MULTILAYERED REGULATION OF TORC1 SIGNALING IN SACCHAROMYCES CEREVISIAE

by

Arron Sullivan

A Dissertation Submitted to the Faculty of the

DEPARTMENT OF MOLECULAR AND CELLULAR BIOLOGY

In Partial Fulfillment of the Requirements

For the Degree of

DOCTOR OF PHILOSOPHY

In the Graduate College

THE UNIVERSITY OF ARIZONA

2018

THE UNIVERSITY OF ARIZONA
GRADUATE COLLEGE

As members of the Dissertation Committee, we certify that we have read the dissertation prepared by **Arron Sullivan** titled **MULTILAYERED REGULATION OF TORC1 SIGNALING IN SACCHAROMYCES CEREVISIAE** and recommend that it be accepted as fulfilling the dissertation requirement for the Degree of Doctor of Philosophy.

Andrew Capaldi Date: (*11/19/2018*)

Ryan Gutenkunst Date: (*11/19/2018*)

Frans Tax Date: (*11/19/2018*)

Ted Weinert Date: (*11/19/2018*)

Guang Yao Date: (*11/19/2018*)

Final approval and acceptance of this dissertation is contingent upon the candidate's submission of the final copies of the dissertation to the Graduate College.

I hereby certify that I have read this dissertation prepared under my direction and recommend that it be accepted as fulfilling the dissertation requirement.

Dissertation Director: *Andrew Capaldi* Date: (*11/19/2018*)

STATEMENT BY AUTHOR

This dissertation has been submitted in partial fulfillment of the requirements for an advanced degree at the University of Arizona and is deposited in the University Library to be made available to borrowers under rules of the Library.

Brief quotations from this dissertation are allowable without special permission, provided that an accurate acknowledgement of the source is made. Requests for permission for extended quotation from or reproduction of this manuscript in whole or in part may be granted by the head of the major department or the Dean of the Graduate College when in his or her judgment the proposed use of the material is in the interests of scholarship. In all other instances, however, permission must be obtained from the author.

SIGNED: Arron Sullivan

ACKNOWLEGEMENTS

I need to thank a lot of people for all their work and support over the year. Andrew Capaldi has been a great mentor and has helped shape me as a scientist. Xiangxia Luo taught me almost everything I know at the bench and we have had many great moments in lab together. Jeremy Worley and I were partners in the high-throughput screen and our teamwork made it a fun challenge. Though we could not have even begin to have completed the screen with out the hard work of Matt Kaplan in the FGC. Jim Hughes-Hallett, Joe Kunkel, Ryan Wallace, Jacob Cecil, and Rachel Wellington have all been my great friends and Jim left me with a fun second project to tackle. Ryan and Rachel also played key roles in the TORC1 body work and I appreciate their contributions and time spent in lab debating how the system works.

I would also like to thank my committee for all their time and work over the years; Ryan Gutenkunst, Frans Tax, Ted Weinert, and Guang Yao. They have listened to me talk about the Tor complex for hours on end and have always had insightful questions, advice, and enthusiasm for my work, of which I have been very appreciative of.

I need to thank my parents Cheryl Sullivan and Michael Hoeper and my siblings Kelli and Devin for playing large roles in supporting my science career and interests over the years and for listening to me tell them about yeast genetics over the holidays. My Uncle John Sullivan helped spark my science interests with many museum visits and electronic building kits when I was younger that I really appreciated. And my grandparents Granville Sullivan and Rose Sullivan, who let me break many things to figure out how they work and who I told I would one day be a scientist.

A huge final thank you goes to Sara Winters for moving to the desert with me so I could complete this work, I cannot thank her enough. She had to deal with many lost weekends and evenings while I was looking at yeast on a microscope.

TABLE OF CONTENTS

LIST OF FIGURES

CHAPTER 2: GENOME-WIDE ANALYSIS OF THE TORC1 AND OSMOTIC STRESS

CHAPTER 3: MULTI-LAYERED REGULATION OF TORC1-BODY FORMATION IN BUDDING YEAST

LIST OF TABLES

CHAPTER 2: GENOME-WIDE ANALYSIS OF THE TORC1 AND OSMOTIC STRESS

ABSTRACT

The Target of Rapamycin Complex 1 (TORC1) is a master regulator of cellular growth in eukaryotes. Much insight has been gained into how amino acid and nitrogen levels regulate TORC1 through the escape from rapamycin-induced growth arrest complex (EGOC), and its regulators including the Seh1-associated complex (SEAC). However, other nutrient levels and environmental stresses also act on TORC1, and far less is known about how these signals are transmitted to the complex. In two projects presented here we investigate the osmotic stress signaling network acting on TORC1 as well as regulators of TORC1 agglomeration that act in glucose and nitrogen starvation conditions.

In the first investigation, we introduce a novel and reproducible high-throughput assay to screen for genes that affect TORC1 activity in stress conditions. We then use these methods to measure the expression of a TORC1 dependent ribosome biogenesis gene, NSR1, in ~4700 strains from the yeast knock-out library during osmotic stress. We show that 440 of these strains are not able to properly repress NSR1 transcription. The genes identified in the screen form a highly-connected network including 17 proteins that directly interact with TORC1. Secondary rapamycin-based assays performed on these strains allowed us to further characterize the network and show that more than 50 of the proteins act downstream of TORC1. The data derived from this work serve as a resource for our lab and others studying TORC1, and the assay itself is customizable and can be used to characterize any gene regulatory network.

In the second study, we sought to further our understanding of the movement of TORC1 from its position distributed across the surface of the vacuolar membrane to a single agglomerate (TORC1-body) in starvation conditions. Previous work suggested that the AMPK in yeast, Snf1, indirectly promoted the phosphorylation of the TORC1 component Kog1. This phosphorylation event sped up aggregation of the complex by ~20 fold. In order to identify other signaling proteins that regulate TORC1-body formation we performed a screen examining the impact that nearly all non-essential kinases and phosphatases in yeast, as well as selected proteins from the previous high-throughput network, have on TORC1 agglomeration. We identified 13 new regulators of TORC1 body formation, including the PI(3)P binding protein Pib2. We also examined the impact of EGOC deletions and mutants had on body formation and discovered that active EGOC was an inhibitor of TORC1 aggregation. Together, we show that seven of the new regulators likely act at or above the EGOC dependent inhibition of TORC1 body formation; while others act at a later step to assist in body formation.

CHAPTER 1: THE TARGERT OF RAPAMYCIN COMPLEX 1: SIGNALING AND REGULATION

1.1 Introduction

Organisms must incorporate data about their surroundings and their own status to ensure proper fitness and survival. One vital question that an organism needs to answer concerning these data is whether or not to grow. Nutrient storage and availability must be accounted for as well as the level of internal and external stressors. Attempting to grow in low nutrients or when some stress is present will cause damage, unwanted mutations, or even death of the organism. This is as true for higher order multicellular organisms as it is for single cellular ones.

After more than 25 years of research since being discovered in *Saccharomyces cerevisiae*, the Target Of Rapamycin Complex 1 (TORC1) has become known as the master regulator of cellular growth in eukaryotes (González & Hall, 2017; Loewith & Hall, 2011; Wullschleger, Loewith, & Hall, 2006). Pro-growth signals such as high levels of nutrients, amino acids, and growth factors activate TORC1, which in turn promotes anabolic cell processes such as ribosomal biogenesis, protein synthesis, lipid synthesis, and overall mass accumulation. Loss of nutrients or energy (ATP), or sub-optimal nutrient sources, turn off or diminish anabolism and turn on catabolic processes such as nitrogen assimilation and autophagy. Similarly, the addition of stresses – oxidative, osmotic, heat shock, hypoxia – inactivate TORC1, even in the presence of optimal growth signals (Barbet et al., 1996; De Virgilio, 2012; Durán & Hall, 2012; Düvel et al., 2010; Efeyan, Comb, & Sabatini, 2015; González & Hall, 2017; Hsu et al., 2011; Loewith & Hall, 2011; Noda & Ohsumi, 1998; Saxton & Sabatini, 2017; Urban et al., 2007a). Although it is known that

TORC1 is activated or deactivated in these conditions, the exact mechanisms of regulation are poorly understood. The exception is amino acid signaling through small GTPases, discussed in more detail below.

1.2 Composition of TORC1

In mammals TORC1 (mTORC1) is composed of the proteins Raptor, mLst8, and the mTor1 kinase and the yeast orthologs are Kog1, Lst8, and Tor1 (Adami, García-Álvarez, Arias-Palomo, Barford, & Llorca, 2007a; Loewith & Hall, 2011; Loewith et al., 2002; Reinke, Anderson, Mccaffery, et al., 2004; Yang et al., 2017; Yip, Murata, Walz, Sabatini, & Kang, 2010). Compared to mammalian systems the yeast TORC1 has two main compositional differences. First, an additional protein Tco89 is part of the complex, though not much is known about its role (Reinke, Anderson, Mccaffery, et al., 2004). Second, Tor1 has a homolog Tor2 which acts in TORC1 when Tor1 is absent, but is normally found in the plasma membrane bound TORC2 complex, which has a different role than TORC1 in the cell (Gaubitz, Prouteau, Kusmider, & Loewith, 2016; Kliegman et al., 2013; Loewith et al., 2002; Riggi et al., 2018). In mammals, the mTor1 kinase is in both complexes. The proteins in TORC1 form a dimer (Adami et al., 2007a; Loewith & Hall, 2011; Yang et al., 2017; Yip et al., 2010).

The Tor1 kinase is a phosphatidylinositol kinase (PIK)-related kinase and from the N to C terminus is composed of two tandem regions of HEAT domain repeats, a FAT domain, a FRB domain, the kinase catalytic domain, and finally a FATC domain (Adami et al., 2007a; Loewith & Hall, 2011).

The HEAT domains offer regions for protein-protein binding between other components of the complex (Wullschleger, Loewith, Oppliger, & Hall, 2005; Yip et al., 2010). PIKK and related kinases are known to have FAT and FATC domains, which have proposed scaffolding and protein binding roles as well as a recently described auto-inhibitory function for the FAT domain by conformational changes in the complex (Bosotti, Isacchi, & Sonnhammer, 2000; Dames, Mulet, Rathgeb-Szabo, Hall, & Grzesiek, 2005; Loewith & Hall, 2011; Yang et al., 2017). The FRB (FKBP12-rapamycin-binding) domain is the location that the TORC1 specific inhibitor rapamycin binds while the molecule is complexed to either FKB12 in humans or FPR1 in yeast--a peptidyl-prolyl cis-trans isomerase that otherwise has no relationship to TORC1 signaling. Rapamycin was a crucial tool in the early investigations and discovery of TORC1 due to its specific inhibitory action on the Tor kinase in TORC1 and not on TORC2 (Cafferkey et al., 1993; Choi, Chen, & Schreiber, 1996; Helliwell et al., 1994; Loewith & Hall, 2011). Finally, the kinase catalytic domain is similar to that of PI3/PI4 kinases however it does not have any propensity to phosphorylate phosphoinositides and instead is a S/T kinase for its substrates (Bosotti et al., 2000; Loewith & Hall, 2011; Urban et al., 2007a).

The Kog1/RAPTOR proteins have a raptor N terminal conserved (RNC) domain followed by HEAT repeat as well as WD40 repeats for complex structure and substrate binding (Adami et al., 2007a; Adami, García-Álvarez, Arias-Palomo, Barford, & Llorca, 2007b; Yip et al., 2010). Further the Kog1 protein, but not RAPTOR, has two intrinsically disordered domains that are rich in glutamines and asparagines. This region is considered prion-like and has been shown to be necessary for aggregation of multiple TORC1 dimers in starvation conditions (Hughes Hallett et

al., 2015). Lst8 and mLST8 have several WD40 repeats and are found bound near the active site of the Tor1/2 kinases in both TORC1 and TORC2, increasing the catalytic activity of the kinases(Loewith & Hall, 2011; Loewith et al., 2002; Wedaman et al., 2003). The yeast specific TORC1 component Tco89 has poorly understood functions in the complex. However, it is essential for the proper activity of TORC1 – and therefore cellular growth – and its absence confers hypersensitivity to rapamycin and decreased cellular integrity (Reinke, Anderson, Mccaffery, et al., 2004).

1.3 TORC1 Localization

In yeast, TORC1 predominantly localizes to the vacuolar outer membrane both when active and when repressed (Binda et al., 2009; Loewith & Hall, 2011; Sturgill et al., 2008; Urban et al., 2007b). It has also been suggested to be in stress granules in heat stress or the nucleus in some fractions where it may regulate ribosomal transcription (H. Li, Tsang, Watkins, Bertram, & Zheng, 2006; Martin, Powers, & Hall, 2006; Takahara & Maeda, 2012). Construction of a tethered version of the major substrate of TORC1, Sch9, to the vacuole showed efficient TORC1 phosphorylation of Sch9, and thus that most of TORC1 signaling happens at the vacuole membrane (Binda et al., 2009; Loewith & Hall, 2011; Urban et al., 2007b). Similarly, in mammals RAGULATOR bound active mTORC1 is found at the lysosomes but may also be found in the nucleus, stress granules, or the cytoplasm in amino acid starvation (Betz & Hall, 2013; Demetriades, Doumpas, & Teleman, 2014; Menon et al., 2014; Rosner & Hengstschlager, 2008; Sengupta, Peterson, & Sabatini, 2010; Thedieck et al., 2013; Zhou et al., 2015).

Recent work has shown that TORC1 also undergoes relocalization on the yeast vacuole (Hughes Hallett et al., 2015; Prouteau et al., 2017). In exponential growth, the yeast TORC1 complex is distributed across the outer membrane of the vacuole, but upon starvation it aggregates into one or more bodies, named TORC1-bodies, but remains on the vacuole surface until nutrients are restored. This is in part due to the prion-like domains in Kog1 protein and signaling by the AMP sensing protein Snf1(the yeast AMPK ortholog) (Hallett et al., 2014; Hughes Hallett et al., 2015). This is a practical way to sequester or modulate a master controller of growth until it is needed again. It is also suggested that the TORC1-bodies may be able to form a higher order structure which would occlude the active site of the Tor kinase, deepening the off state of the complex (Prouteau et al., 2017).

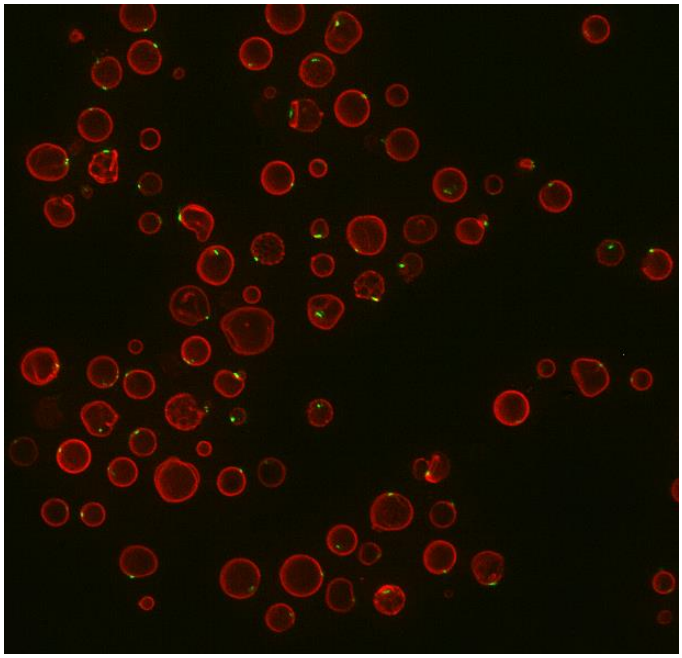

Figure 1. TORC1 bodies (Green; Kog1-YFP) sitting on yeast vacuoles (Red, Vph1-mCherry) in 24-hour glucose starvation.

1.4 Regulation of TORC1 by Nutrients

The investigation of Gasch, et al. in 2000 examining gene expression patterns in various starvation and stress conditions showed that yeast respond to stress and starvation by up-regulating the environmental stress response (ESR) genes and down regulating of pro-growth genes (Gasch et al., 2000). Interestingly, adding the TORC1 specific inhibitor rapamycin triggers analogous expression pattern, once again showing its master regulation of growth status (Hallett et al., 2014). Understanding how the many different nutrient and stress signals regulate TORC1 has been the focus of much work in the past few decades. While much more is now known about how amino acid signals are transmitted to TORC1, there is a lot left to uncover for the numerous other signals that TORC1 must incorporate to make decisions that will affect the fitness and survival of the cell or organism (Bar-Peled & Sabatini, 2014; De Virgilio & Loewith, 2006; González & Hall, 2017; Loewith & Hall, 2011).

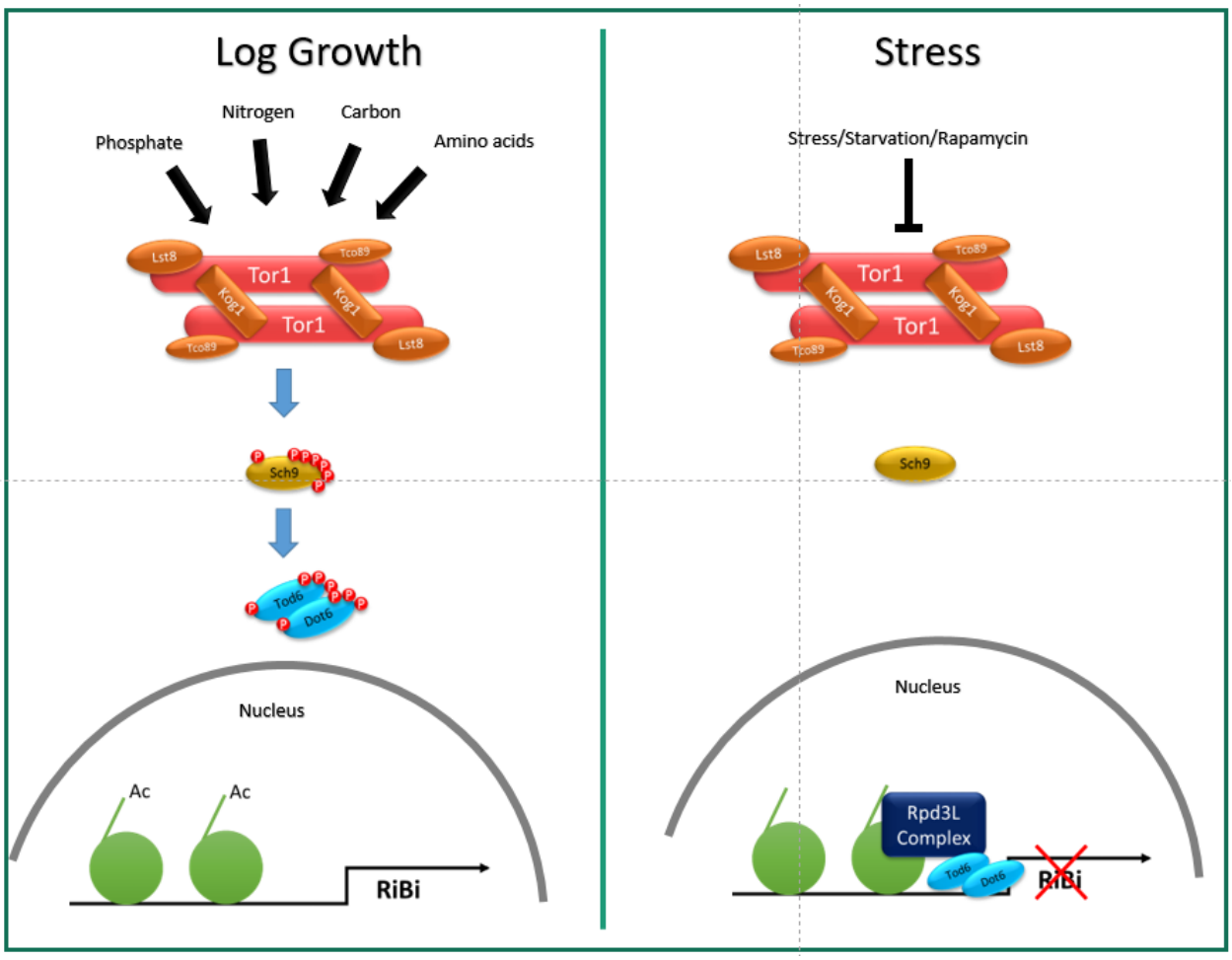

Figure 2. Simple diagram of TORC1 regulation of ribosomal biogenesis (RiBi) genes in growth and stress conditions.

1.4.1 Regulation by EGOC/Ragulator-Rags and amino acid signals

The escape from growth arrest complex, EGOC, in yeast consists of the proteins Ego1-3 and the small Rag GTPases Gtr1/2 (Binda et al., 2009; Dubouloz, Deloche, Wanke, Cameroni, & De Virgilio, 2005; Kira et al., 2016; Powis et al., 2015). The Ego1 protein is tethered to the vacuole outer membrane by palmitoylation and N-myristoylation and together with Ego2/3 acts as a

landing platform for the heterodimer Gtr1/2 (Ashrafi, Farazi, & Gordon, 1998; Binda et al., 2009; Dubouloz et al., 2005). In mammalian cells the overall system is conserved with the Ragulator acting as a platform for the four Rag GTPases RAGA/B/C/D which also act in a heterodimer of RAGA or RAGB with RAGC or RAGD (Bar-Peled & Sabatini, 2014; Chantranupong, Wolfson, & Sabatini, 2015; Sancak et al., 2010). In amino acid replete conditions Gtr1 is GTP loaded by the GEF Vam6, and Gtr2 is loaded with GDP by its GAP Lst4/7 (Binda et al., 2009; Péli-Gulli, Sardu, Panchaud, Raucci, & De Virgilio, 2015). This represents the active form of the heterodimer and is sufficient to activate TORC1 signaling in yeast. Further, Gtr1 is activated by leucine levels via Cdc60 (Bonfils et al., 2012). Deactivation of TORC1 by the EGOC happens through the amino acid sensing Seh1-associated (SEA) complex which acts as a GAP for Gtr1(Algret et al., 2014; Laxman, Sutter, Shi, & Tu, 2014). To date there is no known GEF for Gtr2 (which would inhibit it), and there could be more activators and inactivators for both GTPases yet to be found in yeast (González & Hall, 2017). A similar architecture occurs in humans, where the SEA complex replaced with the GATOR1/2 complex and Lst4/7 replaced with mammalian folliculin and its binding partners (González & Hall, 2017). Besides acting as a scaffold for the RAGs, it has also been shown that the RAGULATOR has GEF activity toward the RAGA/B GTPase(Bar-Peled, Schweitzer, Zoncu, & Sabatini, 2012).

The defining difference between budding yeast and mammalian TORC1 is the growth factor activated small GTPase RHEB and its regulator the tuberous sclerosis complex (TSC). RHEB is required to promote a conformational change in the active site of mTOR1 to promote full catalytic function (Carroll et al., 2016; Yadav et al., 2013; Yang et al., 2017). There is a putative RHEB in

S. cerevisiae (Rhb1), but it is not necessary for TORC1 activity (González & Hall, 2017). Likewise, there is no TSC encoding genes in yeast. It is therefore believed that there is either an unknown RHEB-like activator in yeast or that TORC1 is constituently active and is regulated by blocking the active site or inhibiting substrate binding by other mechanisms (Hughes Hallett et al., 2015; Prouteau et al., 2017; Yang et al., 2013). Together the combination of RHEB and RAGULATOR/RAGs to ensure that the cell has pro-growth factors and amino acids before activating TORC1 is an elegant solution in mammalian systems for incorporating multiple signals before deciding to grow.

1.4.2 Regulation by Glucose/Energy

Another important factor in a cell's decision about whether to accumulate mass, is if there is enough energy to do so. Glucose starvation in yeast confers a rapid deactivation of TORC1 even if other nutrients are present in abundance (Hallett et al., 2014; Hughes Hallett et al., 2015; Prouteau et al., 2017). Low energy levels are recognized in part by the AMP activated Snf1 (AMPK) kinase, which then regulates transcriptional changes for a low energy state of the cell (Braun et al., 2014; Hedbacker & Carlson, 2008; Pé Rez-Sampietro, Casas, & Herrero, 2013). Snf1 is also responsible for phosphorylation of Kog1 at sites that assist its ability to aggregate into TORC1 bodies and maintain the off state of the complex (Hughes Hallett et al., 2015). In mammals, the AMPK inhibits TORC1 by both phosphorylating RAPTOR as well as TSC which then acts as a GAP for RHEB (J. Huang & Manning, 2008; Inoki, Zhu, & Guan, 2003).

There may also be some form of carbon sensing through Gtr1/2/RAGS. One mechanism may be through the vacuolar ATPase (V-ATPase) which senses a lower cytosolic pH in glucose deprivation. Gtr1 has physical interactions with the V-ATPase and may monitor its assembly/activity or it could also be that lower V-ATPase activity, and therefore decreased vacuolar acidity, produces an inactivation signal to EGOC (Dechant et al., 2010). Glucose starvation-directed TORC1 deactivation and the roles of EGOC and the V-ATPase require more exploration to understand cellular growth control.

1.4.3 Regulation of TORC1 by Stress

TORC1 is inactivated in multiple external stress conditions, but for the most part the mechanisms of regulation are unknown. In yeast under osmotic stress the MAPK Hog1 (of the osmosensing High-Osmolarity Glycerol – HOG—signaling pathway) (Saito & Posas, 2012) has been shown to signal to TORC1 for inactivation (Hallett et al., 2014). However, the mechanism for regulation is unclear and a hog1Δ strain still retains about 25% of TORC1 activation in stress providing evidence that one or more other unknown signals are required and are yet unknown (Hallett et al., 2014). Likewise, it is unknown how TORC1 is regulated by oxidative stress, heat, DNA damage, and starvation conditions not already discussed.

Furthermore, TORC1 can be regulated by feedback mechanisms that are not understood. One example of this is that the addition of cycloheximide, a potent translation elongation inhibitor, partially upregulates TORC1 activity (Obrig, Culp, McKeehan, & Hardesty, 1971; Urban et al.,

2007b). It is suggested that this is due to an influx of protein synthesis substrates, such as amino acids, that then signal to TORC1, likely via EGOC, that there are plenty of nutrients for growth (Loewith & Hall, 2011). A recent study has also shown that ribophagy, in starvation conditions, can stimulate TORC1 activity due to the rising levels of recycled amino acids, especially arginine and lysine, which are enriched in ribosomes (Wyant et al., 2018).

1.5 TORC1 Downstream Signaling

TORC1 controls mass accumulation and growth through the production of proteins, lipids, amino acids and more, while at the same time inhibiting catabolic processes such as nitrogen scavenging and autophagy. Using the TORC1 specific inhibitor rapamycin has allowed researchers to discover the pathways and transcriptional programming controlled by the complex over the years. Two main branches of signaling can be categorized; the Sch9-branch, which promotes anabolic processes, transcription, and protein production while the Tap42/PP2A branch promotes catabolic processes in low nutrients (Beck & Hall, 1999; Breitkreutz et al., 2010; Düvel et al., 2010; Huber et al., 2009; Huber, French, Tekotte, & Yerlikaya, 2011; Jorgensen et al., 2004; Lippman & Broach, 2009; Marion et al., 2004; Schawalder et al., 2004; Urban et al., 2007b; Yan, Shen, & Jiang, 2006).

1.5.1 Sch9 Signaling

The Sch9 kinase is directly phosphorylated at six sites by active TORC1 (Urban et al., 2007b). Observation of the levels of phosphorylated Sch9 (or of the S6 kinase in mammals) in the cell is the primary assay used to determine TORC1 activity. Under stress or starvation Sch9 is rapidly and completely de-phosphorylated, followed by subsequent transcriptional reprogramming (Binda et al., 2009; Hallett et al., 2014; Loewith & Hall, 2011; Urban et al., 2007b). While a number of pathways and genes are controlled by active TORC1, the production of ribosomal biogenesis genes (RiBi) and ribosomal proteins (RP) compose the bulk of the transcriptional capacity in the cell and therefore are highly controlled by nutrient and growth inputs to TORC1 (Huber et al., 2011; Roosen et al., 2005; Warner, 1999).

Under nutrient replete conditions TORC1 phosphorylates Sch9, which in turn phosphorylates the genes Dot6 and Tod6 (Huber et al., 2011; Lippman & Broach, 2009; Worley, Luo, & Capaldi, 2013). When phosphorylated these genes remain cytoplasmic, but upon TORC1 inactivation, and therefore Sch9 inactivation, Dot6/Tod6 become dephosphorylated which allows them to move into the nucleus and inhibit transcription. They accomplish this by recruiting the histone deacetylase complex Rpd3L to regions of the chromosome to be repressed, largely promoters of ribosome biogenesis genes (Alejandro-Osorio et al., 2009). Similarly, Sch9 regulates the transcription factor Stb3, which upon TORC1 inactivation recruits Rpd3L to repress ribosomal proteins (Huber et al., 2011; Liko, Slattery, & Heideman, 2007). In opposition, the transcription factor Sfp1 is directly phosphorylated by TORC1 in optimal conditions, which then drives it to the nucleus to promote RiBi and RP gene transcription (Jorgensen et al., 2004; Lempiäinen et al., 2009; Loewith & Hall, 2011; Marion et al., 2004).

1.5.2 Tap42 Signaling

Tap42 is a regulatory subunit of the protein phosphatase 2A complex (PP2A) which includes itself, one of two other regulatory subunits Rrd1 or Rrd2, and one 2A or 2A-related phosphatase (Pph3/21/22, Sit4, or Ppg1) (Loewith & Hall, 2011; Reinke, Anderson, McCaffery, et al., 2004; Yan et al., 2006; Zheng & Jiang, 2005). The number of possible combinations for a complete Tap42-PP2A complex likely contributes to the diverse pathways it has been implicated in playing a role. When the cell is in optimal conditions and TORC1 is fully active, Tap42-PP2A complexes are known to be phosphorylated by and associated with TORC1. When nutrient levels fall or when cells are under stress, Tap42-PP2a is released from its TORC1 association and promotes downstream signaling to stress responses, control of autophagy, amino acid synthesis, and nutrient uptake from the environment (Beck & Hall, 1999; Jiang & Broach, 1999; Loewith & Hall, 2011; Yan, Lai, & Jiang, 2012; Yan et al., 2006). There is evidence that the GTPase Rho1 advances the release of Tap42-PP2A, but how this is accomplished is still not understood and the fact that only a small fraction of Tap42-PP2A is even associated with TORC1 further complicates our understanding of the pathway (Yan et al., 2012).

1.5.3 Other downstream outputs

While a few of the best-known substrates of TORC1 have been discussed above, there are many more both known and implicated through large scale studies. Autophagy is controlled by TORC1 directly and through Tap42-PP2A acting on the key autophagy components Atg13 and Atg1 (Kamada et al., 2000; Noda & Ohsumi, 1998; Stephan, Yeh, Ramachandran, Deminoff, & Herman, 2009; Suzuki & Ohsumi, 2010). TORC1 promotes tRNA and small rRNA synthesis by phosphorylating Maf1 to prohibit it from binding, and therefore inhibiting, RNA polymerase III (Huber et al., 2009; Wei & Zheng, 2009). Stress response is regulated in part by TORC1 dependent dephosphorylation of the transcription factors Msn2/4 (Beck & Hall, 1999; Causton et al., 2001). Furthermore, scores of genes have observed rapamycin dependent phosphorylation events that are either direct targets of TORC1 are target of a kinase/phosphatase under control of TORC1 (Huber et al., 2009; Soulard et al., 2010).

1.6 Aims

It has become quite clear that TORC1 signaling and regulation is a complex problem with many unknown players and mechanisms yet to be discovered. While much focus has been on how amino acid and nitrogen signals regulate TORC1, we wanted to start to shed light on how other stress signals are incorporated in the system.

Chapter 2 relates our development of a novel high-throughput pipeline to probe for genes that are part of the TORC1 signaling network of growth control. We screened the yeast knock-out library to discover which genes, when missing, confer a defect in TORC1 inactivation in acute osmotic

stress. We then placed these genes within a highly connected osmotic stress TORC1-signaling network based on secondary assays and other available data.

Chapter 3 discusses developments and follow up work on the observations that TORC1 aggregates in glucose and nitrogen starvation. Studying the capacity of TORC1 body formation in over 200 mutant strains, we found that the EGOC plays an important role in repressing TORC1 body formation. We also identified 13 new regulators of TORC1 body formation.

Chapter 4 discusses future lines of inquiry based on the results of these two studies.

CHAPTER 2: GENOME-WIDE ANALYSIS OF THE TORC1 AND OSMOTIC STRESS SIGNALING NETWORK IN *SACCHAROMYCES CEREVISIAE*

Jeremy Worley*†, Arron Sullivan*†, Xiangxia Luo†, Matthew E Kaplan‡, and Andrew P. Capaldi†‡§

† Department of Molecular and Cellular Biology and ‡ the Functional Genomics Core facility, University of Arizona, Tucson, AZ, 85721-0206

This work was published in:

G3: GENES, GENOMES, GENETICS February 1, 2016 vol. 6 no. 2 463-474

* Co-first authors

§ Corresponding author: capaldi@email.arizona.edu

2.1 ABSTRACT

The Target of Rapamycin kinase Complex I (TORC1) is a master regulator of cell growth and metabolism in eukaryotes. Studies in yeast and human cells have shown that nitrogen/amino acid starvation signals act through Npr2/3 and the small GTPases Gtr1/2 (Rags in humans) to inhibit TORC1. However, it is unclear how other stress and starvation stimuli inhibit TORC1, and/or act in parallel with the TORC1 pathway, to control cell growth. To help answer these questions, we developed a novel automated pipeline and used it to measure the expression of a TORC1 dependent ribosome biogenesis gene (NSR1) during osmotic stress in 4700 Saccharomyces cerevisiae strains from the yeast knock-out collection. This led to the identification of 440 strains with significant and reproducible defects in NSR1 repression. The cell growth control and stress response proteins deleted in these strains form a highly connected network, including; 56 proteins involved in vesicle trafficking and vacuolar function; 53 proteins that act downstream of TORC1 according to a rapamycin assay--including components of the HDAC Rpd3L, Elongator, and the INO80, CAF-1 and SWI/SNF chromatin remodeling complexes; over 100 proteins involved in signaling and metabolism; and 17 proteins that directly interact with TORC1. These data provide an important resource for labs studying cell growth control and stress signaling, and demonstrate the utility of our new, and easily adaptable, method for mapping gene regulatory networks.

2.2 INTRODUCTION

The Target of Rapamycin (TOR) kinases are conserved across eukaryotes, where they act as master regulators of cell growth and metabolism (LOEWITH AND HALL 2011; LAPLANTE AND SABATINI 2012). In line with their central role in cell signaling, TOR kinases respond to an enormous array of stimuli and control the activity of hundreds of proteins--functions that are supported in part by their recruitment into two distinct complexes, TOR Complex 1 (TORC1) and TOR Complex 2 (TORC2) (BARBET et al. 1996; KIM et al. 2002; LOEWITH et al. 2002; URBAN et al. 2007; HUBER et al. 2009; SOULARD et al. 2010; HSU et al. 2011). TORC1, unlike TORC2, is rapamycin sensitive and in S. cerevisiae is made up of the TOR kinase Tor1 (and in its absence the homolog Tor2), the key regulator Kog1, and two poorly characterized proteins, Lst8 and Tco89 (HEITMAN et al. 1991; LOEWITH et al. 2002; REINKE et al. 2004).

In the presence of adequate nutrients, TORC1 drives growth by activating multiple steps in protein and ribosome synthesis. First, TORC1 directly phosphorylates and activates the transcription factor Sfp1 and the AGC kinase Sch9 (URBAN et al. 2007; LEMPIAINEN et al. 2009). Sch9, in turn, then phosphorylates and blocks the activity of the transcriptional repressors Dot6, Tod6 and Stb3, leaving Sfp1 to promote the high level expression of 400 genes involved in ribosome biogenesis (Ribi) and translation (JORGENSEN et al. 2004; MARION et al. 2004; LIKO et al. 2007; LIPPMAN AND BROACH 2009; HUBER et al. 2011). Second, TORC1 acts in cooperation with Yak1 and the cAMP dependent protein kinase (PKA) pathway, to promote the activity of Fhl1 and upregulate expression of the ribosome protein (RP) genes (MARTIN et al. 2004;

SCHAWALDER et al. 2004; WADE et al. 2004). Third, TORC1-Sch9 phosphorylates and regulates the kinase Maf1, and other factors, to activate Pol I and Pol III and thus rRNA and tRNA synthesis (UPADHYA et al. 2002; HUBER et al. 2009; LEE et al. 2009). Finally, TORC1 promotes translation, in part by blocking phosphorylation of eIF2 (BARBET et al. 1996; LOEWITH AND HALL 2011).

In contrast, when cells are starved for energy, amino acids, or nitrogen, or exposed to noxious stress, TORC1 signaling is inhibited, leading to down-regulation of Ribi and RP gene expression, rRNA and tRNA synthesis, and consequently cell growth (POWERS AND WALTER 1999; GASCH et al. 2000; URBAN et al. 2007; BRAUER et al. 2008). In particular, dephosphosphorylation of Dot6, Tod6 and Stb3 triggers recruitment of the Class I histone deacetylase Rpd3L to the Ribi and RP genes, leading to a rapid decrease in gene expression levels (ALEJANDRO-OSORIO et al. 2009; LIPPMAN AND BROACH 2009; HUBER et al. 2011).

The mechanisms underlying TORC1 inhibition in nitrogen and amino acid starvation conditions are starting to come into focus. Specifically, it is now clear that nitrogen and amino acid starvation trigger activation of the GAP Npr2-Npr3-Iml1 SEAC subcomplex, SEACIT, and this in turn alters the GTP binding state of the small GTPases, Gtr1/2 (KIM et al. 2008; SANCAK et al. 2008; BINDA et al. 2009; NEKLESA AND DAVIS 2009; PANCHAUD et al. 2013). Gtr1/2 then bind TORC1 on the vacuolar membrane and inhibit TORC1 dependent phosphorylation of Sfp1 and Sch9 (URBAN et al. 2007; BINDA et al. 2009; LEMPIAINEN et al. 2009; PANCHAUD et al. 2013). At the same time an interaction between Gtr1/2, the small GTPase Rho1, and TORC1

promotes release of Tap42 from the TOR complex, triggering Tap42-PP2A dependent reprogramming of nitrogen and amino acid metabolism (CARDENAS et al. 1999; DUVEL et al. 2003; YAN et al. 2006; YAN et al. 2012). At least in humans, Gtr1/2 signaling also depends on interactions with the vacuolar ATPase (V-ATPase) and amino acid transporters on the vacuolar membrane (ZONCU et al. 2011; WANG et al. 2015).

Outside of nitrogen and amino acid starvation conditions, however, very little is known about TORC1, and TORC1 pathway, regulation. Npr2/3, Gtr1/2, and Rho1 play little-to-no role in transmitting glucose starvation, osmotic stress, heat stress and oxidative stress signals to TORC1-Sch9 (BINDA et al. 2009; HUGHES HALLETT et al. 2014). Instead, the AMP activated protein kinase Snf1 partially inhibits TORC1 and/or TORC1-Sch9 signaling during glucose/energy starvation, while the MAPK Hog1 plays a small role in regulating TORC1 and/or TORC1-Sch9 signaling in osmotic stress (HUGHES HALLETT et al. 2014). It is also known that TORC1 binds to stress granules during heat shock, but this interaction is not required for the initial stages of TORC1 inhibition (TAKAHARA AND MAEDA 2012). Thus, most of the proteins and pathways that regulate TORC1 and/or TORC1-Sch9 signaling in noxious stress and energy starvation remain to be identified.

It is also unclear how the TORC1 pathway cooperates with other signaling pathways to regulate cell growth. Numerous studies have shown that the ras/PKA pathway regulates expression of the cell growth genes in glucose, primarily by acting in parallel with Sch9 to phosphorylate and regulate Sfp1 and Dot6/Tod6 (JORGENSEN et al. 2004; MARION et al. 2004; MARTIN et al.

2004; ZURITA-MARTINEZ AND CARDENAS 2005; SLATTERY et al. 2008; LIPPMAN AND BROACH 2009). It is also known that the inositol kinases Vip1 and Kcs1, and the inositol pyrophosphates they produce, act in parallel with TORC1 to regulate Rpd3L, and thus the Ribi and RP genes, during stress (WORLEY et al. 2013). However, it is unclear how Kcs1 and Vip1 are regulated and if/how other pathways cooperate with TORC1 to control cell growth.

Therefore, to push our understanding of TORC1 signaling and cell growth control forward, we carried out a screen to identify proteins that are required for the downregulation of Ribi gene expression in osmotic stress. Similar screens have been carried out previously to identify proteins involved in the Unfolded Protein Response (UPR), Heat shock factor 1 (Hsf1) response (in log growth conditions), and the amino acid starvation response--in each case using a GFP reporter placed under a relevant promoter (JONIKAS et al. 2009; NEKLESA AND DAVIS 2009; BRANDMAN et al. 2012). However, a GFP reporter cannot easily be used to study cell growth control since Ribi and RP genes are only transiently downregulated during stress, leading to relatively small (2-fold) changes in Ribi and ribosome protein levels (GASCH et al. 2000; LEE et al. 2011). To get around this problem, we developed a novel automated pipeline that directly measures mRNA levels at the peak of the osmotic stress response (a 32-fold change in gene expression), and used it to measure Ribi gene expression in 4700 strains from the yeast knock-out (YKO) collection (WINZELER et al. 1999). This led to the identification of 440 strains with a reproducible and highly significant ($p<0.001$) defect in Ribi gene repression during stress. We then went on to show that 53 of these strains also have a significant defect in the response to rapamycin, and are therefore missing genes that act downstream of TORC1.

Among the genes that act downstream of TORC1, we find numerous factors involved in transcription and chromatin remodeling including 6 subunits of Rpd3L, 3 subunits of the Elongator complex, 3 histone proteins, 2 histone demethylases and components of the SWI/SNF, INO80 and CAF-1 chromatin remodeling complexes. We also identified 21 ribosome proteins and translation factors in the screen, 9 of which act downstream of TORC1. Other genes in the growth control network have a wide variety of functions, but include 56 proteins involved in vacuolar function and vesicle transport, including 10 components of the V-ATPase, as well as 5 kinases, 5 methyltransferases, and 9 membrane transporters. Finally, 17 genes in the network physically interact with TORC1, suggesting that we have identified numerous direct regulators and effectors of TORC1 signaling.

Overall, the data presented here provide a valuable resource for labs studying TORC1 signaling, cell growth control, or the environmental stress response, and demonstrate the utility of our novel and easily adaptable method for mapping gene regulatory networks in yeast and other organisms.

2.3 METHODS

2.3.1 Automated Pipeline

Inoculation, growth, treatment, and RNA isolation steps were performed on a Biomek FX liquid handling robot (Beckman Coulter) equipped an integrated plate hotel (Cytomat) and shaking incubator (Liconic). All 96 wells plates were labeled with barcodes, and loaded onto the Biomek using a barcode scanner, to ensure that the plates remained in order and maintained their original orientation. OD600 measurements were taken with a plate reader (BioTek Synergy 2) in sterile 96-well plates (Greiner Bio-One) at 30°C. Detailed descriptions of the protocols run on the Biomek are provided in the Supplemental Methods.

2.3.2 Cell Growth and Stress Treatment

YKO collection strains were pinned onto YEPD agar plates using a Singer ROTOR robot and grown for two days at 30°C. The yeast were then pinned from the agar plates into 96-well plates containing 100ul of YEPD per well and grown for 18-22 hours at 30°C. The overnight cultures were then used to inoculate 2.2ml deep-well plates (VWR), containing 550ul of YEPD and one sterile 3.2mm stainless steel mixing bead per well, to an OD600 of 0.05 and loaded into the Liconic Incubator (shaking at 1200rpm and 30°C). Once the median OD600 of a plate reached 0.60 (no wells reached an OD600 of >0.8), 150ul of each culture was transferred to a 2.2ml 96-well plate containing 850ul of RNAse Inactivation Buffer per well (RI Buffer; 4M Ammonium Sulfate, 100mM MES buffer, and 20mM EDTA, pH 4.6) and mixed thoroughly by pipetting. 100ul of 1.875M KCl or 1ug/ml rapamycin in 30°C YEPD was then added to each remaining culture

(yielding final concentration of 0.375M KCl or 200ng/ml rapamycin) and the plate returned to the Incubator for 19min (shaking at 1200rpm and 30°C). The plate was then moved back to the deck of the robot and 150ul of culture removed from each well and added to RI Buffer as described above. The plates containing RI Buffer and yeast were then stored at -20°C.

2.3.3 RNA Purification

Plates containing cells in RI Buffer were defrosted by centrifugation (25min at 3000rpm at room temperature) and the supernatant removed from each well. The pelleted cells were then resuspended in 400ul lysis buffer (4M Guanidine Thiocyanate, 25mM NaCitrate, 0.5% N-lauryl Sarcosine) and transferred to a 700ul 96-well plate (Griener) containing 300ul of zirconia/silica beads per well. The plates were then sealed with sterile foil and shaken for 5min on a mini-Beadbeater-96 (Biospec). After a second round of centrifugation (25min at 3000rpm at 4°C) the plates were loaded into the Biomek where 100ul of lysate was transferred to a sterile 96-well PCR plate (Thermo Scientific). At this point, 70ul of isopropanol was added to each lysate and mixed for 1min before adding 20ul of MagMax binding beads (50% slurry in binding buffer; Ambion) to each well. The isopropanol, lysate and bead mix was then mixed for 7min to ensure all of the RNA in the sample bound to the beads, the plate moved to a magnetic stand-96 (Ambion) for 5min, and the liquid removed from each well. The beads were then washed with 150ul of Wash Buffer 1 for 5min (1.7M Guanidine Thiocyanate, 0.17% N-lauryl Sarcosine, 33% isopropanol, 33mM NaCitrate, pH 7.0) followed by 150ul of Wash Buffer 2 for 5min (2M KCl, 80% Ethanol, 2mM Tris, PH 7.0). The DNA in each sample was then cleaved by treatment with Turbo DNAse (0.25ul of 2 U/μL stock in 50ul DNAse buffer from Life Technologies) for 25 minutes at room

temperature. The RNA was then bound to the magnetic beads again by adding 100ul of 1.5x Wash Buffer 1 and incubating for 5min, the beads washed two more times with Wash Buffer 2 (5min each), and dried for 10min at room temperature. Finally, the purified RNA was eluted by mixing the beads with 30ul of 55°C elution buffer (1mM sterile-filtered RNAse-free Tris pH 8.0) for 5min, the plate was then returned to magnetic stand (to remove the beads), and the eluate transferred to a sterile PCR plate and stored at -80°C.

2.3.4 qPCR

1-step qRT-PCR reactions were performed using 5ul RNA, TaqMan probes/primers from Lifetech (used at the recommended concentrations; probe and primer sequences not provided by company) and 5ul PerfeCTa qPCR ToughMix, Low ROX (Quanta) in a 96-well PCR plate using an Agilent Stratagene Mx3005p cycler. One TaqMan probe bound to the reporter gene Nsr1 (labeled with FAM dye) and the other bound to a control gene, Pex6 or Ntf2 (labeled with JOE dye). The ROX normalized data from each plate was then analyzed using the Stratagene MxPro software and fluorescence thresholds (dRn) of 0.120 for FAM (Nsr1) and 0.60 for JOE (Pex6). Samples that passed the FAM or JOE threshold after >28 cycles were discarded. This filtering caused us to drop data from about 200 strains in the YKO library; most of these strains grew very poorly in the 96 well plates leading to a low RNA yield.

2.3.5 qPCR Normalization

To calculate the normalized NSR1/PEX6 and NSR1/NTF2 ratios, the FAM minus JOE (F-J) value was calculated for every well. The machine learning module, scikit-learn, in Python was then used to calculate the average F-J value for two populations on each plate--strains with expression defects, and strains without expression defects. This was done using Gaussian Mixture Models in the 'scikit.mixture' package with a covariance class of type 'full' for 2-component analysis (http://scikit-learn.org/stable/modules/mixture.html#selecting-the-number-of-components-in-a-classical-gmm). The average F-J value for the strains without an expression defect was then subtracted from the F-J value of the entire plate, setting the mean of the plate (minus the outliers) to 0.0. All values were then multiplied by -1 so that higher RNA concentrations give higher NSR1/PEX6 ratios. This normalization had little impact on the list of strains that we identified as outliers in the screen but adjusts for the 0.3-0.6 cycle variation in the average NSR1/PEX6 ratio that we observe in separate runs on the qPCR machine.

2.3.6 Application of the Method to Other Organisms and Problems

The automated pipeline described here can (in theory) be used to study a wide variety of organisms/cell types. In most cases, this will require knocking down protein targets using siRNA or CRISPRi prior to stress treatment. The lysis step will also have to be optimized for each cell type. However, for organisms that do not have a cell wall it should be possible to perform chemical lysis on the deck of the robot and proceed directly to the RNA purification step. Finally, the primer sets used in the qPCR step will have to be optimized for each pathway and organism. The method described here could also be used to study RNA decay if a transcription inhibitor is added to the cells just prior to stress treatment.

2.3.7 Network Reconstruction

Interactions between the top 440 genes/proteins in our screen were mapped using the protein-protein interaction data from BioGRID (version 3.4.125). TORC1 (Tor1, Kog1, Lst8, Tco89) was also added to our model as one merged node for reference. 275 proteins, including TORC1, form the major network, while 160 genes have no connection to any other of the 440 proteins identified in the screen. Note that the HSP70 family chaperones Ssa1 and Ssb1 and the RNA binding protein Slf1 were removed from the set (along with any proteins that only interact with them) in Fig. 6 to eliminate non-specific interactions (leaving 236 genes).

The interactions within the osmotic stress response network were mapped and clustered using Cytoscape (version 3.2.1). In Figure 7, node centers are colored based on the rapamycin data, with red nodes indicating a normalized F-J score of $\log2 \geq 1$, and grey nodes indicating $\log2 < 1$, or no data. Node borders are colored based on selected GO Slim data (SGD GO Slim Mapper), where maroon indicates nuclear localization and blue indicates endomembrane or vacuolar localization. Edges are colored based on the type of protein-protein data; Affinity Capture-Luminescence, Affinity Capture-MS, Affinity Capture-RNA, Affinity Capture-Western, and Reconstituted Complex are black; Two-hybrid and Protein-Fragment Complementation Assay are orange; finally, Biochemical Activity, Co-crystal Structure, Co-fractionation, Co-localization, Co-purification, and FRET are dotted grey.

2.3.8 DNA Microarrays of Rpd3L mutants

Rpd3L and Rpd3S mutants were constructed using standard methods in an EYO690 (W303) background, as described in detail previously (WORLEY et al. 2013). Overnight cultures of the EY0690 or Rpd3L mutant strains were then used to inoculate 0.75L of YEPD to an OD600 of 0.1 in a 2.8 L conical flask, and grown shaking at 200 rpm and 30°C. Once the cultures reached an OD600 of 0.6, 250 ml of cells were collected by vacuum filtration and frozen in liquid nitrogen. The remaining cells were then subjected to 0.375 M KCl stress for 20min, harvested by vacuum filtration, and frozen in liquid nitrogen. Finally, the mRNA was purified from the frozen cells, converted into cDNA using reverse transcription, labeled with Cy3 or Cy5, and examined using an Agilent microarray, as described previously (CAPALDI 2010; WORLEY et al. 2013)

2.4 RESULTS

2.4.1 Automated Analysis of Gene Expression in Yeast

We developed an automated pipeline and used it to measure the expression of a ribosome biogenesis gene (NSR1) in 4709 a-type strains from the yeast knockout (YKO) collection (WINZELER et al. 1999; GIAEVER et al. 2002). This pipeline included three major steps (Fig. 1a):

First, strains were grown to an OD600 of 0.6 in 96-well plates and exposed to 0.4M KCl, 200nM rapamycin, or mock stress. Then, at the peak of the stress response (20 min), 4M Ammonium sulfate (pH 4.6) was then added to the cultures to promote protein precipitation and block any further RNA synthesis or degradation.

Next, the 96-well plates were centrifuged to pellet the cells and the ammonium Sulfate solution was replaced with lysis buffer and glass beads. The cells were then lysed by bead-beating and the plates centrifuged a second time to remove insoluble debris.

Finally, the RNA was purified from the lysates in each plate using silicon coated magnetic beads and loaded into a 96-well PCR plate. The gene expression levels in each strain were then measured using quantitative PCR--generally following expression of NSR1 and the housekeeping gene PEX6 (Fig. 1b and c).

All of the steps in the pipeline, with the exception of bead-beating and centrifugation, were performed on a Biomek FX liquid handling workstation with an integrated Liconic incubator. This ensured that all wells and plates were treated in an identical way, making it possible to compare data across strains and days (Methods).

2.4.2 Testing the Pipeline

To test our pipeline, we grew a 96-well plate with wild-type yeast in every well and measured NSR1 and PEX6 expression. The NSR1 and PEX6 mRNA levels were consistent across the plate, with a log2 standard deviation of 0.86 and 0.90, respectively (<2-fold average variation). Moreover, when we normalized the NSR1 data using the PEX6 data--to account for well-to-well variation in total RNA levels--we found that the standard deviation from the mean was only 0.37 on a log2 scale (~30% average variation; Fig. S1).

We then grew another plate of wild-type yeast, but this time treated half of the plate with mock stress (YEPD alone, every-other column) and the other half of the plate with 0.4M KCl. The experiment showed that osmotic stress triggers a log2=2.3 fold average decrease in NSR1 expression (Fig. 2). While this expression change is compressed compared to the log2=5 fold decrease we observe using microarray methods, the standard deviation from the mean in stress was only 0.26 on a log2 scale (0.36 for mock stress samples). Thus, the expression change in osmotic stress is approximately ten times greater than the noise in our assay, indicating that our screen should be accurate enough to identify strains with moderate changes in NSR1 expression.

2.4.3 Analysis of the Yeast Knock Out Collection

After we built and tested the automated pipeline, we used it to measure the osmotic stress response in strains from the YKO library (see Methods); collecting two sets of data for 6 of the 96-well plates in the library and one set of data for the other 48 plates in the library. We then normalized the NSR1/PEX6 values to set the average expression level of the library, excluding outlier strains, to log2 =0.0 (see Methods).

Inspecting the data from the screen revealed that most of the strains in the YKO collection have a similar NSR1/PEX6 ratio, with log2 values ranging from -1.0 to +1.0 (Fig. 3a). However, there were also over 400 outlier strains, with NSR1/PEX6 ratios ranging from log2 = 1.5 to 4.5 (Fig. 3a).

To estimate the significance of these results, we analyzed the data from the six plates (560 strains) that were run through the pipeline twice (on separate days; Fig. 3b). Overall, we found a good correlation between replicates, with a Pearson's r of 0.90 and an average difference between measurements of log2= 0.29. Taking this latter value as a good estimate of the average error, we then modeled the log data for the complete screen using a normal distribution with a mean of 0.0 and a standard deviation of 0.3 (Fig. 3a). This model fit the data for strains with NSR1/PEX6 ratios between -1.0 and ~0.5 very well, indicating that the variation in this range is simply due to the error in our assay. By corollary, we could then estimate the probability that a strain has a log2 NSR1/PEX6 ratio larger than 1.0 by chance at less than 0.1% (3.3 Z-score; Fig. 3a).

Our statistical analysis suggested that there are 734 strains with a significant defect in stress dependent repression of NSR1 (log2>1.0; $p<0.001$). However, there were two potential problems with this interpretation of the data. First, our error model is based on data from 6 out of 54 plates in the library and thus, if the error varied from plate to plate, we could be overestimating the number of strains with real defects in NSR1 repression. Second, our analysis assumes that the expression level of the housekeeping gene PEX6 is constant across all YKO collection strains, but some strains may have a higher NSR1/PEX6 ratio than expected due to a decrease in PEX6 expression.

To address these issues we took all of the strains with a normalized NSR1/PEX6 ratio log2>1.3 (rearrayed onto 6 plates containing 494 strains plus 72 center peak [log2=0] controls for

normalization) and ran them through our pipeline again. However, this time we measured the stress dependent changes in the expression level of NSR1 and a different housekeeping gene, NTF2. Just over 85% of the 494 strains had log2>1.0-fold more NSR1/NTF2 than the control strains, leaving 440 strains that have significantly more NSR1 expression ($p<0.001$) than the average strain in the YKO library in two separate assays (Table S1).

2.4.4 Identification of Known Components in the Cell Growth Control Circuit

To estimate the false negative rate in our screen, we examined the screen data for strains missing known components in the Ribi gene control circuit. As described in the introduction, TORC1, Sch9, Kcs1, Vip1, Hog1, and Rpd3L are all known to play a role in downregulating Ribi gene expression during osmotic stress. However, strains missing the TORC1 components Tor1, Kog1, Lst8 and Tco89, and the kinase Sch9 should not (and do not) show up as hits in our screen since; Tor1 acts redundantly with Tor2; Tco89 has a very limited impact on TORC1 signaling; and Kog1, Lst8 and Sch9 are essential genes and thus not in the YKO library (WINZELER et al. 1999; GIAEVER et al. 2002; LOEWITH et al. 2002).

We did find a log2= 3.1, 1.1, and 0.6 increase in NSR1 expression in the kcs1Δ, vip1Δ and hog1Δ strains from the YKO collection. These numbers align reasonably well with those from our previous work, where we found that deletion of Kcs1, Vip1 and Hog1 in the W303 background all caused an approximately 2-fold increase in Ribi gene expression in osmotic stress (WORLEY et

al. 2013; HUGHES HALLETT et al. 2014). The one outlier was the kcs1Δ strain from the YKO library (which has a larger increase in NSR1 expression than expected), but previous work has shown that this strain behaves abnormally and is likely carrying multiple mutations (HUANG AND O'SHEA 2005).

We also found expression changes in YKO collection strains missing some, but not all, of the Rpd3L subunits. Previous studies have shown that Rpd3 and Pho23 are required for Ribi gene repression in stress, but little is known about the role that the other subunits in Rpd3L play in stress conditions (ALEJANDRO-OSORIO et al. 2009). Therefore, to build a more complete picture of Rpd3L function--and calibrate our screen--we made 14 strains, each missing one subunit of Rpd3L (Rpd3, Sin3, Ume1, Pho23, Sap30, Sds3, Cti6, Rxt2, Rxt3, Dep1, Ume6 and Ash1), or as a control Rpd3S (Eaf3, Rco1), and measured their response to 0.4M KCl using DNA microarrays (CARROZZA et al. 2005a; CARROZZA et al. 2005b).

Our microarray analysis revealed that the 14 strains missing Rpd3L or Rpd3S subunits fall into three groups (Fig. 4a). The first group of strains (rpd3Δ, sin3Δ, pho23Δ, dep1Δ, sds3Δ, sap30Δ, and rxt2Δ has a large defect in Ribi and RP gene repression; the second group (ume1Δ, cti6Δ, rxt3Δ, ash1Δ) has a weak to moderate defect in Ribi and RP gene repression; while the third group (ume6Δ, rco1Δ, eaf3Δ) has no defect in Ribi or RP gene repression.

Comparing the microarray and screen data revealed a clear trend; the screen picked up strains with large defects in NSR1 repression but not strains with small to moderate defects in NSR1 repression

(Fig. 4b). In fact, 6/7 gene deletions that caused a strong defect in NSR1 down-regulation were identified as hits (log2>1.0) in the screen (Fig. 4b). The only exception was sds3Δ but in further testing we found that the inconsistency was caused by additional mutations in the strain from the YKO collection (Fig. S2). In contrast, 0/4 gene deletions that caused a small to moderate defect in NSR1 down-regulation in the microarray experiments were identified as hits (Fig. 4b). It is therefore likely that the 440 strains with log2>1.0 more NSR1 expression during stress than the control strains includes most, if not all, of the strains in the YKO library with a strong defect in Ribi gene (NSR1) repression, but few strains with small to moderate defects in Ribi gene repression.

2.4.5 Complexity of Yeast Stress and Cell Growth Control Network

To begin to make sense of the screen data, we set out to organize the strains with high NSR1 expression into groups. As a first step, we ran the 332 strains with NSR1 expression log2>1.4 in KCl (4 plates with center peak controls for normalization; the maximum that can be processed in parallel) through our pipeline, treating them with mock stress. This experiment revealed that most of the strains with high levels of NSR1 expression in stress (top panel, Fig. 5) have normal, or near normal, NSR1 expression levels during log phase growth (middle panel, Fig. 5). In fact, the average NSR1/PEX6 ratio of the 332 strains in mock stress was log2=0.33, just 26% above that of the center peak control strains. Moreover, there were only five strains with log2>1.0 more NSR1 expression than the controls: mch5Δ (log2=2.6), rpl16bΔ (log2=1.8) puf4Δ (log2=1.7), rpl7aΔ (log2=1.2), and rps7bΔ (log2=1.1).

We then ran the 332 strains through our pipeline again, but this time treated them with the potent TORC1 inhibitor rapamycin. This experiment showed that 53 out of the 332 strains only partially downregulate NSR1 in rapamycin (normalized NSR/PEX6 of log2>1.0) and are therefore missing genes that act downstream of TORC1 (bottom panel Fig. 5, Table S1). Many of these 53 genes are involved in gene regulation, including 30 genes that regulate transcription ($p<0.001$ by GO analysis) and 16 genes involved in chromatin organization and biogenesis ($p=2e-4$). In contrast, the 279 genes that act upstream of TORC1, or in parallel with the TORC1 pathway (log2<1.0 normalized NSR1 expression), tend to be involved in vacuolar function (30 genes, $p=4e-7$) or cation homeostasis (15 genes, $p=5e-4$), but not transcription ($p=3e-4$ under-representation).

Next, to organize the hits from our screen into functional modules, we constructed a model of the Ribi gene control circuit using the physical interaction data from BioGRID (STARK et al. 2006). Overall, we found 1076 connections between the 440 genes/proteins with log2>1.0 NSR1 expression in salt (not including self-self interactions; see Methods). To test if this number of connections is significant we also constructed 10,000 random networks, each containing 440 out of the 4709 genes studied in the screen. These networks all had less than 980 interactions (492 interactions on average), suggesting that the probability of finding 1076 connections by chance is less than 0.01%.

Clustering the physical interaction data using Cytoscape (SHANNON et al. 2003) revealed a network made up of two parts (Fig. 6). The upper half includes 118 proteins connected primarily via weak or transient interactions (orange lines representing yeast two-hybrid and other weak

interactions, but not IP data; Fig. 6). These proteins are primarily localized to the vacuole and endomembrane system (56 blue encircled nodes; Fig. 6, Table 1) and form three distinct groups. The first group includes the A, B, C and D subunits of the V1 portion of the vacuolar ATPase (Vma1, Vma2, Vma5 and Vma8), the c, c', c" and d subunits of the Vo portion of the vacuolar ATPase (Vma3, Vma11, Vma16, and Vma6) and three associated proteins (Vma21, Vma22, and Pkr1). The second group includes two components of the EGO complex (a known regulator of autophagy and TORC1 (BINDA et al. 2009); Slm4 and Meh1), two components of the vacuolar transporter chaperone (VTC) complex, and the transporter Gap1 (EGO and VTC; Fig. 6). The third group includes endosomal and vacuolar SNARE proteins (Syn8, Vam3 and Vam7), the vacuolar Rab family GTPase, Ypt7 (involved in vacuole and endosome fusion; (SCHIMMOLLER AND RIEZMAN 1993)), and a component of the CORVET membrane-tethering complex on the vacuole, Pep5. Twenty-two other genes, distributed throughout the upper portion of the network, are also involved in vesicle trafficking (bottom, Table 1), including numerous steps in transporting cargo from the ER through the Golgi and to the Vacuole (Gyp5, Yip5, Emp70, Vfa1, Vab2 and Rcr1) and from the Cytoplasm to Vacuole (Snx4, Pfa3 and Vac8).

Interestingly, almost all of the proteins in the upper portion of the Ribi gene control network, act upstream of TORC1 or in parallel with the TORC1 pathway (grey nodes Fig. 6 and Table 1). Consistent with this, TORC1 itself (green node; Fig. 6) interacts with several proteins in this portion of the network (Table 2), including Vac8, a part of the CVT pathway and Gyp5 (a GTPase-activating protein involved in ER to Golgi transport), and the kinases Nnk1, Fmp48 and Kdx1--

forming a total of 17 interactions with proteins in the upper and lower parts of the network (Table 2).

In the lower half of the network (also 118 genes) we find two highly connected nodes, the histone H3 proteins, Hht1/2 (merged into one node for simplicity and shown in yellow in Fig. 6). Hht1/2 in turn form strong interactions with three major complexes (black lines showing IP data, Fig. 6). The first includes the six core subunits of Rpd3L (Rpd3, Sin3, Pho23, Sap30, Dep1 and Rxt2) as well another Class I HDAC Hos1 and the Sin3 associated transcription factor Stb4 (Table 3). The second includes three components of the Elongator complex (part of the Pol II holoenzyme responsible for transcriptional elongation; Elp3, Elp6 and Iki3) as well as an associated kinase, Vhs1 (Table 3). The third includes 13 ribosomal proteins and 4 ribosome-associated proteins (Table 3).

Hht1/2 also interact with numerous other nuclear proteins involved in NSR1 regulation (54 maroon encircled nodes, Fig. 6), including histone 2a, components of the ISW2, INO80 and SWI/SNF chromatin remodeling complexes, as well as numerous factors involved in translation and RNA decay (bottom, Table 3). Interestingly, many of the proteins in the lower half of the network, particularly those involved in chromatin remodeling and transcription, act downstream of TORC1 as per our rapamycin data (34 red nodes, Fig. 6).

Outside of the portion of the Ribi gene control network connected by known physical interactions, there are many important proteins/genes (Table S1). The only enriched group includes 21 genes

involved in nitrogen metabolism (p=9e-5). However, there are also 56 enzymes in the unconnected portion of the network (including 5 kinases; Adk1, Bud17, Dgk1, Lsb6, and Yfh7, and 5 methyltrasferases; Mtq2, Sam4, Trm12, Trm44, and Ymr310c), along with 9 transmembrane transporters (Dip5, Hxt14, Mep1, Mup3, Pdr10, Sit1, Tom7, Ydr387c, and Yfl040w) and 8 DNA binding proteins (Dal82, Hal9, Hcm1, Hop1, Sip4, Sok2, Su2 and Znf1). These proteins may interact with components in the cell growth control network during osmotic stress—a stimulus rarely applied during large-scale studies of protein interactions and thus missing from the physical interaction network—or alter network activity by affecting the level of key metabolites in the cell.

2.5 DISCUSSION

We have identified 440 strains from the yeast knockout collection that have a strong and reproducible defect in Ribi gene (NSR1) repression during osmotic stress. The proteins/genes knocked out in these strains fall into three major groups.

(1) The NSR1/Ribi regulation network contains 37 proteins involved in vesicle trafficking, 11 components of the vacuolar ATPase, and 50 other proteins that act as part of the endomembrane system (Table 1 and Table S1). These proteins probably influence NSR1 expression in a variety of ways.

Some of these proteins may directly, or indirectly, inhibit TORC1 signaling in stress. In line with this hypothesis, we found that strains missing components of the EGO complex (Meh1 and Slm4) and vacuolar ATPase--known regulators of TORC1 signaling in other conditions (BINDA et al. 2009; ZONCU et al. 2011)--have large defects in NSR1 down-regulation.

Other vacuole or endomembrane proteins may be important for the transport of proteins that interact with, or support the function of, TORC1 and EGO on the vacuolar membrane.

Yet other proteins in this group may be required nutrient transport and storage, and thus deleting them could lead to changes in TORC1 and cell growth signaling. In fact, Cardenas and coworkers have already shown that disruption of the CORVET and HOPS complexes--complexes also identified in our study--cause partial inactivation of TORC1 signaling during log phase growth by inhibiting the activation of the EGO complex members Gtr1/2 (ZURITA-MARTINEZ et al. 2007). This constitutive TORC1 repression may then desensitize the TORC1 pathway to inhibition by osmotic stress (Fig. S3).

(2) The NSR1 regulation network contains at least 24 proteins involved in chromatin silencing, 6 proteins involved in general transcription, and 9 other DNA binding proteins (Table 3). Six of these proteins are subunits of the Class I HDAC Rpd3L--a complex that deacetylates the nucleosomes in Ribi gene promoters whenever TORC1 is inactivated (HUMPHREY et al. 2004; HUBER et al. 2011). However, the other proteins identified in this group have not been linked to Ribi gene regulation previously. Some of these proteins probably cooperate with Rpd3L to

inactivate NSR1 in stress--this is almost certainly the case for the histone H3 and H2A proteins--but others may simply regulate the transcription of critical proteins in the stress response network.

(3) The NSR1 regulation network also contains 17 ribosomal and ribosome associated proteins, and four translation factors (Table 3). Although it is unclear how these proteins interact with the Ribi gene control network, it is well established that blocking translation using the drug cycloheximide triggers hyperactivation of TORC1 (HARA et al. 1998; BEUGNET et al. 2003; URBAN et al. 2007). It therefore seems likely that deletion of at least some of the proteins found in this group will have a similar indirect effect on TORC1 activity by inhibiting translation.

On top of the three major groups listed above, we also found three proteins known to play a role in PKA signaling (Ira2, Gpb1 and Gpr2) in our core 440 gene network, and two others (Pde1 and Pde2) that just missed the log2>1.0 cutoff (Table S1). Four of these proteins (Ira2, Gpb1, Pde1 and Pde2) are involved in limiting PKA pathway activity (BROACH 2012)--suggesting that hyperactivation of the PKA pathway helps compensate for TORC1 inactivation in osmotic stress. Proteins that indirectly limit PKA pathway activity may also be part of the NSR1 regulation network.

Putting the groups of proteins listed above together with the myriad other proteins required for NSR1 repression in stress (listed in Table S1) it is clear that the Ribi, and thus cell growth control, network is highly complex. Over seven percent of the genome (440/5820 genes) is required for proper signaling in osmotic stress conditions alone. Therefore, numerous follow up experiments

will be needed to determine how such a large array of proteins contributes to the osmotic stress response. In this respect, we hope that our screen will serve as a resource that helps guide others toward key proteins and pathways in cell growth control, but remind the reader that some of our data may be misleading as many strains in the YKO collection carry mutations beyond the annotated deletion (HUGHES et al. 2000; TENG et al. 2013; GIAEVER AND NISLOW 2014).

The data presented in this paper also demonstrate the power of our new method for mapping gene regulatory circuits in yeast (and potentially other organisms). It is highly quantitative, reproducible, and works well even when the resulting gene expression changes are short lived or involve a dramatic reduction in mRNA levels. Furthermore, the method can (at least in principle) be adapted to map the regulators of any gene, simply by altering the primers/probes used in the qPCR step.

2.6 FIGURES

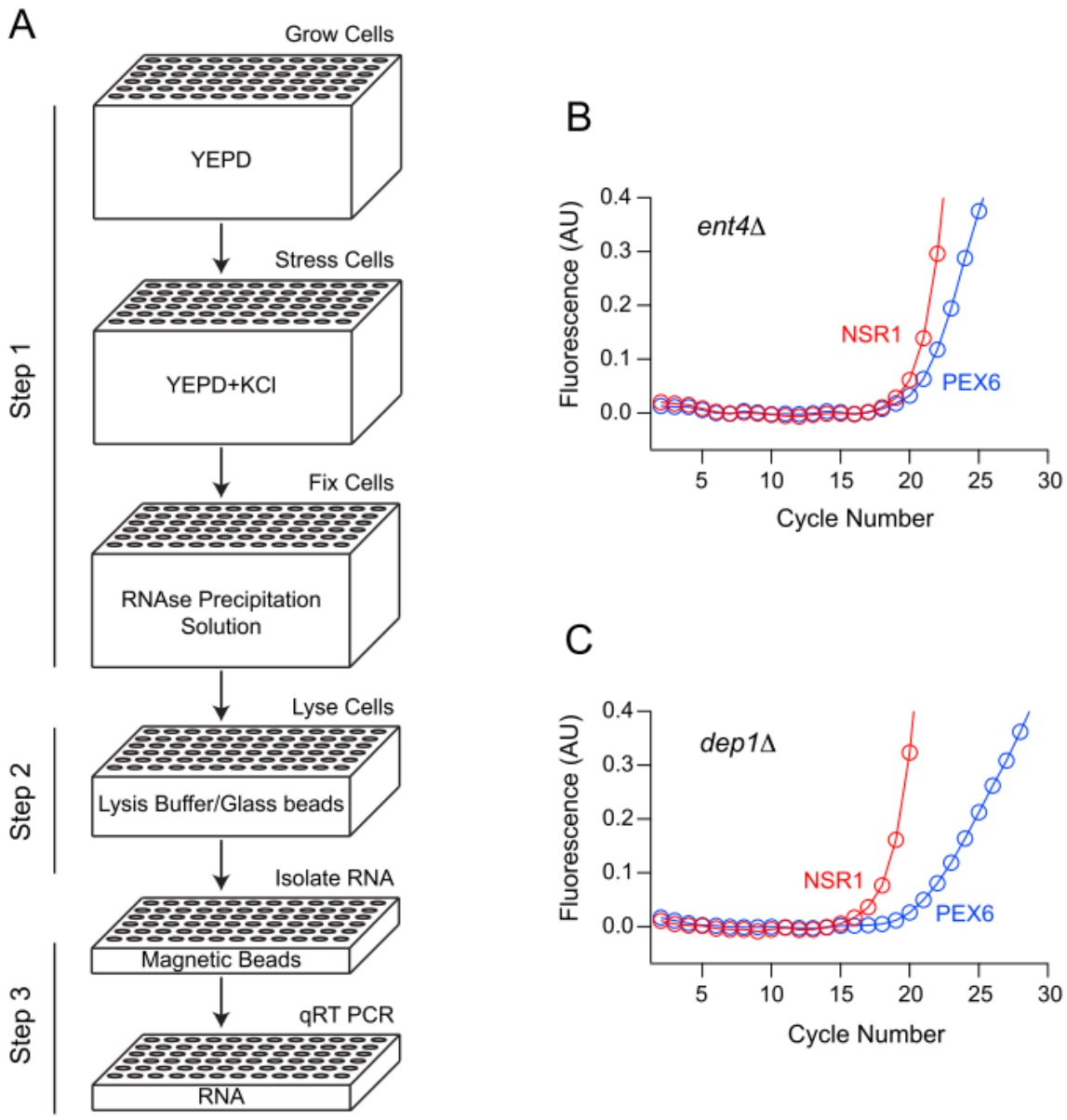

Figure 1. Automated analysis of gene expression in yeast. (A) Strains from the Yeast Knock Out (YKO) collection were inoculated into a 96-well plate containing YEPD medium and grown to an

OD600 of 0.6 in a Biomek FX robot with an integrated Liconic shaking incubator. The plates were then brought onto the deck of the robot, treated with 0.4M KCl, rapamycin, or mock stress, and returned to the incubator. After 20min the plates were retrieved again but this time treated with 4M NH4SO4 (pH 4.6) to block all further RNA synthesis and degradation. Cells were then lysed by bead-beading, and the RNA purified from each well using magnetic beads and loaded into a PCR plate for analysis. (B and C) Duplex quantitative PCR was used to measure the expression of the Ribi gene NSR1 (FAM labeled probe; red) and the housekeeping gene PEX6 (JOE labeled probe; blue) in each well of the plate from the library. In most strains (such as ent4Δ from plate 1) NSR1 and PEX6 expression levels were similar. However, we also found numerous strains (such as dep1Δ from plate 1) with higher levels of NSR1 than PEX6. Quantitation of these data using standard procedures (see Methods) then led to a NSR1/PEX6 ratio for each sample (log2 = -2.8 for dep1Δ and -0.1 for ent4Δ).

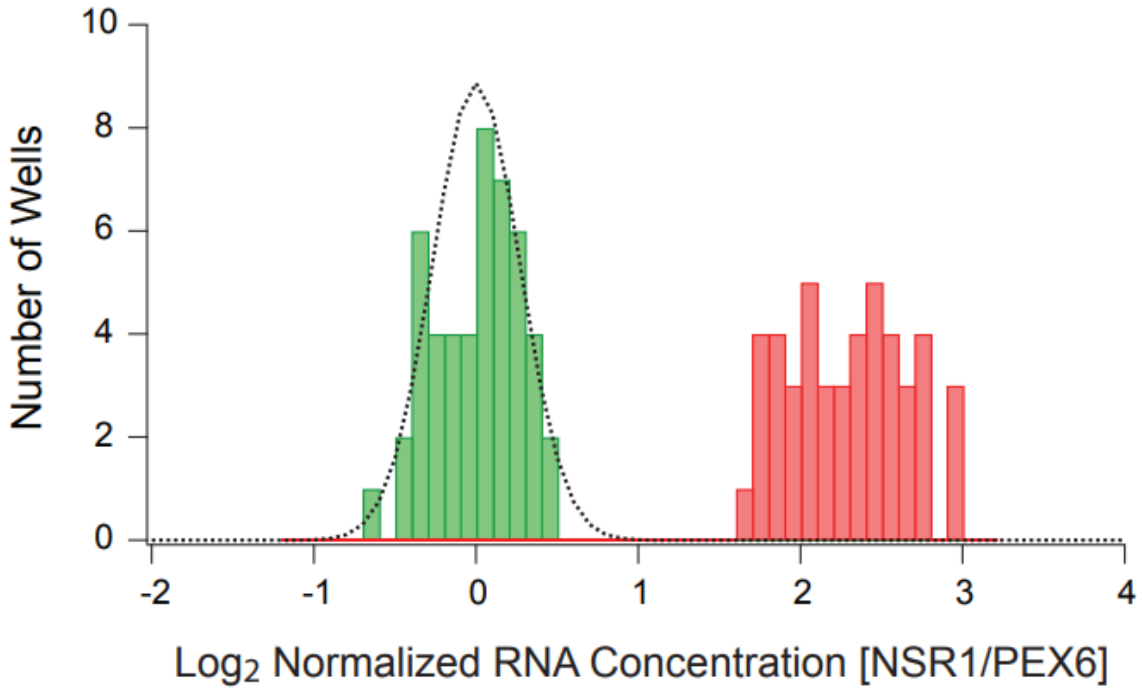

Figure 2. NSR1 expression levels during log growth and 0.4M KCl stress. Histogram showing the distribution of NSR1/PEX6 expression ratios for wild-type cells grown on a single plate and then treated with 0.4M KCl (48 samples, green) or mock stress (48 samples, red). The data was normalized (by adding a single constant to all 96 log NSR1/PEX6 ratios) so that the average signal in stress is 0.0. The dotted line shows the fit to a normal distribution with a standard deviation of 0.26 and an average of 0.0.

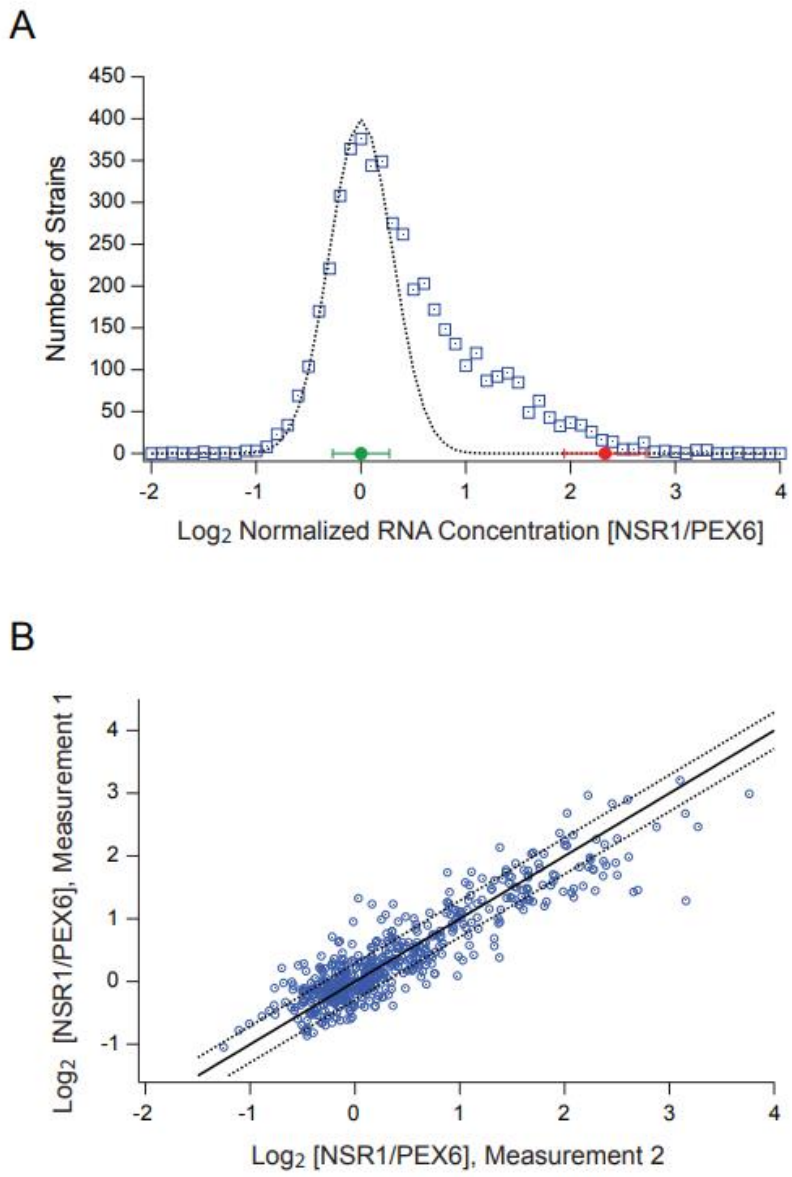

Figure 3. NSR1 expression levels for 4709 strains in the yeast knockout collection. (A) Histogram showing the number of strains in the yeast knockout library with log2 NSR1/PEX6 expression ratios ranging from -2 to 4 in 0.1 increment bins. All data was normalized to set the average expression ratio, minus the outliers, to 0.0 (see Methods). The green point and bar show the average and standard deviation of the NSR1/PEX6 ratio for the wild-type strain in stress (from

Fig. 3). The red point and bar shows the average and standard deviation of the NSR1/PEX6 ratio for the wild-type strain in mock stress (from Fig. 3). The dotted line shows the fit to a normal distribution with an average signal of 0.0 and a standard deviation of 0.30 (B) Scatter plot showing the normalized NSR1/PEX6 expression values for 560 strains run through the automated pipeline on two separate weeks (usually more than a month apart). The solid line show the trend expected if there was a perfect correlation between datasets, the dotted line show the range expected for values that fall one standard deviation (0.3 log2 units) above or below this line.

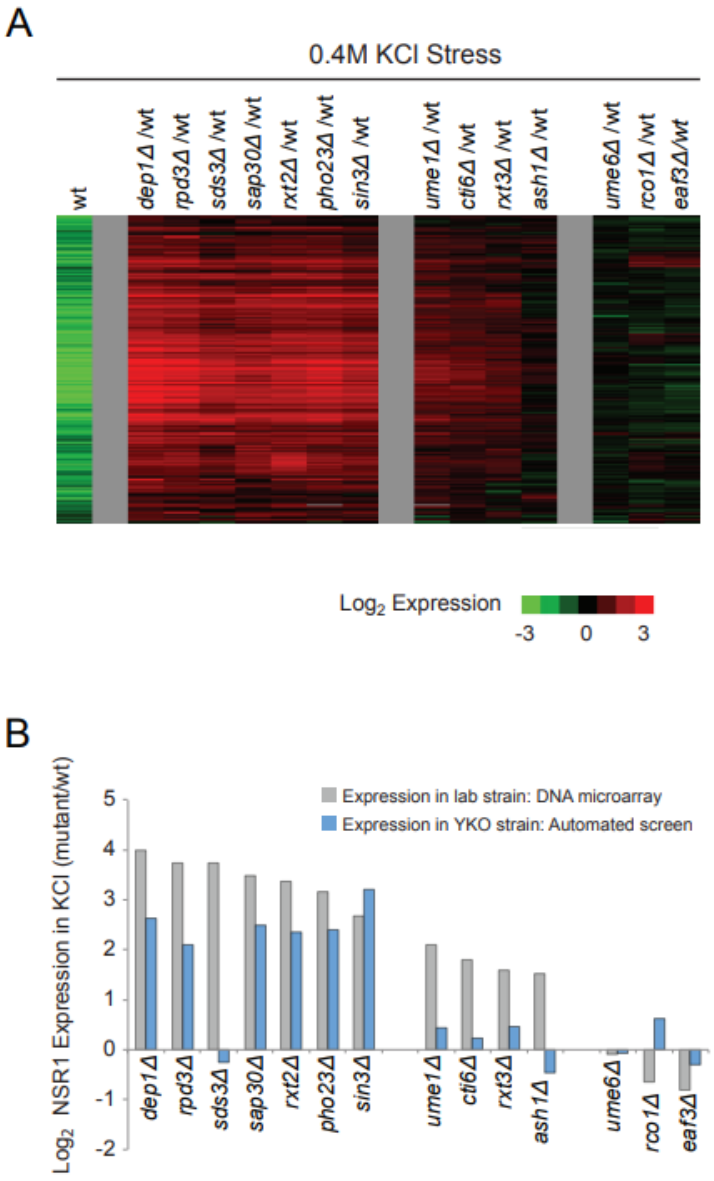

Figure 4. Rpd3L dependent gene expression in osmotic stress conditions. (A) DNA microarrays were use to measure the expression of Ribi genes after 20 min of 0.4M KCl stress in the wild type strain (Column 1) and mutants missing all 14 subunits in the Rpd3L and Rpd3S complexes (Columns 2-15). In the experiment with the wild-type strain, we compared the cDNA from cells treated with stress (labeled with Cy5; red) to the cDNA from cells harvested prior to stress (labeled

with Cy3; green). In experiments with the mutant strains we compared cDNA from the mutant treated with stress (labeled with Cy5; red) to cDNA from the wild-type strain treated with stress (labeled with Cy3; green). Thus, the green bars in the first column show Ribi genes that are repressed in osmotic stress, while the red bars in each subsequent column show the genes that are hyper expressed in stress. (B) Graph showing the change in NSR1 expression caused by deletion of each subunit in Rpd3L/S as measured by DNA microarray analysis of strains made in the W303 background (grey bars) and the automated analysis of the YKO collection (blue bars).

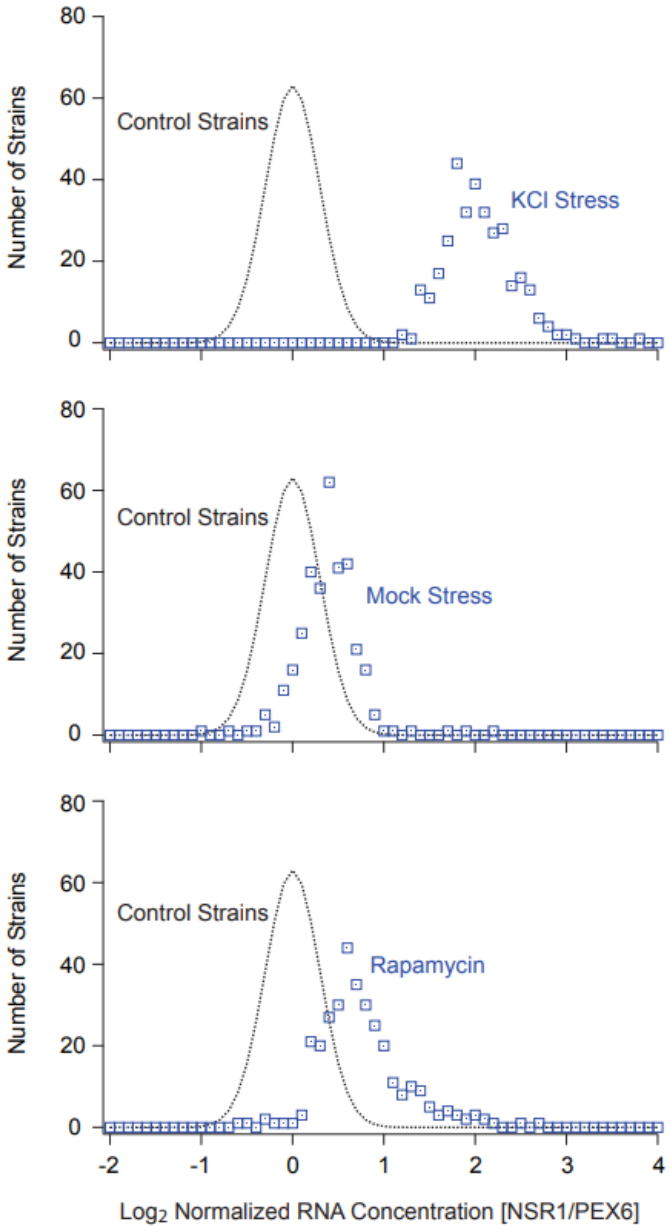

Figure 5. NSR1 expression levels in KCl, mock stress and rapamycin. The top 332 strains in the screen were analyzed to measure the NSR1/PEX6 ratio after 20min in 0.4M KCl stress (upper panel), mock stress conditions (middle panel), or 200nM Rapamycin (lower panel). In all of these experiments the 332 strains were distributed across four 96-well plates, together with 48 strains

from the center of the peak in the original screen. The average NSR1/PEX6 expression level in these control strains was set to 0.0 in each experiment. Strains with defects in repressing NSR1 expression in each condition should therefore have log2 NSR1/PEX6 expression ratios >1.0. The dotted lines show a normal distribution with an average and standard deviation of 0.0 and 0.3 for reference.

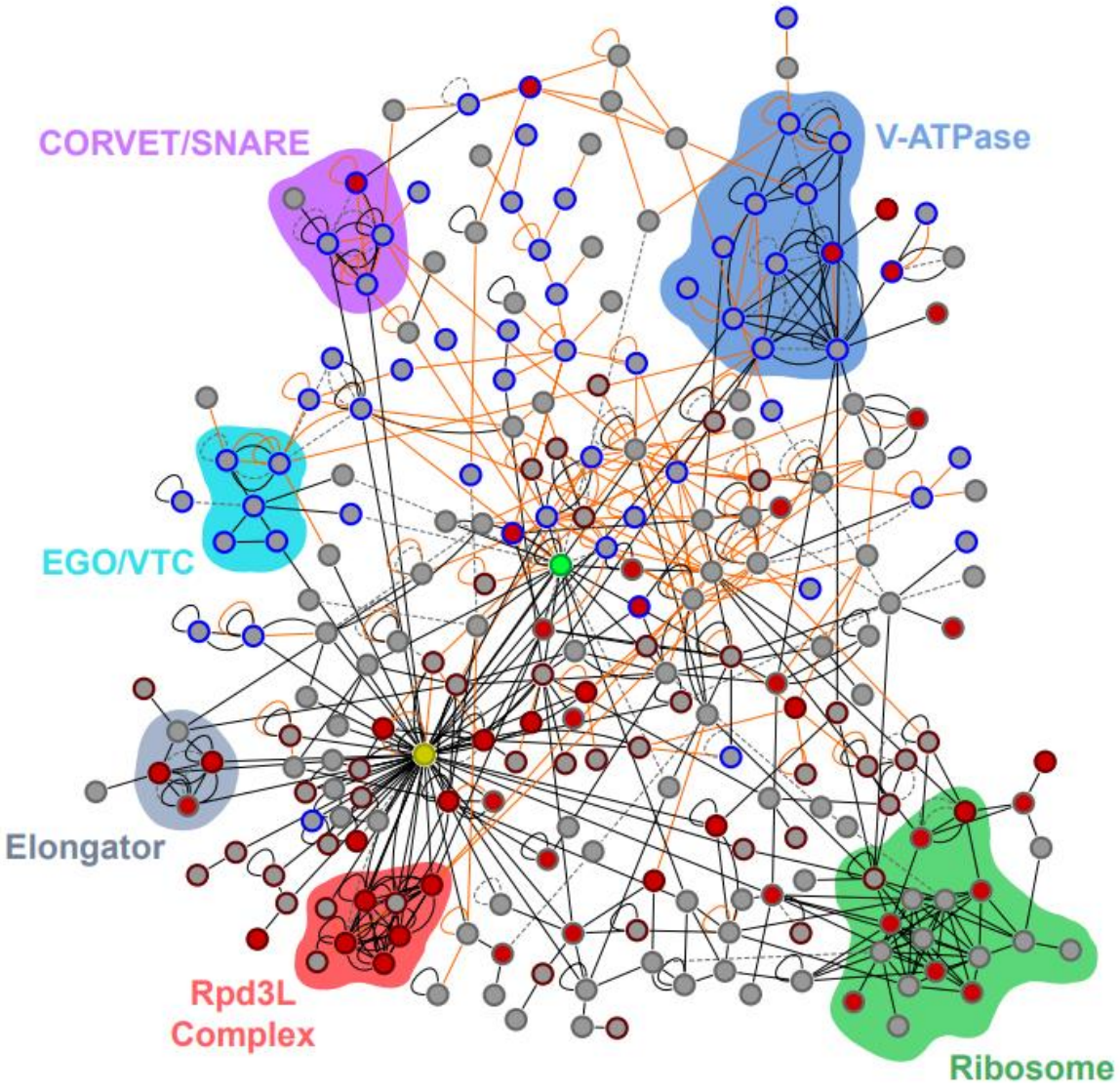

Figure 6. Physical interaction map for genes involved in stress regulated growth control. The network map drawn using Cytoscape (SHANNON et al. 2003) shows physical interactions between the 440 proteins required for robust NSR1 repression in stress, along with TORC1 for reference. Each node shows a single protein, and each edge a single physical interaction from BioGRID (STARK et al. 2006) colored black if it represents affinity capture or reconstituted complex data; orange if it represents two-hybrid or protein-fragment complementation data; and

dotted grey if it represents FRET, biochemical activity, co-purification, or other types of data. The center of each node is colored red if deletion of the protein causes a defect in rapamycin dependent down-regulation of NSR1 (log2>1)--and therefore acts downstream of TORC1--and grey if it does not. Node edges are colored maroon if the protein is the nucleus and blue if it localizes to the endomembrane system or vacuole. The green node is TORC1 and the yellow node Hht1/2. Colored regions highlight key complexes discussed in the text and listed in Tables 1-3. Only proteins with one or more physical interaction (250 in total) are shown in this figure. The highly connected protein chaperones Ssa1 and Ssb1, the RNA binding protein Slf1 and all genes that only connected to them are removed from the network for clarity. The Cytoscape file containing the full network, and all relevant information, is included in the supplementary materials.

2.7 TABLES

Name	Description	Loc	[NSR1]	Down TOR	Phys Net
VMA1	Subunit A of the V1 peripheral membrane domain of V-ATPase	V	2.2	NO	YES
VMA2	Subunit B of V1 peripheral membrane domain of vacuolar H+-ATPase	V	2.3	YES	YES
VMA3	Proteolipid subunit c of the V0 domain of vacuolar H(+)-ATPase	V	1.9	NO	YES
VMA5	Subunit C of the V1 peripheral membrane domain of V-ATPase	V	2.2	NO	YES
VMA6	Subunit d of the V0 integral membrane domain of V-ATPase	V	2.1	NO	YES
VMA8	Subunit D of the V1 peripheral membrane domain of V-ATPase	V	2.1	NO	YES
VMA11	Vacuolar ATPase V0 domain subunit c'	V	1.5	NO	YES
VMA16	Subunit c" of the vacuolar ATPase	V	1.9	NO	YES
VMA21	Integral membrane protein required for V-ATPase function	ER	1.5	NO	YES
VMA22	Protein that is required for vacuolar H+-ATPase (V-ATPase) function	ER	1.9	NO	YES
PKR1	V-ATPase assembly factor	ER	1.9	NO	YES
SLM4	Component of the EGO and GSE complexes	V	3.7	NO	YES
MEH1	Component of the EGO and GSE complexes	V	1.5	NO	YES
VTC1	Subunit of the vacuolar transporter chaperone (VTC) complex	ER/V	1.4	NO	YES
VTC4	Vacuolar membrane polyphosphate polymerase	ER/V	2.3	NO	YES
GAP1	General amino acid permease	V	1.9	NO	YES
SYN8	Endosomal SNARE related to mammalian syntaxin 8		1.8	NO	YES
VAM3	Syntaxin-like vacuolar t-SNARE	V	2.6	NO	YES
VAM7	Vacuolar SNARE protein	V	2.4	NO	YES
YPT7	Rab family GTPase	V	2.5	YES	YES
PEP5	Histone E3 ligase, component of CORVET membrane tethering complex	V	1.9	NO	YES
RCR1	Involved in chitin deposition; may function in endosomal-vacuolar trafficking	ER	2.0	NO	NO
YOP1	Membrane protein that interacts with Yip1p to mediate membrane traffic	ER	1.7	NO	YES
GYP5	GTPase-activating protein (GAP) for yeast Rab family members	G	1.8	NO	YES
RGP1	Subunit of a Golgi membrane exchange factor (Ric1p-Rgp1p)	G	1.4	NO	NO
SYS1	Integral membrane protein of the Golgi	G	1.8	NO	YES
TVP15	Integral membrane protein; localized to late Golgi vesicles	G	1.8	NO	YES
TVP38	Integral membrane protein; localized to late Golgi vesicles	G	1.9	NO	YES
VPS52	Component of the GARP (Golgi-associated retrograde protein) complex	G	1.3	NO	NO
YIP5	Protein that interacts with Rab GTPases; localized to late Golgi vesicles	G	1.6	NO	YES
EMP70	Endosome-to-vacuole sorting	V	1.6	NO	YES
SNX4	Sorting nexin; involved in the retrieval of late-Golgi SNAREs	Endo	2.0	NO	YES
SNX41	Sorting nexin; involved in the retrieval of late-Golgi SNAREs	Endo	2.0	NO	YES
VFA1	Protein that interacts with Vps4p and has a role in vacuolar sorting	Endo	1.8	NO	YES
VPS5	Nexin-1 homolog; moves proteins from endosomal compartment to Golgi	Endo	1.7	NO	YES
PFA3	Palmitoyltransferase for Vac8p	V	2.4	NO	YES
VAC8	Phosphorylated and palmitoylated vacuolar membrane protein	V	2.9	NO	YES
LST4	Protein possibly involved in a post-Golgi secretory pathway		2.7	YES	NO
EDE1	Scaffold protein involved in the formation of early endocytic sites		1.6	NO	YES
ENT2	Epsin-like protein required for endocytosis and actin patch assembly		1.8	NO	YES
KIN2	Serine/threonine protein kinase involved in regulation of exocytosis		1.7	?	YES
VAB2	Subunit of the BLOC-1 complex involved in endosomal maturation		2.4	?	YES

MDR1	Cytoplasmic GTPase-activating protein; regulation of Golgi secretory function		2.4	NO	NO
APL4	Gamma-adaptin	Endo	1.8	NO	YES
APM1	Mu1-like medium subunit of the AP-1 complex	G	1.8	NO	YES
CHC1	Clathrin heavy chain		1.5	?	YES
DYN1	Cytoplasmic heavy chain dynein		1.7	?	YES

Table 1. Vacuolar, endomembrane and vesicle trafficking genes required for the down regulation of the Ribi gene NSR1 in stress. The top three groups of genes encode proteins highlighted in the top portion of the physical interaction network shown in Fig. 7; V-ATPase, EGO/VTC and CORVET/SNARE respectively. The fourth group lists other genes found in our screen encoding vacuolar, vesicle transport of endomembrane proteins. The third column (Loc) lists the localization of each protein; V is vacuole, ER is endoplasmic reticulum, G is Golgi, and Endo is other parts of the Endomembrane system. The fourth column [NSR1] lists the log2 NSR1/PEX6 expression ratio from the screen. The fifth column notes if the gene acts downstream of TORC1 (has log2 >1 normalized NSR1/PEX6 ratio in rapamycin). The sixth column (Phys Net) states whether the genes is part of the physical interaction network shown in Fig. 6.

Name	Description	Loc	[NSR1}	Down TOR
VAC8	Vacuolar membrane protein; CVT pathway	C	2.9	YES
GYP5	GTPase-activating protein for Rab proteins; ER to Golgi transport	C	1.8	NO
DAL82	Positive regulator of allophanate inducible genes	N	2.6	NO
FMP48	Protein kinase	C/M	1.7	NO
KDX1	Protein kinase	M	1.5	NO
NNK1	Protein kinase	C	1.8	NO
SAP185	Protein that forms a complex with the Sit4p protein phosphatase	C/M	1.9	YES
POP2	RNase of the DEDD superfamily	C	1.4	YES
TIF1	Translation initiation factor eIF4A	C	1.6	?
MRPS17	Mitochondrial ribosomal protein of the small subunit	C	1.5	?
GAS1	Beta-1,3-glucanosyltransferase	C/M/N	1.1	?
HXT2	High-affinity glucose transporter of the major facilitator superfamily		1.9	?
ICL1	Isocitrate lyase	C	2.1	NO
SAC6	Fimbrin, actin-bundling protein	C	1.8	NO
TPO3	Polyamine transporter of the major facilitator superfamily	C	1.7	?
YKU80	Subunit of the telomeric Ku complex (Yku70p-Yku80p)	N	1.5	?
YLR108C	Protein of unknown function	N	1.8	YES

Table 2. Proteins required for the downregulation of the Ribi gene NSR1 in stress that physically interact with TORC1. The third column (Loc) lists the localization of each protein; C is cytosol, M is membrane, N is nucleus. The fourth column [NSR1] lists the log2 NSR1/PEX6 expression ratio from the screen. The fifth column notes if the gene/protein acts downstream of TORC1 (has log2 >1 normalized NSR1/PEX6 ratio in rapamycin). A question mark means that the protein/gene was not analyzed in the rapamycin subscreen.

Name	Description	Loc	[NSR1]	Down TOR	Ph Net
ELP3	Subunit of Elongator complex	N	2.8	YES	YES
ELP6	Subunit of Elongator complex		1.8	YES	YES
IKI3	Subunit of Elongator complex	N	1.8	YES	YES
VHS1	Cytoplasmic serine/threonine protein kinase		2.5	NO	YES
RPD3	Histone deacetylase, component of Rpd3S and Rpd3L	N	2.1	NO	YES
SIN3	Component of Rpd3S and Rpd3L	N	2.6	YES	YES
PHO23	Component of Rpd3L	N	2.4	YES	YES
SAP30	Component of Rpd3L	N	2.2	YES	YES
DEP1	Component of the Rpd3L	N	2.6	YES	YES
RXT2	Component of Rpd3L	N	2.4	YES	YES
HOS1	Class I histone deacetylase	N	1.9	NO	YES
STB4	Putative transcription factor	N	2.4	NO	YES
RPS6A	Protein component of the small (40S) ribosomal subunit	R	2.4	YES	YES
RPS7B	Protein component of the small (40S) ribosomal subunit	R	1.4	YES	YES
RPS9A	Protein component of the small (40S) ribosomal subunit	R	1.9	NO	YES
RPS22A	Protein component of the small (40S) ribosomal subunit	R	1.4	NO	YES
RPS17A	Protein component of the small (40S) ribosomal subunit	R	2.4	YES	YES
RPL2B	Ribosomal 60S subunit protein L2B	R	1.3	NO	YES
RPL6A	Ribosomal 60S subunit protein L6A	R	2.1	NO	YES
RPL6B	Ribosomal 60S subunit protein L6B	R	2.6	YES	YES
RPL7A	Ribosomal 60S subunit protein L7A	R	2.1	NO	YES
RPL13A	Ribosomal 60S subunit protein L13A	R	1.8	NO	YES
RPL16B	Ribosomal 60S subunit protein L16B	R	1.8	NO	YES
RPL22A	Ribosomal 60S subunit protein L22A	R	1.9	NO	YES
RPL24A	Ribosomal 60S subunit protein L24A	R	2.0	YES	YES
SSZ1	Hsp70 protein that interacts with Zuo1p (a DnaJ homolog)		2.0	YES	YES
ZUO1	Ribosome-associated chaperone	R/N	1.9	YES	YES
NOP12	Nucleolar protein involved in pre-25S rRNA processing	N	2.1	NO	YES
RQC1	Component of the ribosome quality control complex (RQC)	R	2.0	NO	YES
RPL38	Ribosomal 60S subunit protein L38	R	2.0	YES	NO
RPL43B	Ribosomal 60S subunit protein L43B	R	1.6	NO	NO
RPS27A	Protein component of the small (40S) ribosomal subunit	R	2.1	NO	NO
CLU1	Subunit of the eukaryotic translation initiation factor 3 (eIF3)		2.3	YES	YES
EFT1	Elongation factor 2 (EF-2), also encoded by EFT2	R	1.6	NO	YES
TIF1	Translation initiation factor eIF4A	R	1.6	NO	YES
YGR054W	Eukaryotic initiation factor (eIF) 2A	R	2.2	NO	YES
CAF20	Phosphoprotein of the mRNA cap-binding complex		2.0	NO	YES
ASK10	Component of RNA polymerase II holoenzyme	N	2.4	NO	YES
CAF130	Subunit of the CCR4-NOT transcriptional regulatory complex		1.6	NO	YES
ELA1	Elongin A; Required for Pol II degredation	N	2.6	NO	YES
ELC1	Elongin C; Required for Pol II degredation	N	1.5	NO	YES
PGD1	Subunit of the RNA polymerase II mediator complex	N	2.0	NO	YES
NUT1	Component of the RNA polymerase II mediator complex	N	1.7	NO	YES
GIS1	Histone demethylase and transcription factor	N	1.7	NO	YES
HIR2	Subunit of HIR nucleosome assembly complex	N	2.0	NO	YES
HIR3	Subunit of the HIR complex	N	2.5	NO	YES
HPA2	Tetrameric histone acetyltransferase		1.9	NO	YES
HTA1	Histone H2A	N	2.4	YES	YES

IES4	Component of the INO80 chromatin remodeling complex	N	1.8	YES	YES
ITC1	Subunit of Isw2p-Itc1p chromatin remodeling complex	N	1.6	NO	YES
DPB4	Subunit of ISW2 chromatin accessibility complex	N	2.0	NO	YES
JHD2	JmjC domain family histone demethylase	N	2.2	YES	YES
RLF2	Largest subunit (p90) of the Chromatin Assembly Complex (CAF-1)	N	2.5	YES	YES
SAS5	Subunit of the SAS complex (Sas2p, Sas4p, Sas5p)	N	2.2	NO	YES
SWI3	Subunit of the SWI/SNF chromatin remodeling complex	N	2.5	YES	YES

Table 3. Ribosomal and nuclear genes required for the down regulation of the Ribi gene NSR1 in stress. The top three groups of genes encode proteins highlighted in the bottom portion of the physical interaction network shown in Fig. 7; VElongator, Rpd3L and Ribosome respectively. Note that three ribosomal proteins not connected to the others by physical interactions were included in the list. The fourth group lists other genes found in our screen involved in transcription and chromatin remodeling, all of which are part of the lower half of the physical interaction network in Fig. 7. The third column (Loc) lists the localization of each protein; R is ribosome, N is nuclear. The fourth column [NSR1] lists the log2 NSR1/PEX6 expression ratio from the screen. The fifth column notes if the gene acts downstream of TORC1 (has log2 >1 normalized NSR1/PEX6 ratio in rapamycin). The sixth column (Phys Net) states whether the genes is part of the physical interaction network shown in Fig. 6.

2.8 SUPPLEMENTAL FIGURES AND METHODS

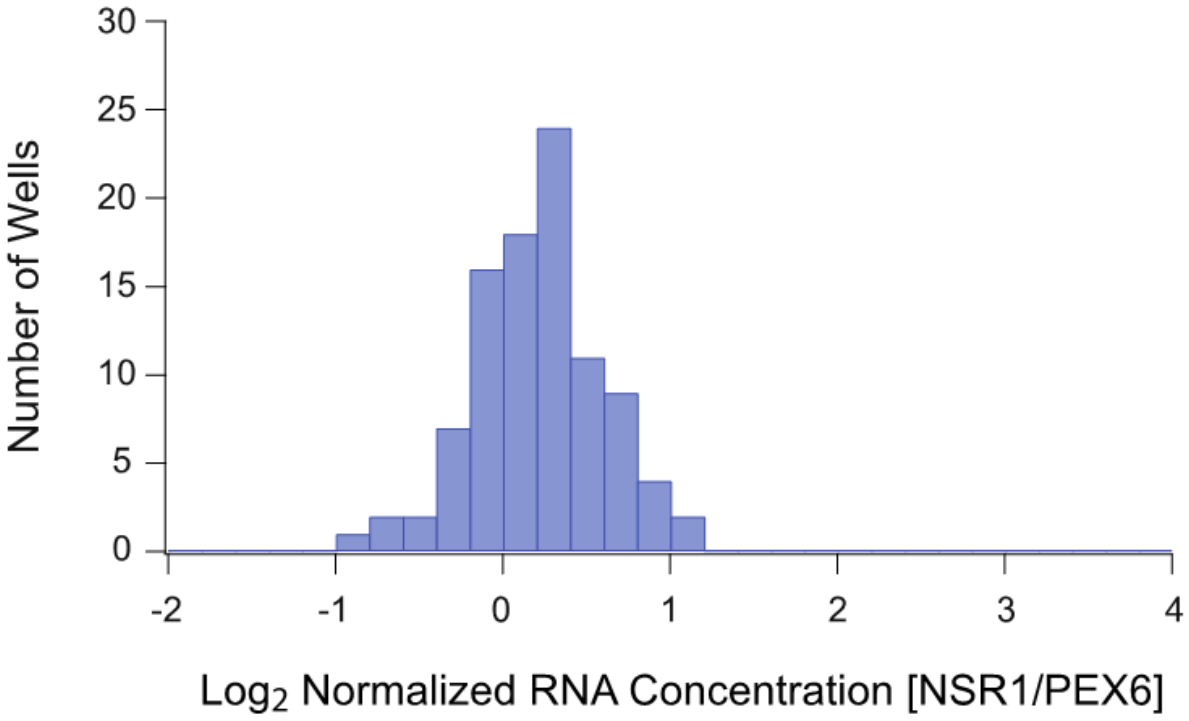

Figure S1. NSR1 expression levels during log growth. Histogram showing the distribution of NSR1/PEX6 expression ratios for wild-type cells grown on a single 96-well plate and then treated with mock stress (YEPD medium). The data was normalized (by adding a single constant to all 96 log NSR1/PEX6 ratios) so that the average signal in stress is 0.0. The standard deviation for the 96 measurements of NSR1/PEX6 expression is log2 = 0.37.

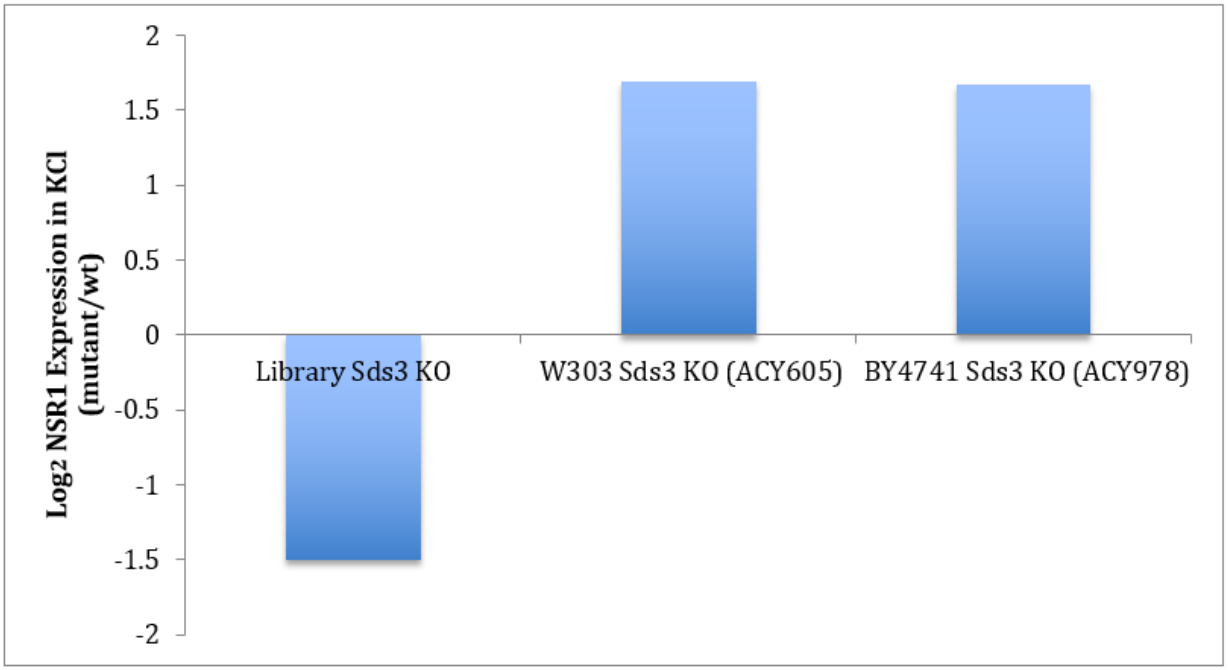

Figure S2. Graph showing the change in NSR1/PEX6 expression caused by deletion of Sds3 in the W303 background (ACY605 strain used in microarray analysis), the BY4741 background used in the YKO collection (ACY978), and the sds3Δ strain from the YKO collection. Each bar shows the expression level compared to that found in the wild-type strain (both 20min after treatment with 0.4M KCl), as measured by qPCR (Methods). In this experiment cells were grown and harvested as described for the DNA microarray experiments but the mRNA was purified using a RiboPure RNA purification kit (Ambion).

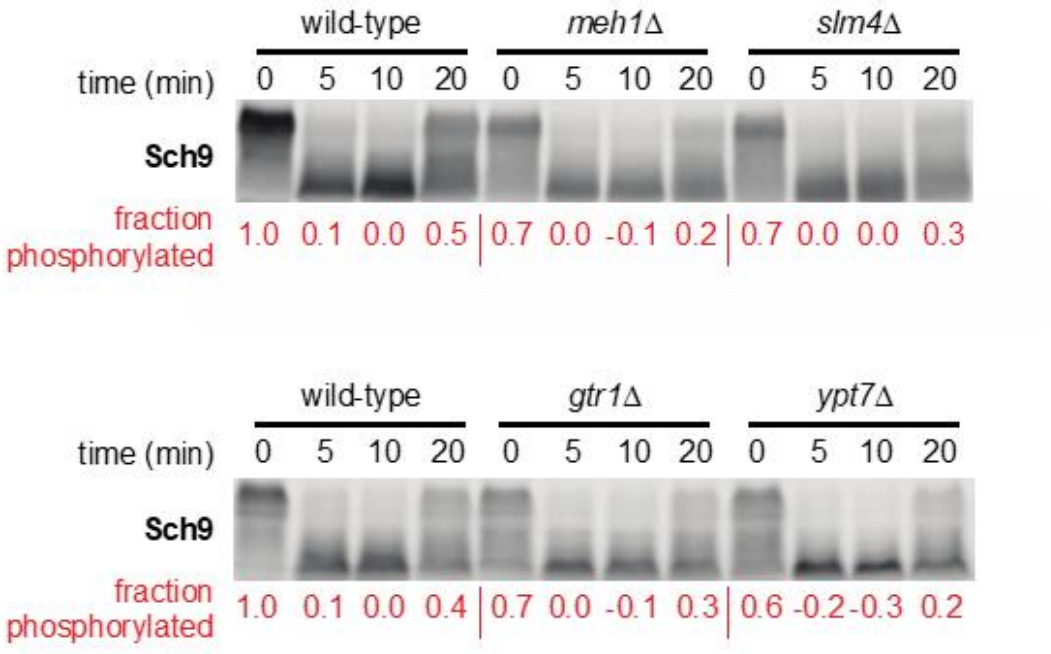

Figure S3. Deletion of the EGO complex components Slm4, Meh1 and Gtr1 causes constitutive repression of TORC1. TORC1 activity was measured by following Sch9 phosphorylation during growth in YEPD medium (time=0) and then 5, 10 and 20 min after treatment with 0.4M KCl stress, using a bandshift assay developed by Loewith and coworkers (URBAN et al. 2007). The protein mobility shift data was quantified using a custom MATLAB script as described in (HUGHES HALLETT et al. 2014) and normalized so that the wild-type values are 1.0 at time=0 min, and 0.0 at time=10 min (red numbers). The data show that deletion of Slm4, Meh1 and Gtr1 all cause a 30% decrease in Sch9 phosphorylation in YEPD medium. This may explain why the slm4Δ, meh1Δ and gtr1Δ strains have significant defects in the osmotic stress screen (Table S1; gtr1Δ the log2=1.2 fold). Specifically, constitutive TORC1 repression may trigger feedback mechanisms that then limit TORC1 pathway repression in stress. However, if this is the case, the changes in

the TORC1 pathway must occur at a level below TORC1, as TORC1 dependent inhibition appears to be normal during osmotic stress in all three strains (values ranging from 0.0 to -0.1 at time=10 min). We also found a constitutive TORC1 signaling defect in the strain missing Ypt7--a protein involved in vacuolar function but not thought to regulate EGO or TORC1 (BINDA et al. 2009). Thus, Slm4, Meh1, Gtr1 and/or Ypt7, may also block NSR1 inhibition in stress by disrupting vacuolar function (see Discussion). Note that other gene deletions, and mutations that lock Gtr1/2 in their active state, do not influence TORC1 signaling in osmotic stress (HUGHES HALLETT et al. 2014).

SUPPLEMENTAL METHODS

Program I (Grow, Stress, and Harvest)

The operator loads 1-8 sets of barcoded plates into the Biomek. Each set includes: one overnight culture plate, one 2.2 ml square well plate with 550ul of YEPD and a sterile 3.2mm stainless steel mixing bead in each well (media plate), two 2.2 ml square well plates containing 850ul of RI buffer in each well (RI buffer plates), one 2.2ml square well plate containing 1.875M KCl or 1ug/ml rapamycin in YEPD in each well (stress plate; volume depends on the number of plates that are being processed), and one 300ul optical read plate. The media and stress plates are then transferred into the Liconic incubator (shaking at 1200rpm and 30C) while the RI buffer plates, overnight plate, and a set of P50 and P200 aerosol resistant tips are transferred into the Cytomat. Then, when the operator activates the inoculation routine, a barcode matched overnight culture, media, and optical read plate are moved to the deck of the robot (the media plate is loaded onto a peltier position on the deck and held at 30C). The yeast in the overnight culture plate is then resuspended

by pipetting 39ul up and down 6 times, and 6ul of culture is transferred into the media plate and mixed by pipetting 39ul up and down six more times. The media plate is then moved from the peltier position to an orbital shaker, vortexed at 900rpm for 20s, and moved back to the peltier position. 250ul of culture is then transferred into the optical read plate (using two steps with P200 tips) and the OD600 read by the operator. Once the OD is read the cultures are transferred back from the optical read plate into the media plate and all of the plates returned to the incubator. The last transfer (from the optical read plate to media plate) uses a custom pipetting template to ensure that yeast are removed from the edge of each well. Specifically, the transfer volumes were split in 40 aspirations, each of which is shifted 10 degrees around the perimeter of the well. The inoculation steps are then repeated for up to seven additional sets of plates (at intervals chosen by the operator, usually 1hr).

During cell growth, the operator is able to read the OD of any plate in the robot. Here again, the operator activates a routine where the media plate is moved to a peltier position on the deck of the robot (held at 30C), 250ul of culture is transferred to the optical read plate, the OD600 read, the cultures transferred back to the media plate, and then all plates are moved back into the Liconic incubator. In general, the OD600 was read 2-3 times after the initial inoculation, so that we could accurately predict the time-point at which cells reach an OD600 of 0.6.

Once the cells reached an OD600 of 0.6, the stress treatment routine is activated. First, the media plate and salt stress (or rapamycin) plates are retrieved from the incubator and the RI buffer plates and P200 tips are retrieved from the Cytomat. Then, 150ul of culture is transferred from the media

plate to the first RI buffer plate, and mixed by aspirating 150ul from 1mm above the bottom of the plate and dispensing it again at 15mm above the bottom of the plate, at 100ul/s for 2 min. 100ul of YEPD containing KCl or rapamycin is then transferred from the stress plate to the media plate using a moving dispense step, starting at the bottom of the plate and ascending to 14.5mm above the bottom at 75ul/s, followed by three 25ul mixes at 100ul/s, and the samples are shaken at 900rpm for 10s and returned to the incubator. Approximately 19min later the media plate is moved back to peltier position on the deck and 150ul of culture transferred to the second RI buffer plate (as described above). The plates containing cells in RI buffer were then stored at -20C.

Program II (Aspirate RI Buffer and resuspend cells in Lysis Buffer)

After the yeast in RI buffer are thawed by centrifugation they are loaded into the Biomek along with a plate containing 400ul lysis buffer and 300ul zirconia beads. Then, the RI buffer is removed from each plate, 150ul at a time (using a P200 tip). During this aspiration step the tip is placed 1mm above the bottom of the well, off center by 80% of the well diameter, and the liquid removed at 20ul/s to ensure that the cell pellet remains intact. RI buffer is then dispensed into a position on the deck loaded with a plate shaped funnel made using a 3D printer (that transfers the liquid to a beaker so that a reservoir does not have to be emptied multiple times during the program). Once the RI buffer is removed, the robot pauses and waits for a prompt from the user (to make sure they are ready to move the plate to the bead beater). Once activated, the robot then transfers 400ul of lysis buffer to the plates containing the cell pellet, moves the plate to the orbital shaker on the deck of the robot, and then performs a mixing loop four times. This mixing loop involves aspirating 150ul from 0.8mm above the bottom of the well at 90ul/s and dispensing the buffer at 2mm above the bottom of the well at 90ul/s, 3 times per loop, and then shakes the plate at 1000rpm for 10s.

At the end of the mixing procedure, 390ul of yeast in lysis buffer is transferred into the lysis plate containing glass beads, and immediately loaded into the bead beater by the operator. Once bead-beating is complete, the plates were centrifuged at 4C and then loaded back into the robot for RNA purification.

Program III (RNA Purification)

The operator loads 1-8 sets of barcoded plates into the Biomek (4 sets is the most that can processed in a single 12hr day) along with aerosol resistant P200 and P50 tips. Each set includes: the cell lysate plate, an empty RNA plate (rigid, full skirt, PCR plate), an empty binding reaction plate (rigid, full skirt, PCR plate), and an empty 2.2ml well waste plate. The lysate plates are then moved into the Liconic incubator (at 4C) and the remaining sets of plates and tips are moved into the Cytomat. The user then loads a reservoir containing elution buffer onto the peltier position, and reservoirs containing wash buffer 1, wash buffer 2, RNA rebinding buffer (1.5x wash buffer 1), a 700ul plate containing Turbo DNAse, a rigid PCR plate with MagMAX RNA isolation beads, and a magnetic stand (Ambion #AM10027) onto other positions on the deck. The Turbo DNAase was then moved to the Liconic incubator (at 4C). Note that we used a 3D printer to make a 1.8mm plate that sat over the pins on the magnetic stand. This lowered the position of the beads on the side of the tube so that we could elute the RNA in a lower volume.

Once the plates and reservoirs are loaded, the first lysate plate is moved to the deck, and 100ul of cell lysate is moved to the binding reaction plate using P200 tips. To avoid pulling glass beads into the tips the aspiration was done in 12 steps, each step involves: Aspirating 0.1x of the volume at 11.4 mm above the bottom of the well (at the level of the top of the beads) at 60 ul/s, pausing in place for 0.5s, and dispensing 0.02x of the volume at 80ul/s. After 12 cycles the robot aspirates

0.04X of the volume and then dispenses the liquid into the binding plate at 1mm above the bottom of the plate. 150ul of isopropanol is then added to the binding plate, and mixed for 1 minute by aspirating 150ul at 0.8mm above the bottom of the well at 80ul/s and dispensing 150ul at 3.5mm above the bottom of the well at 150ul/s. The robot then resuspends the magMAX binding beads by performing the following sequence 20 times using p50 tips:

- Aspirate 150ul at 1.2mm above the bottom of the well at 80ul/s
- Move the tip to 10mm above the bottom of the well on center
- Move the tip to 1.2mm off center (the side of the well) at 45 degrees (2 o'clock) and 10mm above the bottom of the well.
- (1) Dispense the volume at 150ul/s
- (2) Move the tip to 10mm above the bottom of the well on center
- (3) Aspirate 30ul at 1.2mm above the bottom of the well at 80ul/s
- (4) Move the tip to 10mm above the bottom of the well on center
- Move the tip to 1.2mm off center at 135 degrees (10 o'clock) and 10mm above the bottom of the well.
- Repeat steps 1-4 from above
- Move the tip to 1.2mm off center at 225 degrees (8 o'clock) and 10mm above the bottom of the well.
- Repeat steps 1-4 from above
- Move the tip to 1.2mm off center at 315 degrees (5 o'clock) and 10mm above the bottom of the well.

- Repeat steps 1-4 from above
- Dispense the volume at 150ul/s

The robot then transfers 20ul of the MagMAX bead slurry to each well in the binding plate. The robot then uses P200 tips to mix the isopropanol, lysate and beads for 7min. The pipetting sequence used is:

- Aspirate 150ul at 0.8mm above the bottom of the well at 80ul/s
- Move the tip to 10mm above the bottom of the well on center
- Move the tip to 1.2mm off center (the side of the well) at 45 degrees (2 o'clock) and 10mm above the bottom of the well.
- (1) Dispense the volume at 150ul/sec
- (2) Move the tip to 10mm above the bottom of the well on center
- (3) Aspirate 150ul at 0.8mm above the bottom of the well at 80ul/sec
- (4) Move the tip to 10mm above the bottom of the well on center
- Move the tip to 1.2mm off center at 135 degrees (10 o'clock) and 10mm above the bottom of the well.
- Repeat steps 1-4 from above
- Move the tip to 1.2mm off center at 225 degrees (8 o'clock) and 10mm above the bottom of the well.
- Repeat steps 1-4 from above
- Move the tip to 1.2mm off center at 315 degrees (5 o'clock) and 10mm above the bottom of the well.

- Repeat steps 1-4 from above
- Dispense the volume at 150ul/s
- Move the tip to 10 mm above the bottom of the well on center

The robot then moves the binding plate to the magnetic stand and pauses for 4min. The robot then moves the supernatant to the waste plate using the following pipetting steps and P200 tips:

- Aspirate 75ul at 0.9mm above the bottom of the well at 10ul/s
- Dispense 75ul at 1.2mm below the top of the well at 75% off center, 90 degrees (12 o'clock)
- Aspirate 75ul at 0.9mm above the bottom of the well at 10ul/s
- Dispense 75ul at 1.2mm below the top of the well at 75% off center, 90 degrees (12 o'clock)
- Aspirate 50ul in four parts at 20ul/s

• 12.5ul while descending from 1mm above the bottom of the well to -0.1mm above the bottom of the well (to be sure to push on the bottom of the well)

• Pause 50 ms

• 12.5ul while ascending from -0.1mm above the bottom of the well to 1mm above the bottom of the well

• Pause 50ms

• 12.5ul while ascending from 1mm above the bottom of the well to -0.1mm above the bottom of the well

• Pause 50ms

- 12.5ul while ascending from -0.1mm above the bottom to 1mm above the bottom
- Pause 50ms

o Dispense 50ul at 1.2mm below the top of the well at 75% off center, 90 degrees (12 o'clock)

Next, the robot removes the binding reaction plate from the magnetic stand and transfers 150ul of wash buffer 1 to the binding plate using a P200 tip and mixes the beads and buffer for 2min. During this, and other wash steps, we found that it is critical to dispense buffer at different points around the tube. In prototype versions of the protocol missing this step we got highly variable data due to beads sticking to the sides of some tubes. The pipetting sequence we used is:

o Aspirate 115ul at 0.8mm above the bottom of the well at 80ul/s

o Move the tip to 10mm above the bottom of the well on center

o Move the tip to 1.2mm off center (the side of the well) at 45 degrees (2 o'clock) and 10mm above the bottom of the well.

o (1) Dispense the volume at 150ul/s

o (2) Move the tip to 10mm above the bottom of the well on center

o (3) Aspirate 115ul at 0.8mm above the bottom of the well at 80ul/s

o (4) Move the tip to 10mm above the bottom of the well on center

o Move the tip to 1.2mm off center at 135 degrees (10 o'clock) and 10mm above the bottom of the well.

o Repeat steps 1-4 from above

- Move the tip to 1.2mm off center at 225 degrees (8 o'clock) and 10mm above the bottom of the well.
- Repeat steps 1-4 from above
- Move the tip to 1.2 mm off center at 315 degrees (5 o'clock) and 10mm above the bottom of the well.
- Repeat steps 1-4 from above
- Dispense the volume at 150ul/s
- Move the tip to 10mm above the bottom of the well on center

The robot then moves the binding reaction plate to the magnetic stand again, pauses for 2min, and then transfers the supernatant to the waste plate using the following pipetting steps and P200 tips:

- Aspirate 75ul at 0.9mm above the bottom of the well at 10ul/s
- Dispense 75ul at 1.2mm below the top of the well at 75% off center, 90 degrees (12 o'clock)
- Aspirate 75ul at 0.9mm above the bottom of the well at 10ul/s
- Dispense 75ul at 1.2mm below the top of the well at 75% off center, 90 degrees (12 o'clock)
- Aspirate 50ul in four parts at 20ul/s (as defined above)
- Dispense 50ul at 1.2mm below the top of the well at 75% off center, 90 degrees (12 o'clock)

The robot then removes the binding plate from the magnetic stand again and repeats the procedures described above, but this time using wash buffer 2. Once the washing procedures are complete,

the Turbo DNase plate is brought out onto the deck of the robot and 50ul of Turbo Dnase in buffer is added to each well. The robot then mixes the beads and Dnase for 25min. The pipetting sequence is:

- Aspirate 50ul at 1mm above the bottom of the well at 80ul/s
- Move the tip to 10mm above the bottom of the well on center
- Move the tip to 1.2mm off center (the side of the well) at 45 degrees (2 o'clock) and 10mm above the bottom of the well.
- (1) Dispense the volume at 150ul/s
- (2) Move the tip to 10mm above the bottom of the well on center
- (3) Aspirate 50ul at 1 mm above the bottom of the well at 80ul/s
- (4) Move the tip to 10mm above the bottom of the well on center
- Move the tip to 1.2mm off center at 135 degrees (10 o'clock) and 10mm above the bottom of the well.
- Repeat steps 1-4 from above
- Move the tip to 1.2mm off center at 225 degrees (8 o'clock) and 10mm above the bottom of the well.
- Repeat steps 1-4 from above
- Move the tip to 1.2mm off center at 315 degrees (5 o'clock) and 10mm above the bottom of the well.
- Repeat steps 1-4 from above
- Dispense the volume at 150ul/s

- Move the tip to 10mm above the bottom of the well on center

The robot then adds 100ul of RNA rebind solution to the reaction plate, and mixes the solution for 5min. The pipetting sequence is:

- Aspirate 150ul at 1 mm above the bottom of the well at 80ul/s
- Move the tip to 10mm above the bottom of the well on center
- Move the tip to 1.2mm off center at 45 degrees (2 o'clock) and 10mm above the bottom of the well.
- (1) Dispense the volume at 150ul/s
- (2) Move the tip to 10mm above the bottom of the well on center
- (3) Aspirate 150ul at 1mm above the bottom of the well at 80ul/s
- (4) Move the tip to 10mm above the bottom of the well on center
- Move the tip to 1.2mm off center at 135 degrees (10 o'clock) and 10mm above the bottom of the well.
- Repeat steps 1-4 from above
- Move the tip to 1.2 mm off center at 225 degrees (8 o'clock) and 10 mm above the bottom of the well.
- Repeat steps 1-4 from above
- Move the tip to 1.2mm off center at 315 degrees (5 o'clock) and 10mm above the bottom of the well.
- Repeat steps 1-4 from above
- Dispense the volume at 150ul/s

- Move the tip to 10mm above the bottom of the well on center

The robot then moves the binding reaction plate to the magnetic stand and pauses for 2min before carrying out an additional round of washing with wash buffer 2. Once the final washes are complete 30ul of Elution Buffer (heated to 55C on the peltier position) is added to the beads in the binding plate (off the magnet) using P50 tips, at a position 5.8mm above the bottom of the well. The robot then mixes the beads and elution buffer using the following pipetting sequence:

- Aspirate 30ul at 1mm above the bottom of the well at 80ul/s
- Move the tip to 10mm above the bottom of the well on center
- Move the tip to 1.2mm off center (the side of the well) at 45 degrees (2 o'clock) and 10mm above the bottom of the well.
- (1) Dispense the volume at 150ul/sec
- (2) Move the tip to 10mm above the bottom of the well on center
- (3) Aspirate 30ul at 1 mm above the bottom of the well at 80ul/s
- (4) Move the tip to 10 mm above the bottom of the well on center
- Move the tip to 1.2mm off center at 135 degrees (10 o'clock) and 10mm above the bottom of the well.
- Repeat steps 1-4 from above
- Move the tip to 1.2mm off center at 225 degrees (8 o'clock) and 10mm above the bottom of the well.
- Repeat steps 1-4 from above

- Move the tip to 1.2mm off center at 315 degrees (5 o'clock) and 10mm above the bottom of the well.
- Repeat steps 1-4 from above
- Dispense the volume at 150ul/s
- Move the tip to 10mm above the bottom of the well on center

The robot then moves the binding reaction plate to the magnetic stand, and pauses for 2min, while it retrieves the RNA plate from the Cytomat. 30ul of eluate is then transferred from the binding plate to the RNA plate using a P50 tip, using both a 30ul pipetting step and a 10ul pipetting step (at 0.9mm above the bottom of the well) to ensure all liquid is transferred. The robot then transfers the RNA plate to the Liconic incubator (at 4C) and moves to the next plate in the sequence. The plates containing RNA were stored at -80C and later analyzed by qPCR.

2.9 ACKNOWLEDGEMENTS

We would like to thank Christopher Martinez and Gabrielle Martinez for help programming and running the Biomek robot. This work was supported by the National Institutes of Health (NIH) grants 1R01GM097329 and 5T32GM008659.

CHAPTER 3: MULTI-LAYERED REGULATION OF TORC1-BODY FORMATION IN BUDDING YEAST

Arron Sullivan, Ryan L. Wallace, Rachel Wellington, Xiangxia Luo, and Andrew P. Capaldi[1]

Published Online: Molecular Biology of the Cell 28 Nov 2018

https://doi.org/10.1091/mbc.E18-05-0297

Department of Molecular and Cellular Biology

University of Arizona, Tucson AZ 85721-0206

[1] Corresponding author: capaldi@email.arizona.edu

3.1 ABSTRACT

The Target of Rapamycin Kinase Complex 1 (TORC1) regulates cell growth and metabolism in eukaryotes. In *Saccharomyces cerevisiae*, TORC1 activity is known to be controlled by the conserved GTPases, Gtr1/2, and movement into and out of an inactive agglomerate/body. However, it is unclear if/how these regulatory steps are coupled. Here we show that active Gtr1/2 is a potent inhibitor of TORC1-body formation, but cells missing Gtr1/2 still form TORC1-bodies in a glucose/nitrogen starvation dependent manner. We also identify 13 new activators of TORC1-body formation and show that seven of these proteins regulate the Gtr1/2 dependent repression of TORC1-body formation, while the remaining proteins drive the subsequent steps in TORC1 agglomeration. Finally, we show that the conserved PI(3)P binding protein, Pib2, forms a complex with TORC1 and overrides the Gtr1/2 dependent repression of TORC1-body formation during starvation. These data provide a unified, systems-level model of TORC1 regulation in yeast.

3.2 INTRODUCTION

The Target of Rapamycin kinase Complex I (TORC1) is a key regulator of cell growth and metabolism in eukaryotes (Gonzalez and Hall, 2017; Loewith and Hall, 2011; Saxton and Sabatini, 2017). In the presence of pro-growth hormones and ample nutrients, TORC1 is active and drives protein, lipid, and nucleotide synthesis by phosphorylating a wide range of proteins (Bodenmiller et al., 2010; Gonzalez and Hall, 2017; Hsu et al., 2011; Loewith and Hall, 2011; Robitaille et al., 2013; Saxton and Sabatini, 2017). In contrast, when hormone, nutrient, or energy levels fall—or

cells are exposed to noxious stress—TORC1 is inhibited, causing the cell to switch from anabolic to catabolic metabolism and eventually enter a quiescent state (Barbet et al., 1996; Duvel et al., 2010; Gonzalez and Hall, 2017; Loewith and Hall, 2011; Noda and Ohsumi, 1998; Saxton and Sabatini, 2017).

TORC1 is made up of three essential proteins, called mTOR, Raptor and mLst8 in humans and Tor1, Kog1 and Lst8 in yeast (Kim et al., 2002; Loewith et al., 2002). Biochemical and structural studies show that these proteins form a stable, ring-like structure containing two of each subunit (Adami et al., 2007; Aylett et al., 2016; Yang et al., 2017; Yip et al., 2010). Kog1/Raptor recruits substrates to the TOR kinase (Tor1) and is required for the regulation of Tor1 activity (Aylett et al., 2016; Hara et al., 2002; Kim et al., 2002). Lst8, on the other hand, binds directly to Tor1 and may help stabilize the TOR complex (Kim et al., 2002). In yeast, TORC1 also includes the non-essential and poorly characterized subunit Tco89 (Reinke et al., 2004).

TORC1 activity is controlled by a variety of proteins and pathways (Gonzalez and Hall, 2017; Loewith and Hall, 2011; Nicastro et al., 2017; Saxton and Sabatini, 2017), but in the model organism Saccharomyces cerevisiae, two major modes of regulation have been identified:

First, nitrogen and amino acid signals are transmitted to TORC1 via a pair of small GTPases called Gtr1 and Gtr2 (Rag A/B and Rag C/D in humans) (Binda et al., 2009; Kim et al., 2008; Sancak et al., 2008). Gtr1 and 2 form a heterodimer that is tethered to the vacuolar/lysosomal membrane by a palmitoylated and myristoylated complex made up of Ego1, Ego2 and Ego3 (EGO-TC, or

Ragulator in humans) (Binda et al., 2009; Nadolski and Linder, 2009; Powis et al., 2015; Roth et al., 2006; Sancak et al., 2010). In the presence of abundant nitrogen/amino acids, Gtr1 and 2 are in their GTP and GDP bound forms, respectively, and bind tightly to Kog1/Raptor and Tco89 (Binda et al., 2009; Gao and Kaiser, 2006; Sancak et al., 2008). In contrast, when nitrogen/amino acid levels fall, Npr2, Npr3 and Iml1 (SEACIT in yeast and GATOR1 in humans) bind to Gtr1 and induce its GTPase activity (Bar-Peled et al., 2013; Neklesa and Davis, 2009; Panchaud et al., 2013; Su et al., 2017). The resulting switch--from GTP bound Gtr1, to GDP bound Gtr1--then causes a conformational change that weakens the interaction between Gtr1/2 and TORC1, and rapidly inhibits (τ = 1-2 min) TORC1 signaling (Binda et al., 2009; Hughes Hallett et al., 2014; Sancak et al., 2008).

TORC1 is also rapidly (τ = 1-2 min) inactivated in glucose starvation conditions, but this transition occurs normally in strains carrying mutations that lock Gtr1/2 in their active (GTP and GDP bound) conformations (Hughes Hallett et al., 2014; Urban et al., 2007), indicating that either glucose does not signal through Gtr1/2 (in contrast to the Rags (Efeyan et al., 2013)) or that other regulators dominate the response.

Second, glucose and nitrogen starvation cause Kog1, Tco89 and--as shown in recent studies--Tor1 (Kira et al., 2016; Prouteau et al., 2017) to move from their position spread across the vacuolar membrane, to a single focus on the edge of the vacuole (Hughes Hallett et al., 2015). TORC1-body formation is sped-up approximately 20-fold by Snf1/AMPK dependent phosphorylation of Kog1 at Ser 491 and 494, and over 100-fold by two glutamine-rich prion-like domains in Kog1

(Hughes Hallett et al., 2015). Analysis of strains with mutations that limit TORC1-body formation show that the TORC1-bodies are not required for rapid TORC1 inactivation (in contrast to Gtr1/2) but rather increase the threshold for TORC1 activation in cells that have been starved for a significant period of time (Hughes Hallett et al., 2015). This creates hysteresis in the TORC1 pathway to help ensure that cells remain committed to a starvation state until they are exposed to optimal conditions.

It is currently unclear, however, if/how Gtr1/2 and Ego1-3 (EGOC) influence TORC1 localization, or what signaling proteins/pathways besides Snf1 regulate TORC1-body formation. As a result, there is no unified model of TORC1 regulation in yeast.

Here, to address these questions, we examine the influence that Gtr1/2, Ego1-3, and 209 additional proteins (including nearly all non-essential kinases and phosphatases in yeast) have on TORC1 agglomeration using fluorescence microscopy. We show that the active (GTP bound) form of Gtr1 is a potent inhibitor of TORC1-body formation, but cells missing Gtr1 and Gtr2 still form TORC1-bodies in a glucose/nitrogen starvation-dependent manner. We also identify 13 new regulators of TORC1-body formation and show that they act in two steps: First, the PKC pathway, Sit4, Gcn2, and Cka1 work together with SEACIT to override the Gtr1/2 dependent inhibition of TORC1 agglomeration. Then, Ypk1, Cmk1, Yak1, Sak1 (all stress/starvation signaling proteins), and the intrinsically disordered TORC1 subunit Tco89, help drive TORC1 into bodies. Finally, we show that the conserved PI(3)P binding protein, Pib2, forms a complex with TORC1, and overrides the Gtr1/2-dependent repression of TORC1-body formation during starvation.

Taken together, our data provides a comprehensive, network level, view of TORC1 regulation, and show that starvation signals have to be transmitted through Gtr1/2, before Pib2 and other stress/starvation signaling proteins can trigger TORC1-body formation and lock the TORC1 pathway in an inactive state.

3.3 RESULTS

3.3.1 EGOC dependent control of Kog1-body formation

To measure the influence that EGOC has on TORC1-body formation, we followed Kog1-YFP localization in a wild-type strain and a strain missing Gtr1/2 (and thus all interactions between EGOC and TORC1). Cells were kept in log phase growth for at least 12 hrs (in SD medium), loaded into chamber slides, and 3D images were acquired using a fluorescence microscope. The cells were then washed with medium missing glucose, and additional images were acquired at regular time intervals.

The wild-type strain formed bodies in two phases; 8 ± 5% of cells had bodies at time zero, and this increased to ~50% with a time constant of approximately 10 min, and then >90% with a time constant of 260 ± 100 min (Fig. 1a, b and (Hughes Hallett et al., 2015)). In contrast, the gtr1Δgtr2Δ

strain formed bodies in a single phase: 32 ± 4% of cells had bodies at time zero, and this increased to 73 ± 1% of cells with a time constant of 9 ± 2 min (Fig. 1a, b). These data show that deleting Gtr1/2 increases the fraction of cells containing TORC1-bodies in nutrient replete conditions (from 8 ± 5% to 32 ± 4%), and speeds up body formation during starvation. Thus, EGOC acts to repress TORC1-body formation, especially in nutrient replete conditions.

Next, to determine if starvation signals transmitted through EGOC control TORC1-body formation, we followed Kog1-YFP localization in strains carrying mutations that lock Gtr1 in its active state (npr2Δ and GTR1Q65L (Binda et al., 2009; Panchaud et al., 2013)). These strains had gross defects in TORC1-body formation in both glucose and nitrogen starvation conditions (Fig. 1a, b and S1), indicating (1) that the active form of EGOC--normally found in nutrient replete conditions--is a potent inhibitor of TORC1-body formation, and (2) that EGOC is converted into its inactive form during both glucose and nitrogen starvation, and this in turn allows TORC1 to form bodies.

3.3.2 Kog1 and EGOC colocalize during starvation

To learn more about the influence that EGOC has on TORC1-body formation, we followed EGOC localization during glucose and nitrogen starvation.

Recent studies have shown that EGOC localizes to both the vacuolar membrane, and distinct puncta associated with the vacuolar membrane, during growth in nutrient replete (SD) medium

(Binda et al., 2009; Kira et al., 2016; Kira et al., 2014). Nitrogen starvation then increases the fraction of cells with EGOC puncta, while mutants that disrupt EGOC decrease the fraction of cells with EGOC puncta (Kira et al., 2016).

To confirm and extend these results, we tagged Gtr1, Ego1, Ego2 and Ego3 with YFP and followed their movement in both glucose and nitrogen starvation conditions, using the same procedures described above for the Kog1-YFP experiments.

In line with previous results, we found that EGOC localizes to the vacuolar membrane in all cells, and to foci located on the vacuolar membrane in around 70% of cells, during log phase growth (Fig. 2a, b). EGOC then moves into foci in an additional 10 and 20% of cells during nitrogen and glucose starvation, respectively; but maintains vacuolar membrane localization in all cells (Fig. 2a, b).

The finding that EGOC foci are formed during log phase growth—before TORC1 moves into bodies—lead us to ask if TORC1-bodies assemble at the EGOC foci. To do this, we examined the localization of Kog1 labeled with RFP (Kog1-DuDre) in strains carrying Gtr1-YFP and Ego2-YFP, in glucose starvation conditions. These experiments showed that TORC1 and EGOC foci colocalize in the vast majority of cells containing TORC1-bodies (98% overlap between Ego2 and Kog1 foci (n=97), and 95% overlap between Gtr1 and Kog1 foci (n=103), in cells containing Kog1-foci; Fig. 2d). Thus, TORC1 interacts with the pool of EGOC located on the vacuolar

membrane in log growth conditions, and then moves to the pool of EGOC located in foci during starvation.

3.3.3 The role of EGOC foci in TORC1-body formation

The microscopy data described above suggest that EGOC foci act as nucleation sites for TORC1-body formation. If this is true, then eliminating the EGOC foci should slow down TORC1-body formation in strains that maintain interactions between Gtr1/2 and TORC1.

To test this prediction, we followed Kog1-YFP localization in strains missing Gtr1 alone and Gtr2 alone, since they do not form EGOC foci (Fig. 2c; (Kira et al., 2016)), but may maintain weak interactions between Gtr2 and TORC1, and Gtr1 and TORC1, respectively. These strains form more TORC1-bodies than the wild-type strain in log growth conditions (indicating that the repression of TORC1-body formation by active EGOC requires an intact Gtr1/2 complex) but then form TORC1-bodies (7-11 times) slower than the wild-type strain (Fig. 1b; $\tau = 107 \pm 27$ and 67 ± 37 min for the gtr1Δ and gtr2Δ strains, versus τ 11 ± 3 min for the wild-type strain).

We then followed Kog1-YFP localization in strains missing Ego1 alone, and Ego3 alone, since they also fail to form EGOC foci (Fig. 2c) but probably maintain some interaction between Gtr1/2 and TORC1. These strains form the same number of TORC1-bodies as the wild-type strain in log growth conditions (indicating that Gtr1/2 represses TORC1-body formation efficiently even when it isn't tethered to the vacuolar membrane), and then—as predicted—form bodies (6-10 times)

slower than the wild-type strain (Fig. 1b; $\tau = 58 \pm 19$ and 99 ± 52 min for ego1Δ and ego3Δ strains, versus τ 11 ± 3min for the wild-type strain).

Thus, while the main role of EGOC is to repress TORC1-body formation during log phase growth, it appears that interactions between TORC1 and the EGOC in foci (or TORC1 and other proteins in the EGOC foci) helps speed up TORC1-body formation during starvation (see the supplemental text and Fig. S2 for further discussion).

3.3.4 Activators of TORC1-body formation

To identify additional regulators of TORC1-body formation, we measured Kog1-YFP localization in 209 strains--each missing one of 139 non-essential kinases/phosphatases in yeast (Breitkreutz et al., 2010), or one of 70 genes of interest--many of which were found to interact with the TORC1 pathway in a previous screen (Worley et al., 2015). Cells were kept in log phase growth for at least 12 hrs, transferred into glucose free medium for 60 min, and then 3D images were acquired using a fluorescence microscope. Most of the strains formed more TORC1-bodies than the wild-type parental strain during starvation, but there were 40 outliers--all with significant (>2-fold) defects in TORC1-body formation (Fig. 3a). To follow this up, we grew the 45 strains that formed the fewest bodies in the screen (green bar, Fig. 3a), and the 13 strains that formed the largest number of bodies in the screen (red bar, Fig. 3a), and measured Kog1-YFP localization as a function of time in both glucose and nitrogen starvation conditions (Fig. 3b). These experiments confirmed the findings from the initial screen and led to the identification of 13 strains that have

dramatic defects in TORC1-body formation (<10% of cells with bodies after two hours of glucose starvation versus 78% of cells with bodies in the wild-type strain), namely; pib2Δ, rom2Δ, tco89Δ, sit4Δ, yak1Δ, ypk1Δ, bck1Δ, sak1Δ, gcn2Δ, cmk1Δ, ypl150wΔ, cka1Δ, and slt2ΔFig. 3b and c The defect in the pib2Δstrain was especially pronounced (blue line, Fig. 3c), and in subsequent experiments we found that <5% of pib2Δcells form Kog1-bodies after 24 hours of starvation (versus >90% in the wild-type strain).

To determine if the genes that regulate TORC1-body formation also control the rapid inactivation of TORC1, we measured TORC1 activity during glucose starvation in 14 different strains--each missing one gene that is important for TORC1-body formation (including all 13 genes listed above). To do this we followed the phosphorylation of the key TORC1 substrate, Sch9, during glucose starvation (Hughes Hallett et al., 2014; Urban et al., 2007). These experiments showed that TORC1 was repressed as normal (or somewhat over-repressed) in 12 of these strains (Fig. 3d and S3), and while the other two strains (rom2Δ and sak1Δ) do have defects in TORC1 repression (Fig. 3e and S3), the defects are minor compared to those caused by the deletion of Snf1/AMPK—a gene we previously identified as regulating TORC1 activity in glucose starvation conditions (Fig. 3e; (Hughes Hallett et al., 2014)). Thus, the major regulators of TORC1-body formation identified in this study act downstream of, and/or in parallel with, the canonical TORC1 regulatory circuit to control TORC1 agglomeration and lock TORC1 in an inactive state.

3.3.5 Activators of TORC1-body formation acting upstream and downstream of Gtr1/2

Activators of TORC1-body formation could act (1) at, or above, the level of EGOC to promote release from the Gtr1/2 dependent repression of TORC1-body formation, or (2) at a subsequent step to drive TORC1 agglomeration. To distinguish between these possibilities, we created a series of double mutant strains, each missing Gtr1 and one of the 13 regulators of TORC1-body formation identified in the screen. We also made a strain missing Gtr1 and Npr2, and a strain missing Gtr1 and carrying glutamine to alanine mutations in both prion like domains of Kog1 (PrDm1+2 (Hughes Hallett et al., 2015)), as controls for scenarios (1) and (2), respectively. All of these strains grew relatively well, except for bck1Δgtr1Δ (which we continued to study) and ypl150wΔgtr1Δ (which we dropped from the experiment), as described in the Methods.

Measurement of TORC1-body formation in the double mutants revealed that the newly identified regulators fall into two distinct groups. Deletion of Gtr1 rescued the TORC1-body formation defects found in the bck1Δ, slt2Δ, and rom2Δstrains (all proteins in the PKC pathway; (Levin, 2011)), as well as the defects found in the gcn2Δ, pib2Δ, cka1Δ, npr2Δ, and sit4Δ strains (Fig 4). In contrast, deletion of Gtr1 had very little impact on TORC1-body formation in the ypk1Δ, cmk1Δ, sak1Δ, tco89Δ, yak1Δ, and prDm1+2 strains (Fig. 4). Thus, 7/13 genes we identified in the screen work together with Npr2 to promote release from the Gtr1/2-dependent repression of TORC1-body formation, while the remaining genes, including the intrinsically disordered TORC1 subunit Tco89, drive the subsequent steps in TORC1 agglomeration along with the prion-like domains in Kog1.

Remarkably, most (6/7) of the proteins that act on, or at the level of, Gtr1 to promote TORC1-body formation are repressed by, or in a pathway that is repressed by, TORC1, including: Sit4, a type 2A related phosphatase repressed by TORC1 via Tap42, involved in regulating a wide range of processes, including cell cycle regulation (Di Como and Arndt, 1996; Jacinto et al., 2001; Loewith and Hall, 2011); Slt2/Mpk1, a MAPK in the PKC pathway repressed by TORC1 and involved in the regulation of cell wall integrity, cell cycle progression, and proteasome activity (Krause and Gray, 2002; Moreno-Torres et al., 2015; Rousseau and Bertolotti, 2016; Torres et al., 2002); Rom2, an upstream activator in the PKC pathway (Levin, 2011; Ozaki et al., 1996); Bck1, a MAPKKK in the PKC pathway that interacts with TORC1 (Breitkreutz et al., 2010; Levin, 2011); Cka1, the alpha catalytic subunit of casein kinase 2 (CK2), recently found to be repressed by TORC1, and involved in regulating RNA Pol III activity and other proteins/pathways ((Sanchez-Casalongue et al., 2015; Shekhar-Guturja et al., 2016); and Gcn2, a kinase repressed by TORC1 that has also been reported to act upstream of TORC1, involved in regulating amino acid biosynthesis (Cherkasova and Hinnebusch, 2003; Yuan et al., 2017).

These connections suggest that the inhibition of TORC1 signaling in starvation conditions helps drive the release of TORC1 from the EGOC dependent repression of TORC1-body formation via feedback. This probably helps to ensure that all of the TORC1 molecules in a cell are primed to move into bodies during long term starvation.

However, TORC1-body formation is also controlled by an additional group of proteins (Yak1, Ypk1, Cmk1 and Sak1) that activate TORC1-body formation once TORC1 is released from the

EGOC dependent repression of TORC1 agglomeration. With the exception of Yak1 (Martin et al., 2004), these proteins are not linked to the TORC1/EGOC signaling pathway and, instead, respond to membrane stress as part of the TORC2-Ypk1 pathway (Ypk1; (Muir et al., 2014; Roelants et al., 2011)), calcium signals (Cmk1; (Cyert, 2001)), and glucose/energy starvation (Sak1; (Elbing et al., 2006; Hedbacker and Carlson, 2008)). It therefore appears that the second layer of regulation helps to ensure that multiple stress/starvation pathways are activated before a cell commits to the starvation state by forming TORC1-bodies.

3.3.6 Cooperation between Pib2 and EGOC

One of the most interesting findings from the double mutant analysis is that Pib2—a protein that is required for TORC1-body formation in wild-type cells (Fig. 3) and known to interact with both EGOC and TORC1 (Kim and Cunningham, 2015; Michel et al., 2017; Tarassov et al., 2008)—becomes dispensable for TORC1-body formation in the absence of Gtr1 (Fig. 4). But how? One possibility is that Pib2 is required for the starvation dependent inactivation of Gtr1, and thus release of the Gtr1/2 dependent repression of TORC1-body formation, like Npr2. However, full-length Pib2 has been shown to activate TORC1 kinase activity (Kim and Cunningham, 2015; Michel et al., 2017; Tanigawa and Maeda, 2017; Varlakhanova et al., 2017), while Npr2 represses TORC1 kinase activity (Neklesa and Davis, 2009; Panchaud et al., 2013)—indicating that Pib2 drives TORC1-body formation via a different mechanism than Npr2. Therefore, to learn more about the role that Pib2 plays in TORC1-body formation, we examined the impact that each domain in Pib2 has on Kog1-YFP localization.

Previous studies have shown that Pib2 contains four distinct domains (Kim and Cunningham, 2015; Michel et al., 2017): (1) an N-terminal domain that inhibits TORC1 activity; (2) a central domain that binds to Kog1; (3) a FYVE domain that binds to PI(3)P and recruits Pib2 to the vacuolar membrane, and; (4) a C-terminal domain, including a critical (and highly conserved) 15 amino acid stretch from amino acid 620-635, that activates TORC1 (Fig. 5a; see supplemental text and Figs. S4-S6 for further details).

Deletion of the N-terminal Inactivation Domain (NID) of Pib2 increased the fraction of cells that form TORC1 bodies in nutrient replete conditions (from 8 ± 5% to 21 ± 1%), and on the one-hour time scale (from 56 ± 1% to 80 ± 2%)--indicating that this region of Pib2 inhibits TORC1-body formation (Fig. 5b). In contrast, deletion of the C-terminal activating domain (CAD), Kog1-binding domain (KBD), and FYVE domain (FYVE) slowed or blocked TORC1-body formation, indicating that these domains promote TORC1-body formation (Fig. 5b).

The data showing that the Kog1-binding domain in Pib2 is required for TORC1-body formation is especially interesting since previous studies have shown that this domain is dispensable for TORC1 activity (in SD medium). Moreover, it suggests that Pib2 drives TORC1-body formation via a direct interaction with Kog1/TORC1.

To test this idea, we created a strain carrying GFP-Pib2 and Kog1-DuDre, and followed their localization during glucose starvation. This experiment revealed that: (1) Pib2 is located on both

the vacuolar membrane, and foci associated with the membrane, in nutrient replete medium--just like EGOC--and (2) that Kog1 and Pib2 both reside in the TORC1-body (also occupied by EGOC) during starvation (93% overlap, n=128 cells with Kog1 foci; Fig. 6a). We also performed co-immunoprecipitation experiments (after crosslinking) to see if Pib2, EGOC and TORC1 bind to each other during log growth (when TORC1 is distributed across the vacuolar membrane) and/or in starvation conditions (when TORC1 is in a body). These experiments showed that Pib2 and Kog1, and Gtr1 and Kog1, interact at similar levels in both nutrient replete and starvation conditions (Fig. 6b).

Thus, Pib2, EGOC, and TORC1 form a complex that blocks TORC1-body formation when EGOC is active (in nutrient-replete conditions), but permits TORC1 to form bodies when EGOC is inactive (during starvation). In this complex, EGOC constantly acts to inhibit TORC1-body formation, likely via direct binding to TORC1. However, when Gtr1/2 are in the inactive state, Pib2 overwhelms the repressive effect of EGOC so that TORC1-bodies can form.

3.4 DISCUSSION

3.4.1 Regulation of TORC1-body formation

In our original study of TORC1 localization (Hughes Hallett et al., 2015), we followed the movement of Kog1-YFP, Tco89-YFP, and Tor1 with a triple GFP insertion (Sturgill et al., 2008), in different stress and starvation conditions. Those experiments showed that Kog1-YFP and

Tco89-YFP move into a body during glucose and nitrogen starvation (with a time constant of 10 min) while Tor1D330-3xGFP remains on the vacuolar membrane/cytoplasm--leading us to conclude that TORC1 dissociates in starvation conditions so that Kog1 and Tco89 can move into a "Kog1-body". However, recent experiments examining the localization of GFP-Tor1, have shown that Tor1 also moves into a body (Kira et al., 2016; Prouteau et al., 2017) indicating that the internal 3xGFP tag disrupts Tor1 localization. We have confirmed these results (data not shown), and therefore refer to TORC1-bodies, rather than Kog1-bodies, throughout this paper.

In the same study, we showed that AMPK/Snf1 phosphorylates Kog1 during glucose starvation at two novel sites (Ser 491 and 494), and that these phosphorylation events help drive the formation of TORC1-bodies (TORC1-bodies form 20-fold slower in Kog1S491/494A and snf1Δ cells). We also showed that two glutamine-rich, prion-like domains in Kog1 help drive TORC1-body formation (TORC1-bodies form >100-fold slower in the strongest prion mutant; PrDm1+2). Then, by studying strains with mutations that limit TORC1-body formation (Kog1S491/494A, PrDm1+2, and others) we showed that TORC1-bodies are not required for the rapid inactivation of TORC1, but instead increase the threshold for TORC1 activation in cells that have been starved for a significant period of time (from around 0.02% glucose, to around 2% glucose). In other words, TORC1-body formation creates hysteresis (memory) in the TORC1 pathway to help ensure that cells remain committed to a starvation state until they are exposed to optimal conditions. In line with this, cells carrying Asp or Glu mutations at Ser 491 and 494 in Kog1 (phosphomimetics) fail to grow—even in rich medium.

Here, to build on our previous work, we set out to learn more about how TORC1-body formation is regulated and, in particular, if/how the major TORC1 regulators Gtr1/2 (Rag A/B and C/D in humans) impact TORC1-body formation--with the goal of building an integrated model of TORC1 regulation in yeast.

Our new data show that TORC1-body formation and TORC1 inhibition are tightly coupled events. Specifically, we show that glucose and nitrogen starvation both trigger inhibition of the Gtr1/2 complex (i.e. a switch from the GTP/GDP to the GDP/GTP-bound state). This signaling event is well known to help drive inhibition of TORC1 kinase activity (Binda et al., 2009; Nicastro et al., 2017): In the case of nitrogen starvation, Gtr1/2 inhibition is responsible for about 50% of the rapid and complete repression of TORC1 activity (Hughes Hallett et al., 2014). In the case of glucose starvation, Gtr1/2 inhibition is responsible for only about 20% of the rapid and complete repression of TORC1 activity, since Snf1/AMPK and other unknown pathways play a dominant role in the response (Hughes Hallett et al., 2014). At the same time, Gtr1/2 inhibition also allows TORC1 to form bodies. Importantly, however, it is not TORC1 inhibition itself that promotes TORC1-body formation, since TORC1 is fully repressed in numerous mutant strains that have dramatic defects in TORC1-body formation (some of which can be rescued by deletion of Gtr1). Instead, it appears that Gtr1/2 has a dual role; (1) helping control TORC1 activity, particularly in response to nitrogen and amino acid signals and (2) acting as a glucose and nitrogen starvation dependent gate for TORC1-body formation. This dual role ensures that starvation signals are sent through the Gtr1/2--at least partially inactivating TORC1--before TORC1 can agglomerate and lock the pathway in a hyper-repressed state.

Our data also point to a second mechanism coupling TORC1 inhibition to TORC1-body formation: Most (6/7) of the proteins that are required for the release from Gtr1/2 dependent repression of TORC1-body formation, are repressed by, or are in a pathway that is repressed by, TORC1 itself. It therefore appears that TORC1 inhibition promotes TORC1-body formation by activating several feedback loops.

While TORC1-body formation is tightly coupled to TORC1 inhibition via Gtr1/2 and feedback, it is important to note that the late steps in TORC1-body formation (those that occur after the release from the Gtr1/2 dependent repression of body formation) depend on stress and starvation signaling proteins that are not directly linked to the TORC1 pathway (Sak1, Ypk1 and Cmk1). Further work will be needed to pick apart the influence that of these proteins have on TORC1 signaling, but it seems likely that they help limit TORC1-body formation until multiple stress/starvation pathways are activated.

Our data also provide important insight into the mechanism underlying the Gtr1/2 dependent gating of TORC1-body formation. We show that Gtr1/2 inhibits TORC1-body formation in nutrient replete conditions (when it is active) but becomes dispensable for TORC1-body formation during starvation (when it is inactive). We also show that the inactivation of the Gtr1/2 dependent repression of TORC1-body formation requires Pib2—a protein that forms a complex with TORC1 in both log growth and starvation conditions. These results suggest that that the tight interaction between Gtr1/2 and TORC1 in nutrient replete conditions pins TORC1 in a conformation that has

a low propensity to agglomerate and/or covers a surface of TORC1 that is needed for body formation (e.g. the prion-like domains in Kog1; Fig. 7). Then, when the interaction between Gtr1/2 and TORC1 is weakened in starvation conditions (by a switch to the inactive GDP/GTP bound form of Gtr1/2), Pib2 pulls TORC1 into a new conformation that is primed to agglomerate (Fig. 7).

The discovery that Pib2 is required for the Gtr1/2 dependent regulation of TORC1-body formation builds on previous work showing that Pib2 and Gtr1/2 work together to control TORC1 activation (Kim and Cunningham, 2015; Michel et al., 2017; Tanigawa and Maeda, 2017; Varlakhanova et al., 2017; Worley et al., 2015). We therefore propose that EGOC and Pib2 act as a single complex machine—to control both Gtr1/2 dependent TORC1 activation and TORC1-body formation. In this context, it will be interesting to determine if/how the related protein, LAPF/phafin-1, modulates Rag GTPase function in humans.

3.4.2 Comparison between TORC1-bodies and TOROIDS

While we were completing this work, Prouteau et. al. (2017) published a new study of TORC1 localization. They report that TORC1 moves rapidly into and out of foci, on a timescale that matches Sch9 phosphorylation and dephosphorylation (τ = 2min). They also report that active Gtr1/2 limits TORC1-body formation, and that deletion of Gtr1/2 leads to TORC1 agglomeration in 60% of cells, even in nutrient-replete medium—leading them to conclude that Gtr1/2 are the dominant regulators of TORC1 agglomeration.

The differences between their results, and our results, may be due to different experimental setups since Prouteau et. al. examined TORC1 localization in cells that were transitioning in and out of stationary phase (adding and subtracting nutrients where appropriate) while we followed TORC1 localization in cells that had been kept in log growth phase for >12 hours. There may also be some strain-to-strain differences in the exact rates and levels of TORC1-body formation.

Prouteau et. al. also analyzed the structure of TORC1 purified from cells in stationary phase using CryoEM. Their analysis shows that TORC1 molecules can pack in a helical array to form a hollow tube with a length of up to 1uM. This packing occludes the active site of the complex. Using STORM microscopy, the authors then confirm that some (<20%) of the TORC1 agglomerates formed in vivo are elongated. To test the impact that these TORC1 fibers (called TOROIDS) have on TORC1 activity, Prouteau et. al. then introduced the same Tor1D330-3XGFP construct that we used in our original study (and found does not move to bodies), arguing that the 3xGFP is in an ideal position to disrupt TOROID assembly. They find that Sch9 is phosphorylated at a high level in the Tor1D330-3XGFP strain, even during glucose starvation—leading them to conclude that TOROID formation is required for TORC1 inactivation in glucose starvation conditions.

The argument that TORC1 agglomeration is required for rapid TORC1 inactivation is incompatible with our data showing that 14 different strains with major defects in TORC1-body formation all turn off TORC1 signaling normally (or nearly normally) in glucose starvation conditions (GTR1Q65L and the 13 mutants identified in the screen; Fig. 3 and S3). Instead, we

believe there are two possible explanations for the TORC1 signaling defect found in the Tor1D330-3XGFP strain. The first is simply that the insertion of three GFPs into Tor1 blocks the access of a key regulatory protein to TORC1. The second is that interactions between individual TORC1 molecules (like those found in the TOROID) do help inactivate TORC1 in starvation conditions (leading to the signaling defect in the Tor1D330-3XGFP strain), but the assembly into a higher order agglomerate--visible in the microscope and disrupted in our mutants--is only required to stabilize the off state of TORC1. A model of this type could also help resolve additional conflicts between our data and the data of Prouteau et al. Namely, (1) that the TOROID structure does not include Tco89 (a key driver of TORC1 agglomeration) or explain why the prion-like domains in Kog1 help drive TORC1 agglomeration and (2) that in our microscopy experiments, we never see the kind of highly elongated fibers found in the structural studies of Prouteau et. al. Therefore, it may be that the individual TORC1-TORC1 interactions identified in the CryoEM structure form in vivo, but the interactions formed with, and between, Tco89, the prion domains in Kog1, Pib2 and EGOC pull small TORC1 agglomerates into globular bodies and block the formation of the long fibers seen in vitro.

Further experiments will be needed to resolve these issues and integrate the exciting findings of Prouteau et. al. with our data and two-step model of TORC1 regulation (rapid TORC1 inhibition followed by TORC1-body formation; Fig. 7). However, from the work completed to date, it is clear that the movement of TORC1 into and out of higher order structures is a carefully controlled process that plays an important role in regulating TORC1 activity. Moving forward, it will

therefore be interesting to determine precisely how TORC1-body formation tunes signaling through the TORC1 pathway, and to see if other kinases are regulated by reversible agglomeration.

3.5 MATERIALS AND METHODS

3.5.1 S. cerevisiae strains

Most of the strains used in this study were generated in a haploid S. cerevisiae strain, W303 background (trp1, can1, leu2, his3, ura3), using standard methods. The exceptions were as follows: (1) To make the strain carrying a Gtr1Q65L allele at the native Gtr1 locus, we first knocked out GTR1 using the pCORE cassette, containing both a URA3 and Kan markers (Storici and Resnick, 2006). We then cloned the mutant form of GTR1 out of a plasmid provided from the De Virgilio lab, and introduced it into the gtr1Δ cell line. Finally, we selected for cells that had integrated the mutant GTR1 at the native locus via selection with 5FOA and by searching for colonies that die on Kanamycin (G418) plates. (2) We also used the pCORE cassette to build the strains carrying truncated forms of Pib2 at the native locus. PCR was used to create truncated versions of the Pib2 gene, and the fragments were integrated at the native Pib2 locus by transforming them into strains that had the entire Pib2, or part of the Pib2 gene, replaced with the pCORE cassette. (3) GFP-Pib2 was created by cloning the tagged gene out of a plasmid provided by the Cunningham lab, and integrating it at the native locus--as described above for the truncation mutants. In cases 1-3, the integrity of the final gene product was confirmed by sequencing the Pib2 or Gtr1 gene and

surrounding regions. (4) Strains carrying Kog1-DuDre and Ego1-YFP, or Gtr1-YFP and the strains carrying Kog1-YFP and Ego1/Ego3/Gtr1-DuDre were made by mating and tetrad dissection.

The double mutant strains examined in Fig. 4 were made by knocking each of the relevant Kog1-body regulators out in the gtr1Δstrain. In all but two cases (ypl150wΔ gtr1Δand bck1Δgtr1Δ) the transformation led to a standard number of positive colonies and the resulting strain grew at a rate similar to that of the gtr1Δparental strain. However, since previous reports indicated that the gtr1Δpib2Δ strain is inviable (Kim and Cunningham, 2015), we checked that we had not made a mistake by building it several times. In all cases, we identified a standard number of colonies and the strains grew at approximately the same rate as the gtr1Δ strain.

All strains used in this study are listed in Table S2.

3.5.2 Fluorescence microscopy

Cells were taken from a fresh YEPD plate and grown for 5-6 hrs in SD medium in a 35 ml test tube on a rotator at 30°C, until they reached an OD600 of approximately 0.1. The starter cultures were then used to inoculate 20 ml of SD medium in a 125 ml conical flask to an OD600 of approximately 0.001, and allowed to grow shaking at 200 rpm and 30°C, until they reached mid-log phase. At this point, 400 µl samples were transferred to a chamber slide (Ibidi u-slide, 8-well; 80827) that had been treated with 2 mg/ml concanavilin A, and examined on the microscope. The slides were then washed three times with 400 µl starvation medium (either SD minus glucose or

SD minus nitrogen (no amino acids or ammonium sulfate)), loaded into a 30°C chamber on the microscope, and protein localization was followed over time.

Images were acquired using a DeltaVision Elite Microscope equipped with an Olympus 100x, 1.4NA, objective and a sCMOS camera. We collected a Z-series of 16 images with 0.4 μm spacing in the YFP (YFP filter; Ex. 496–528 nm, Em. 537–559 nm), GFP (GFP filter; Ex. 425-495 nm, Em. 500–550 nm), and/or RFP (RFP filter; Ex. 555–590 nm, Em. 600-675nm) channels at each time-point to ensure that all of the fluorescent foci in the cell were detected. Image files were then processed in ImageJ (Schneider et al., 2012) to create the maximum projection from the stack.

We calculated the fraction of cells containing one or more TORC1-body using a custom pipeline in CellProfiler (Carpenter et al., 2006). In all cases the results were checked by manual inspection, and adjusted if necessary. Where appropriate time-course data was fit to a single exponential equation, $A*(1-e-t/\tau) + c$, or double exponential equation, $A1*(1-e-t/\tau1) + A2*(1-e-t/\tau2) + c$, where A (or A1+A2) is the fraction of cells that form bodies during the time-course, τ is the apparent time-constant, and c is the fraction of cells that have bodies at the start of the time-course. In cases where there was no change in TORC1-body levels during the time-course, the data was fit to a line. All fitting was done in Igor Pro 6.3 (WaveMetrics) and the errors reported are the standard deviation estimated from the fit.

3.5.3 Sch9 bandshift experiments

Bandshift measurements were performed as described previously (Hughes Hallett et al., 2014, 2015; Urban et al., 2007), except that the data were quantified using Image Studio software (LiCor), by comparing the total intensity of the upper (phosphorylated) bands to the total intensity of the upper and lower (phosphorylated and dephosphorylated) bands at each timepoint (to calculate the fraction Sch9 phosphorylated). The values for all time-points and strains were then multiplied by a single constant so that the fraction of Sch9 phosphorylated at time zero in the wild-type strain is set to 1.0.

3.5.4 Co-Immunoprecipitation experiments

Cells were grown in 750 ml of SD medium, shaking at 200 rpm and 30°C, until they reached mid-log phase (OD600 between 0.55 and 0.6). At that point, 1/3 of the culture was harvested by filtration and flash frozen. Approximately one minute later, the other two thirds of the culture was collected on a separate filter, washed with SD medium missing glucose, and added to a flask containing 500 ml of SD medium missing glucose, and grown for an additional 2 or 4 hours before it was collected using filtration.

Immunopurifications were performed using a modified version of the protocol by Murley and Nunnari (Murley et al., 2017) designed to identify protein-protein interactions on membranes. Cells were resuspended in 4 ml of lysis buffer (20 mM Hepes, 150 mM potassium acetate, 2 mM magnesium acetate, 1 mM EGTA and 0.6 M sorbitol at pH 7.4), containing Roche complete protease and phosphatase inhibitors, and lysed by bead beating (6 x 1 min). The lysates were then

cleared by centrifugation at 3000 rpm for 5 min on a benchtop centrifuge, and treated with 1mM dithiobis succinimidyl propionate (a reversible crosslinker; Thermo Fisher Scientific) for 30 min at 4°C. The reaction was then quenched by the addition of 100 mM Tris HCl (pH 7.5) to the sample and incubation on ice for 30 min. Membranes were then solubilized by the addition of 1% digitonin (Cayman) and nutation at 50 rpm and 4°C for 60 min, and the lysates cleared by centrifugation at 12,000 g for 10 min at 4°C.

In the GFP-Pib2 purifications, the clarified lysates were incubated with 50 µl of µMACs monoclonal mouse anti-GFP magnetic microbeads (Miltenyi Biotec) at 4°C for 30 min. µMAC columns were then equilibrated in the lysis buffer + 1% digitonin and protease inhibitors, loaded with the beads, washed three times with 800 µl lysis buffer, 0.1% digitonin, and Roche protease inhibitors, and then washed two times with 800 µl lysis buffer. The proteins were then eluted in 50 mM Tris HCl (pH 6.8), 50 mM DTT, 1% SDS, 1 mM EDTA at 95°C.

In the Kog1-FLAG purifications, the clarified lysates were incubated with 10 µg of anti-FLAG M2 antibody (Sigma) for 3 hrs, and then Protein A/G Ultralink resin (Pierce) for an additional 2 hrs, all at 4°C with slow rotation. The resin was then washed three times with 800 µl lysis buffer, 0.1% digitonin, and Roche protease inhibitors, and two times with 800 µl lysis buffer, before boiling the resin in SDS PAGE loading buffer to elute Kog1 and associated proteins.

The protein samples from each experiment (3 time points for each IP and the matching controls) were run on a single 8% SDS PAGE gel and transferred to a nitrocellulose membrane using

standard procedures. The membrane was then cut in half to separate the higher and lower molecular weight regions (using a pre-stained ladder as a guide). The high molecular weight portion of the membrane was then incubated with anti-FLAG antibody (M2, Sigma) to detect Kog1-FLAG, while the lower weight portion of the membrane was incubated with anti-GFP to detect GFP-Pib2 (4B10B2, Roche) or anti-myc (9E10; Roche) to detect Gtr1-myc.

3.6 ACKNOWLEDGMENTS

We thank Claudio De Virgilio for sharing the GTR1Q65L plasmid; Kyle Cunningham for sharing the GFP-Pib2 plasmid; and Takeshi Noda for sharing the GFP-Tor1 strain. This work was supported by the National Institutes of Health (NIH) grants R01GM097329 and T32GM008659.

3.9 SUPPLEMENT

3.9.1 Influence of EGOC-foci on TORC1-body formation

To determine if TORC1 moves into the EGOC foci during body formation, we set out to follow EGOC and TORC1 localization in a single strain.

As a first step, we tagged Kog1 and all five EGOC subunits using mCherry and mRuby. These constructs all had very low signal. To overcome this problem, we tagged Kog1 with DuDre, a tandem array of DsRed Express 2 (Li et al., 2015). As expected, the Kog1-DuDre construct was

brighter, making it possible to follow TORC1-body formation. However, after careful analysis we found that 30% of cells expressing Kog1-DuDre contain TORC1-bodies during log phase growth (3-fold higher than in Kog1-YFP and other previously studied strains)—indicating that the large tag on Kog1 disrupts interactions with EGOC and/or other inhibitors of TORC1-body formation. Nevertheless, we crossed the strain expressing Kog1-DuDre with the strains carrying YFP-tagged EGO subunits, and found that TORC1-bodies co-localize with EGOC-foci during both log growth and starvation (Fig. 2 and associated text)

To try and get around the problems associated with the Kog1-DuDre construct, we next tagged four out of the five EGOC subunits with DuDre. The Ego1-DuDre, Ego3-DuDre and Gtr1-DuDre constructs all had strong signals and were therefore crossed with a strain carrying Kog1-YFP. However, the resulting dual marker strains formed TORC1-bodies at a much lower rate than the parental strain expressing Kog1-YFP alone (Figs. 1 and S2). The resulting dual marker strains also formed far fewer EGOC-foci in log growth conditions than the constructs expressing EGOC-YFP alone, and in the case of Ego3, less than the construct tagged with Ego3-DuDre alone (Figs 2 and S2). Thus, the EGOC-DuDre tags and Kog1-YFP tags clash/interfere with each other and disrupt EGOC-foci and TORC1-body formation. Again, however, when TORC1-bodies do form they co-localize with EGOC–foci (Fig. S2).

Putting all the data together, it appears that EGOC-foci form before TORC1-bodies and may help to nucleate/accelerate TORC1-body formation. This model is supported by: (1) the data in Figs. 1 and 2 showing that EGOC-foci are formed in 60-70% of cells during log phase growth (before

TORC1-bodies start to form), and that TORC1-bodies ultimately co-localize with the EGOC-foci. (2) The observation that mutants that disrupt EGOC-foci formation, but still carry Gtr1 and/or Gtr2, form TORC1-bodies slower than the wild-type strain (Figs. 1 and 2). (3) The observation that strains carrying Ego1-DuDre, Ego3-DuDre or Gtr1-DuDre with Kog1-YFP all have reduced levels of EGOC-foci formation in log growth conditions and also have a reduced rate of TORC1-body formation (Fig. S2). (4) The observation that EGOC-foci formation always precedes TORC1 body formation (Fig. 1, 2 and Fig. S2).

However, there are other models that could fit with the data described above. For example, EGOC-foci could dock onto the TORC1-body after it forms (in this case the low rate of TORC1-body formation in EGOC mutants would have to be explained by other mechanisms). Therefore, to confirm that TORC1-bodies assemble at the site of preformed EGOC-foci we attempted to follow Kog1 and EGOC localization over time in single cells. Unfortunately, due to the low signals from TORC1 and EGOC (and the resulting long exposure times needed to follow TORC1-body and EGOC-foci formation) there was too much photobleaching to follow TORC1 and EGOC localization at multiple time-points in a single cell.

3.9.2 Properties of the Pib2 truncation mutants

The Pib2 truncation mutants were originally built and studied on plasmids (Michel et al., 2017). That work showed that removal of the N-terminal domain of Pib2 (residues 1-164) conferred resistance to rapamycin (as expected if TORC1 is hyper-activated in the mutant) while removal of

the extreme C-terminus of the protein (residues 620-635) causes sensitivity to rapamycin (as expected if TORC1 activity is repressed in the mutant). The original study also showed to that deletion of Pib2 limits TORC1 activation by glutamine (as measured by monitoring the phosphorylation of Sch9). However, the N-terminal truncation did not influence TORC1 activity in the Sch9 phosphorylation assay, and the authors did not measure the impact that other Pib2 truncations have on TORC1 activity using the Sch9 assay.

In this work, we built each of the previously reported Pib2 truncation mutants (and some hybrids) at the native locus to ensure that the mutant proteins are expressed uniformly across the population of cells under study. To test if these constructs behave as expected, we first measured the sensitivity of each strain to rapamycin in the Kog1-YFP background. In line with the previous results, we found that deletion of the C-terminal domain conferred sensitivity to rapamycin (Fig. S4, upper panel) while deletion of the N-terminal domain confers resistance to rapamycin (Fig. S4, lower panels). Although we note that our pib2Δ strain is less sensitive to rapamycin than the strain studied by Michel et al (this may be due to differences in the base strain).

To further explore the impact that each domain in Pib2 has on TORC1 signaling, we measured TORC1 activity before and during nitrogen starvation in key truncation mutants. As expected, the pib2Δ strain had significantly less TORC1 activity in rich medium (during log growth) than the wild-type strain (~75% of wild-type levels based on duplicate measurements; Fig. S5), but deletion of the N-terminal and C-terminal domains did not cause an appreciable change in TORC1 activity or repression by nitrogen starvation (Fig. S6).

3.9.3 Pib2 overexpression

Deletion of Pib2 blocks TORC1-body formation. To test if Pib2 overexpression speeds up TORC1-body formation we cloned full length Pib2, and GFP-Pib2, into a p415 plasmid containing a CYC1-promoter and introduced them into Kog1-YFP pib2Δ and pib2Δ strains, respectively. Pib2 expression from the plasmid was 2.6 ± 0.2-fold above native levels (as measured by comparing the GFP-Pib2 signal from the native locus to that from the overexpression plasmid) -- and covered for deletion of Pib2--but slowed TORC1-body formation (Fig. S6). This indicates that Pib2 levels are already sufficient in wild-type cells to drive the maximum rate of TORC1-body formation and that excess Pib2 perturbs TORC1-body formation.

3.8 FIGURES

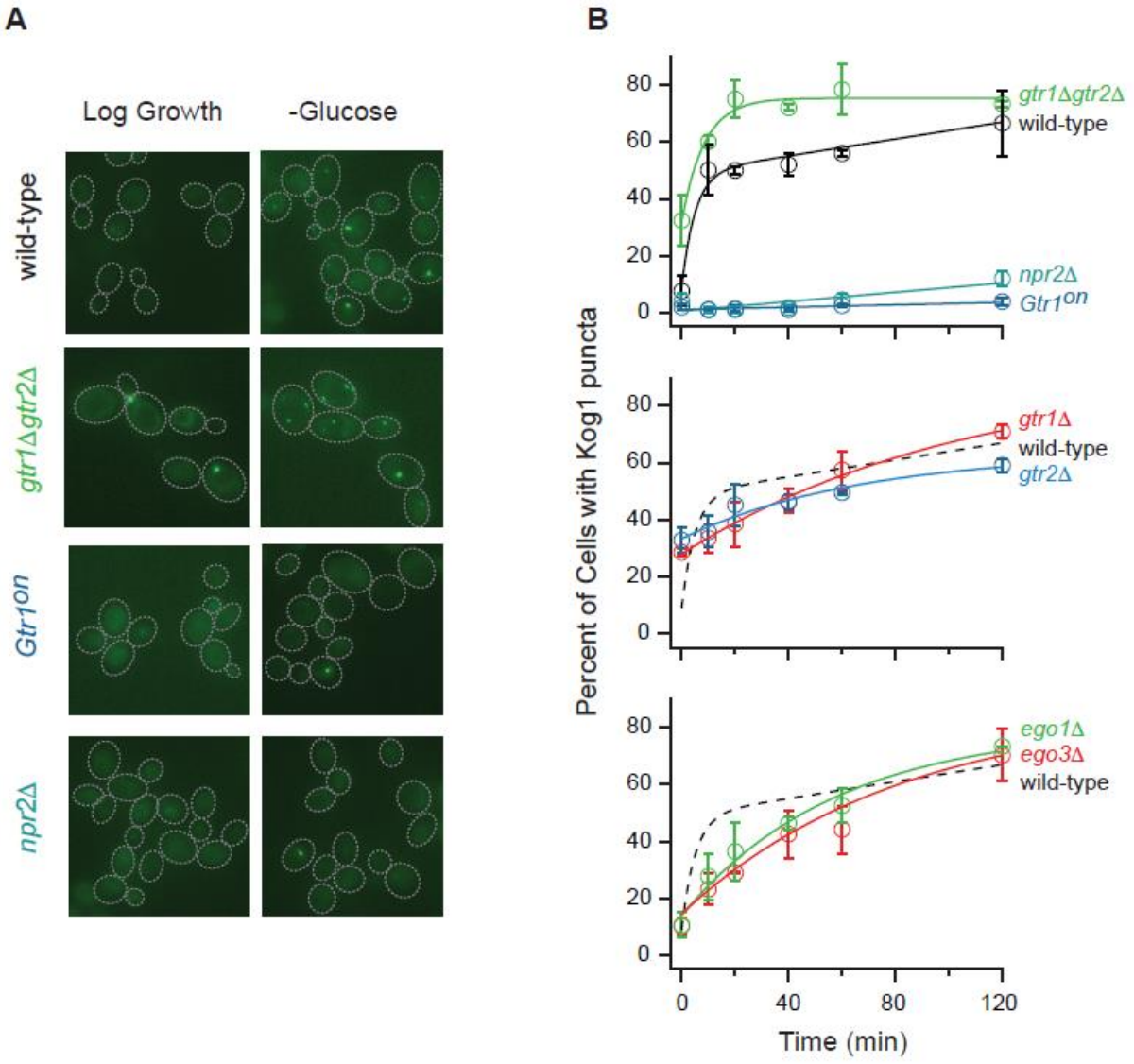

Fig. 1. EGOC regulates TORC1-body formation. (A) Kog1-YFP localization before (log growth) and 60 min after glucose starvation in the wild-type strain, and strains missing Gtr1/2 (gtr1Δgtr2Δ), Npr2 (npr2Δ), or carrying a constitutively active GTR1Q65L allele (Gtr1on). The dashed lines show the position of each cell in the bright-field image. (B) Time-course data showing the fraction

of cells containing Kog1-YFP puncta in the wild-type strain and strains missing Npr2, Gtr1, Gtr2, Gtr1/2, Ego1, Ego3, or carrying a constitutively active Gtr1 allele (Gtr1on), during glucose starvation (as labelled). Each time point shows the average and standard deviation from experiments carried out on three different days, with 75-300 cells, per time point, per replicate. The solid lines show the best fit to a single exponential for the gtr1Δgtr2Δ, ego1Δ, ego3Δ, gtr1Δ and gtr2Δstrains, a double exponential for the wild-type strain, and a straight line for the npr2Δand Gtr1on strains. The broken lines in the lower panels show the best fit to the wild-type data (from the top panel) for comparison.

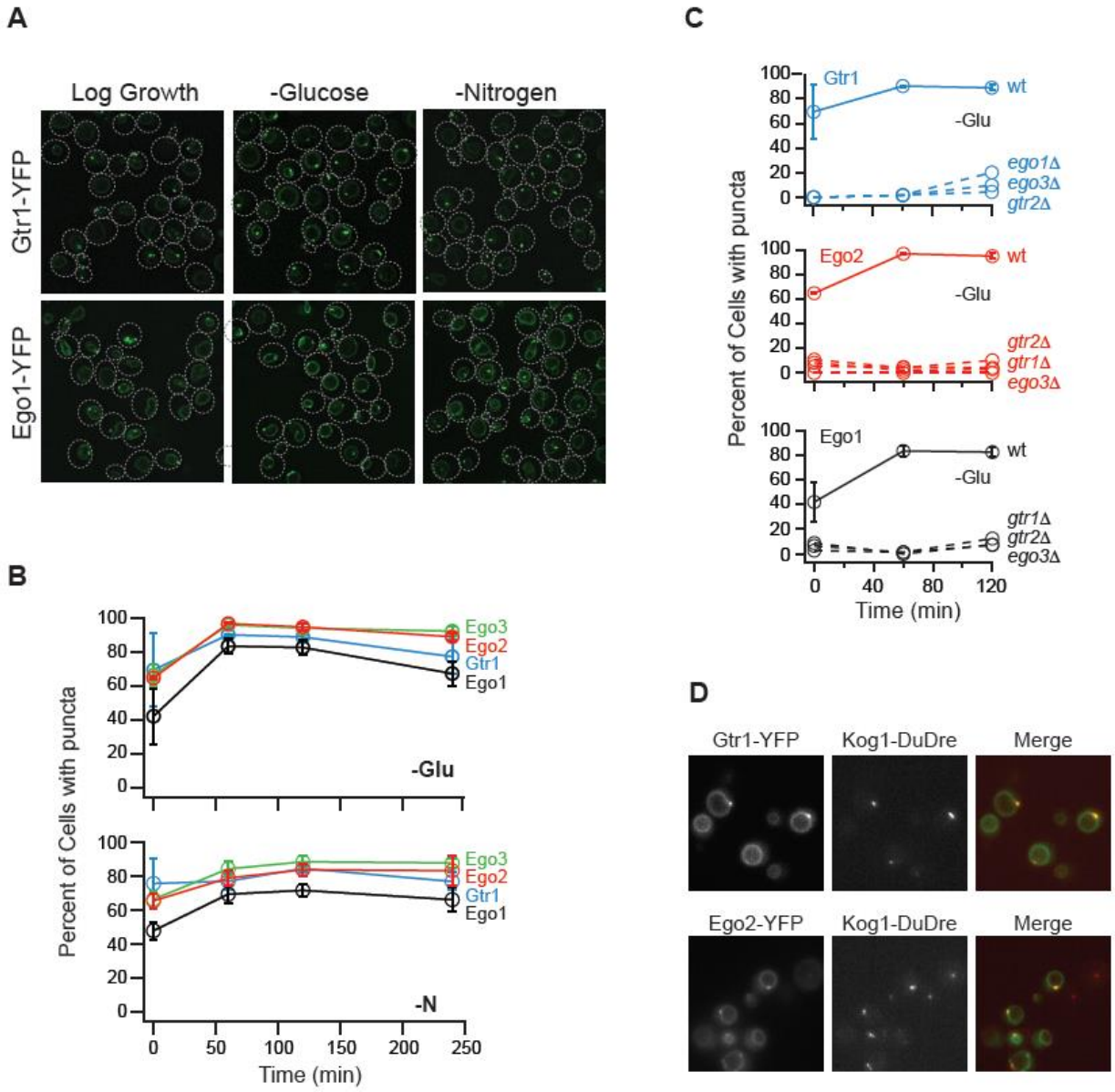

Fig. 2. EGOC forms puncta in log growth and starvation conditions. (A) Gtr1-YFP and Ego1-YFP localization before (log growth), and 60 min after, glucose and nitrogen starvation. The dashed lines show the position of each cell in the bright-field image. (B) Time-course data showing the fraction of cells containing Ego1-YFP, Ego2-YFP, Ego3-YFP and Gtr1-YFP puncta during glucose and nitrogen starvation (top and bottom panels, respectively). (C) Time-course data

showing the fraction of cells containing Gtr1-YFP, Ego1-YFP and Ego2-YFP puncta in strains missing Gtr1, Gtr2, Ego1, or Ego3 (as labelled). For (B and C) each time point shows the average and standard deviation from experiments carried out on two different days, with 100-300 cells, per time point, per replicate. (D) Localization of Gtr1-YFP and Kog1-DuDre (top panel) and Ego2-YFP and Kog1-DuDre (lower panel) after 60 min of glucose starvation.

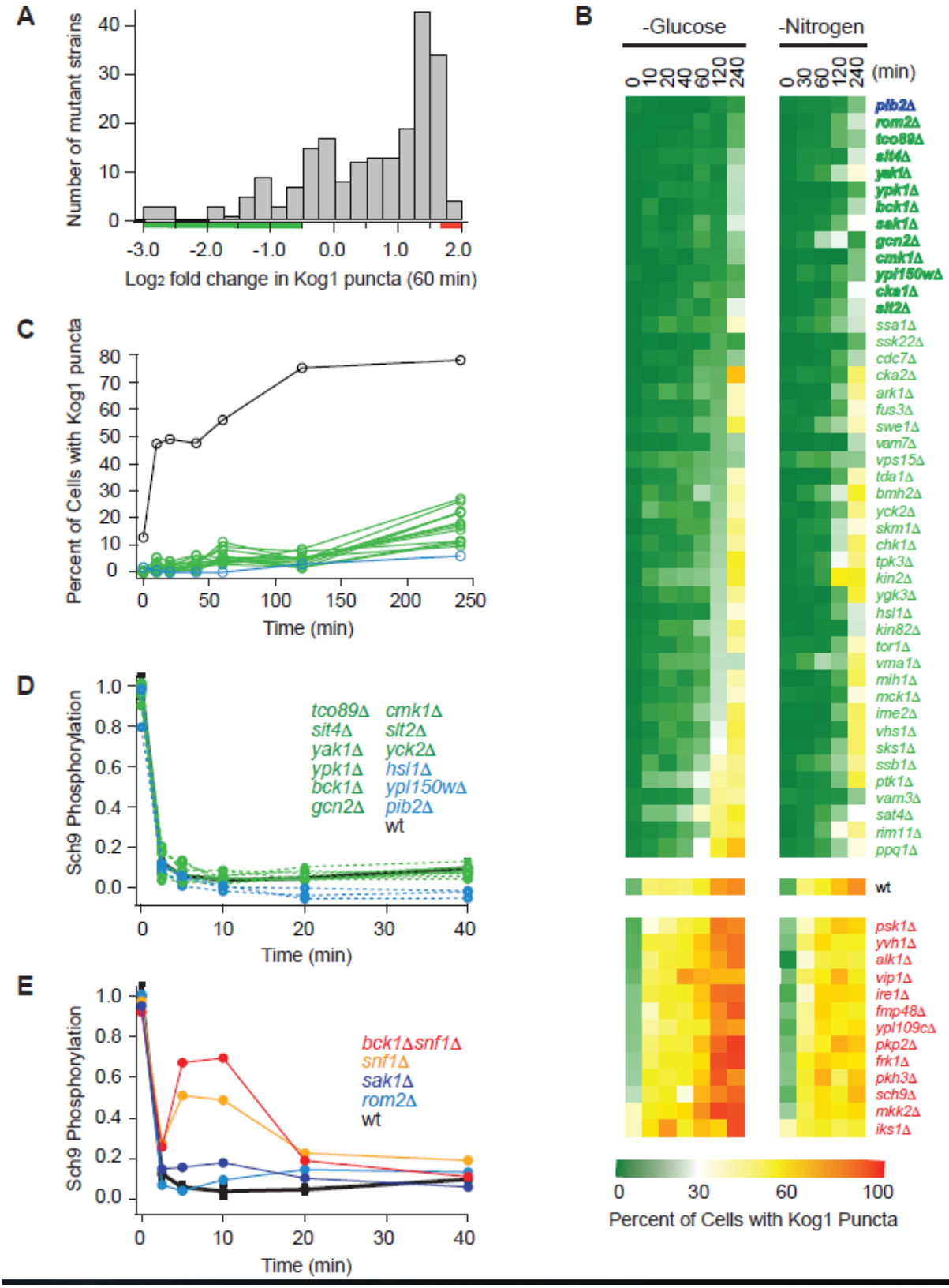
A
Number of mutant strains
Log2 fold change in Kog1 puncta (60 min)
B
-Glucose
-Nitrogen
(min)
pib2Δ
rom2Δ
tco89Δ
slt4Δ
yak1Δ
ypk1Δ
bck1Δ
sak1Δ
gcn2Δ
cmk1Δ
ypl150wΔ
cka1Δ
slt2Δ
ssa1Δ
ssk22Δ
cdc7Δ
cka2Δ
ark1Δ
fus3Δ
swe1Δ
vam7Δ
vps15Δ
tda1Δ
bmh2Δ
yck2Δ
skm1Δ
chk1Δ
tpk3Δ
kin2Δ
ygk3Δ
hsl1Δ
kin82Δ
tor1Δ
vma1Δ
mih1Δ
mck1Δ
ime2Δ
vhs1Δ
sks1Δ
ssb1Δ
ptk1Δ
vam3Δ
sat4Δ
rim11Δ
ppq1Δ
wt
psk1Δ
yvh1Δ
alk1Δ
vip1Δ
ire1Δ
fmp48Δ
ypl109cΔ
pkp2Δ
frk1Δ
pkh3Δ
sch9Δ
mkk2Δ
iks1Δ
Percent of Cells with Kog1 Puncta
C
Percent of Cells with Kog1 puncta
Time (min)
D
Sch9 Phosphorylation
tco89Δ
sit4Δ
yak1Δ
ypk1Δ
bck1Δ
gcn2Δ
cmk1Δ
slt2Δ
yck2Δ
hsl1Δ
ypl150wΔ
pib2Δ
wt
Time (min)
E
Sch9 Phosphorylation
bck1Δsnf1Δ
snf1Δ
sak1Δ
rom2Δ
wt
Time (min)

Fig. 3. Screen for regulators of TORC1-body formation. (A) Histogram summarizing the influence that deleting 209 different genes (including all 139 non-essential kinases and phosphatases in yeast) has on Kog1-YFP foci formation. The score for each strain is based on the percent of cells that form foci after 60 min of glucose starvation (based on data from at least 100 cells) and is normalized using wild-type data to calculate fold change. The raw data for each strain is included in Table S1. (B) Heat map showing time-course data for the 45 strains that formed the fewest bodies in the initial screen (green/blue gene names), the 13 strains that formed the most bodies in the initial screen (red gene names), and the wild-type strain (wt), in glucose and nitrogen starvation conditions. Each colored square shows the fraction of cells with Kog1-puncta at a particular time-point, based on images of at least 100 cells. (C) Time course data for the 13 strains with the largest defects in body formation (green and blue lines; gene names shown in bold in panel B), and the wild-type strain (black line). (D-E) Quantification of band-shift data measuring Sch9 phosphorylation during glucose starvation in strains missing key regulators of TORC1-body formation. The data was normalized so that the level of Sch9 phosphorylation in the wild-type strain at time zero is set at 1.0. The raw bandshift data for each strain is shown in Fig. S3.

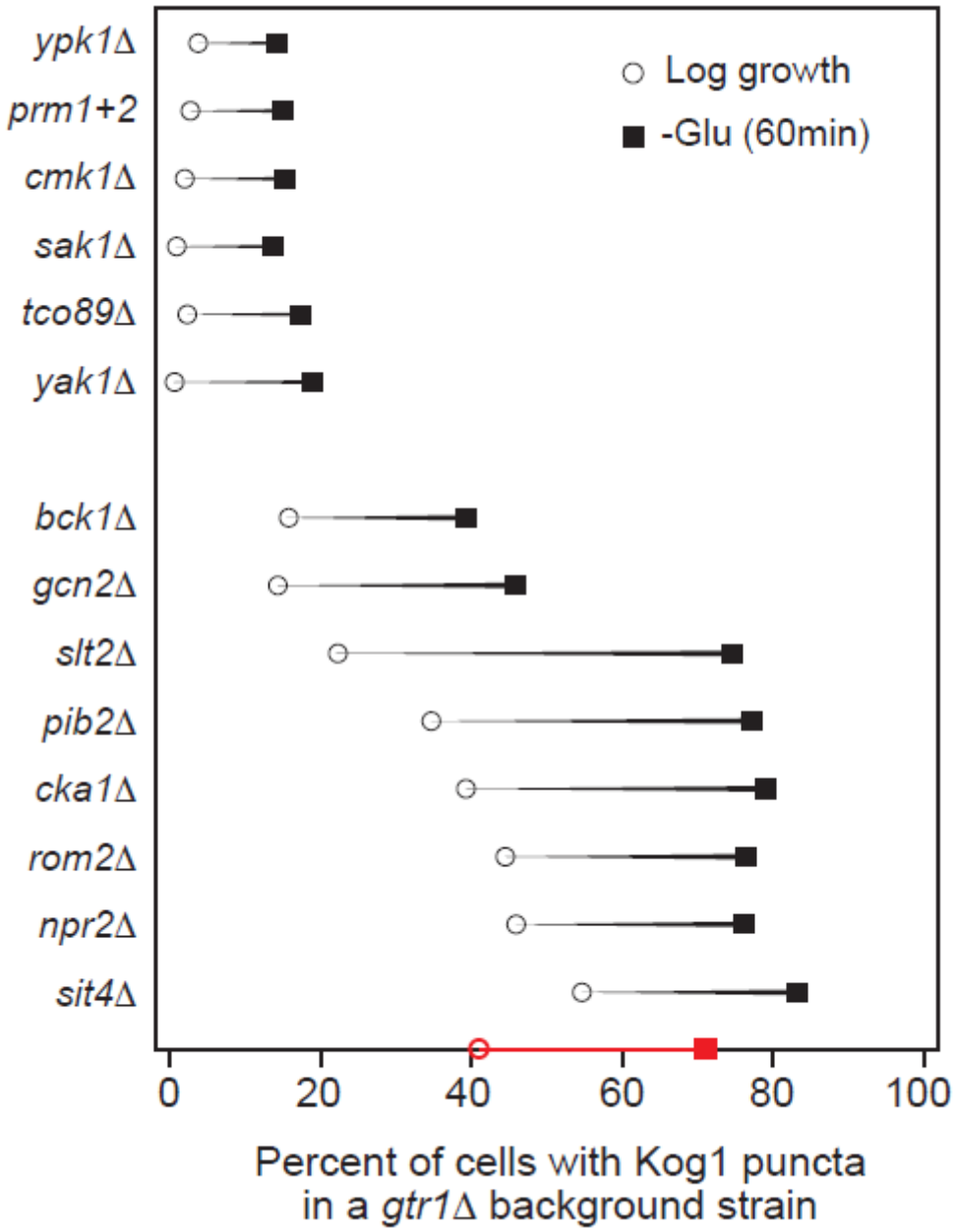

Fig. 4. Cooperation between Gtr1 and key regulators of TORC1-body formation. Impact that deleting key regulators of TORC1-body formation, or mutating the prion domains in Kog1

(PrDm1+2), has on Kog1-YFP puncta formation in a gtr1Δ background. Black circles show the percent of cells with bodies in log growth cultures, while black squares show the percent of cells with bodies after 60 min of glucose starvation. The values shown are the average from experiments carried out on at least two different days with >100 cells per time-point, per replicate. The standard deviation is <5% for all mutants and time points except for sak1Δ (60 min), gcn2Δ60 min), pib2Δ60 min), cka1Δ0 min), sit4Δ0 min) which have standard deviations of 5-10%; npr2Δ0 min), sit4Δ0 min) and sit4Δ60 min) which have standard deviations of 10-15%; and slt2Δ60 min) and npr2Δ60 min) which have standard deviations of 15-20%. The red circle and square on the x-axis shows the data for the gtr1Δsingle mutant for comparison.

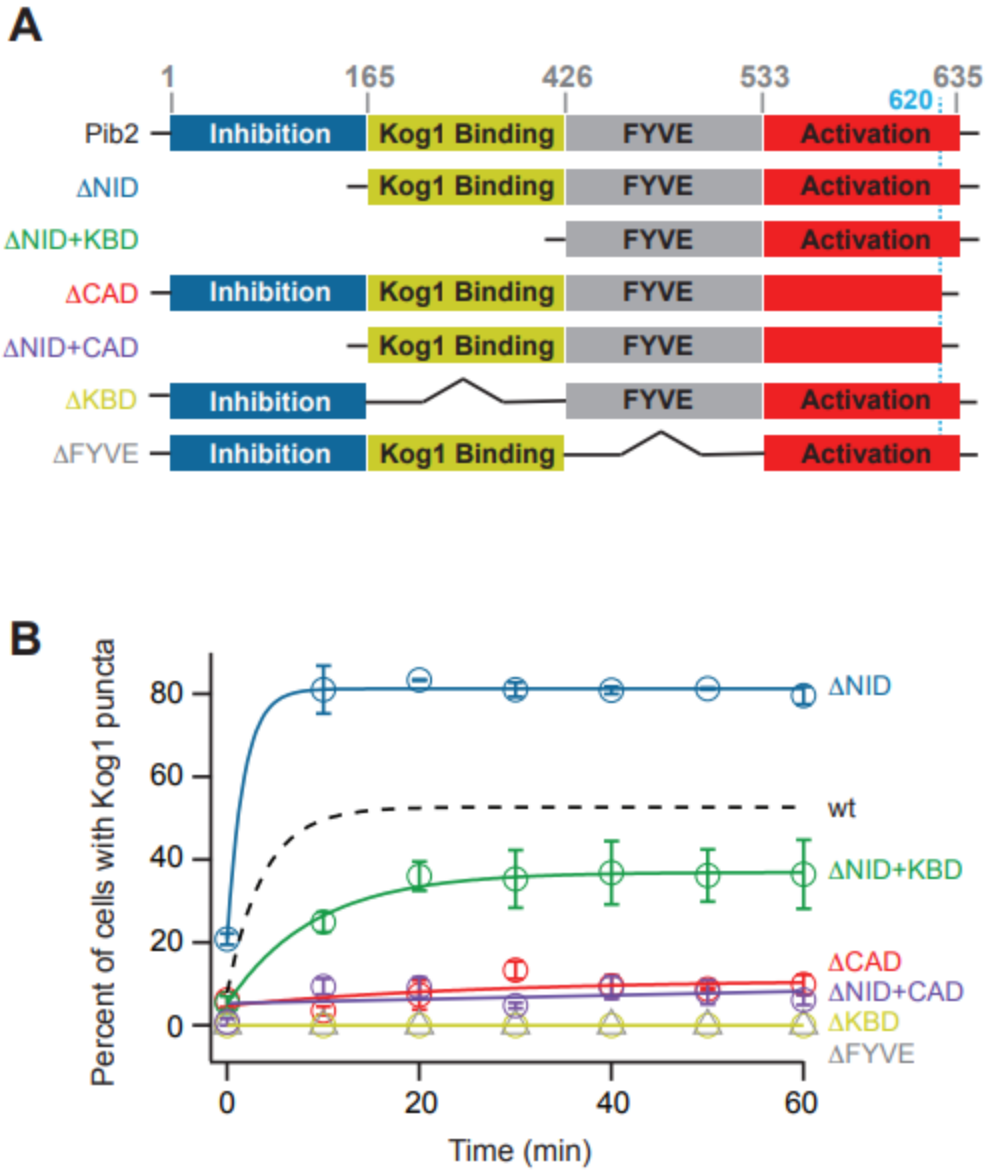

Fig. 5. Impact of Pib2 domains on TORC1-body formation. (A) Map of the different domains in Pib2 (as described in the text), and the structure of the Pib2 truncation mutants we constructed. The black lines in the ΔKBD and ΔFYVE mutants show that the neighboring domains are connected and do not represent polypeptide. (B) Time-course data following Kog1-YFP localization in strains carrying truncated forms of Pib2 at the Pib2 locus. Each time point shows

the average and standard deviation from experiments carried out on two different days, with 70-200 cells per time point, per replicate (except t=0, ΔNID+CAD which had >40 cells per replicate). The solid lines show the best fit to a single exponential for the ΔNID, ΔNID+KBD, ΔCAD, and ΔNID+CAD strains, and a straight line for the ΔKBD and ΔFYVE strains. The broken line shows the best fit to the wild-type data (from Fig. 2) for comparison. Overexpression of Pib2 had little impact on TORC1-body formation, see Fig. S6 and supplemental text for details.

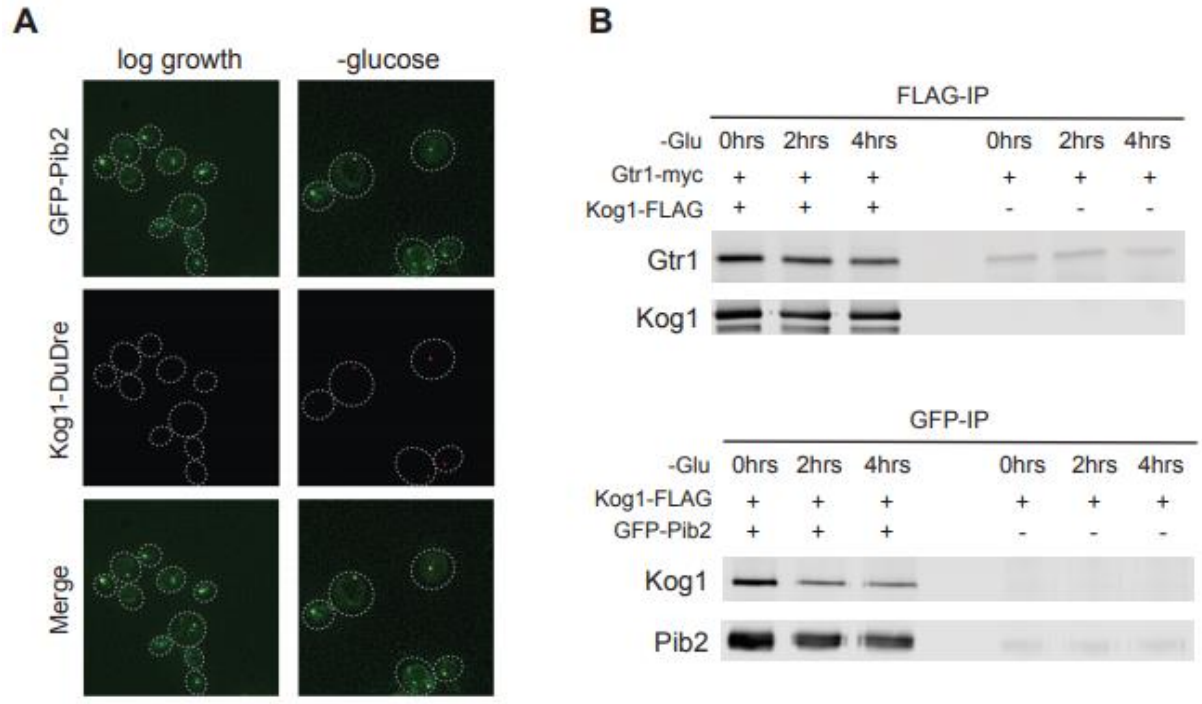

Fig. 6. Pib2, EGOC and TORC1 interact in log growth and starvation conditions. (A) Localization of GFP-Pib2 and Kog1-DuDre during log growth (left panels) and after 60 min of glucose starvation (right panels). The dashed lines show the position of each cell in the bright-field image. (B) Co-immunoprecipitation experiments following interactions between Gtr1 and Kog1 (top panel) and Pib2 and Kog1 (lower panel) before (0 min) and after 2 and 4 hrs of glucose starvation. The right-hand side of each blot shows the data for a mock IP (IP from cells missing the epitope tag on Kog1 or Pib2) used to measure the background levels of Gtr1 and Kog1 in the precipitate.

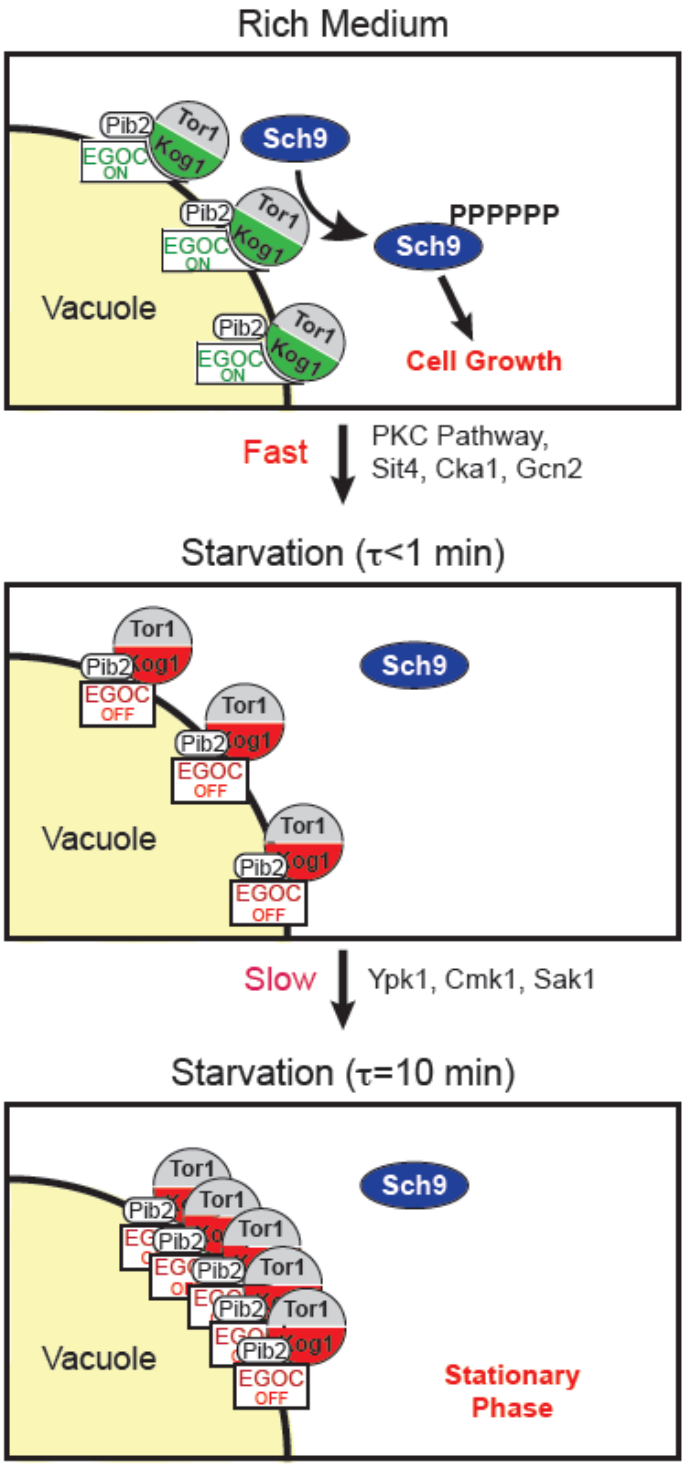

Fig. 7. Working model of TORC1 regulation. See text for details.

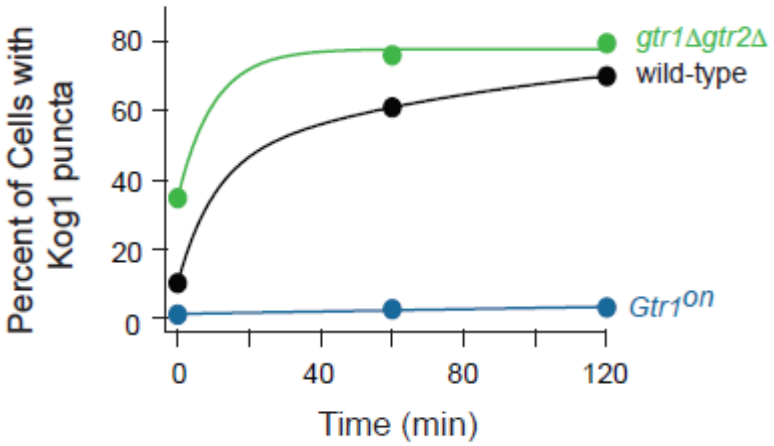

Fig. S1. EGOC regulates TORC1-body formation in nitrogen starvation. Time-course data showing the fraction of cells containing Kog1-YFP puncta in the wild-type strain and strains missing Gtr1/2, or carrying a constitutively active Gtr1 allele (Gtr1on), during nitrogen starvation (as labelled). Each time point shows the data from 90-180 cells, per time point. The solid lines show the best fit to a single exponential for the gtr1Δgtr2Δ strain, a double exponential for the wild-type strain, and a straight line for the Gtr1on strain, using the same rate constants found in glucose starvation.

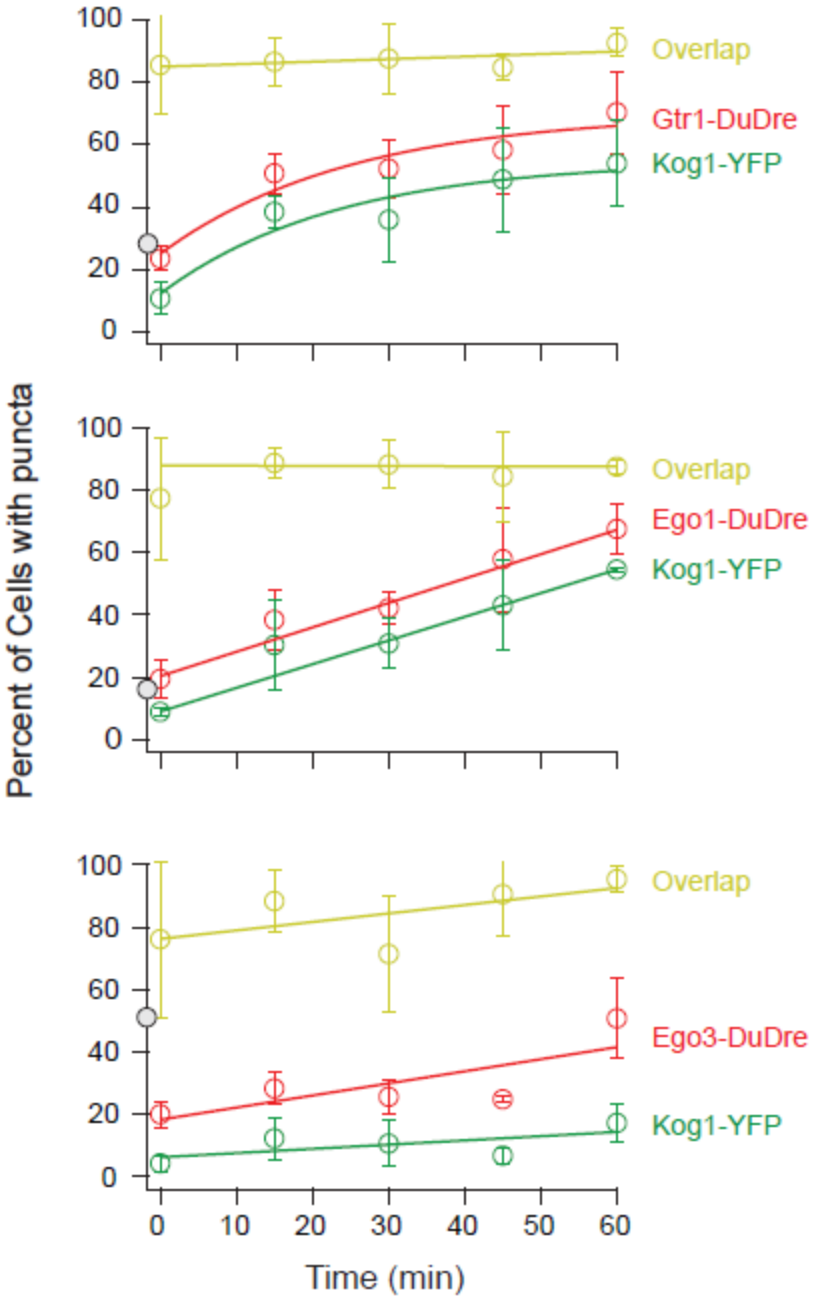

Fig. S2. EGOC and TORC1 co-localization during starvation. Time-course data showing the fraction of cells containing EGOC puncta and/or TORC1-bodies during glucose starvation as

measured in strains expressing Kog1-YFP and Gtr1-DuDre, Ego1-DuDre or Ego3-DuDre (top, middle and bottom panels, respectively). The yellow points and lines show the percent of TORC1 bodies that co-localize with EGOC foci. Each time-point shows the average and standard deviation from three experiments, with 100-300 cells per time-point, per replicate. The grey points (on the y-axis) show the number of cells with EGOC foci in SD medium in cells carrying the relevant EGOC subunit tagged with DuDre, but no Kog1-YFP.

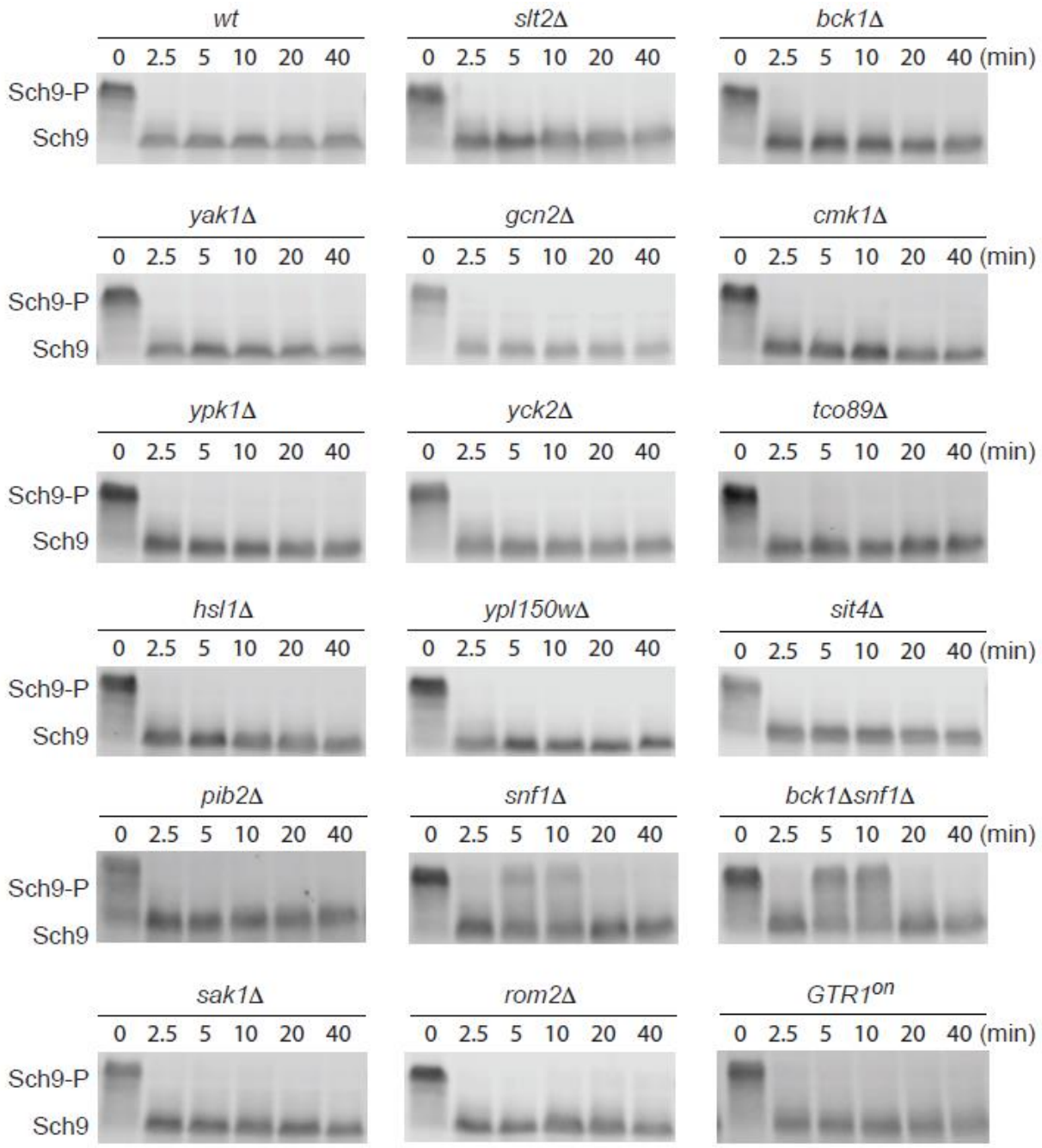

Fig. S3. Sch9 phosphorylation during glucose starvation. Western blots following Sch9 phosphorylation during glucose starvation in the wild-type strain, and mutant strains with severe defects in TORC1-body formation.

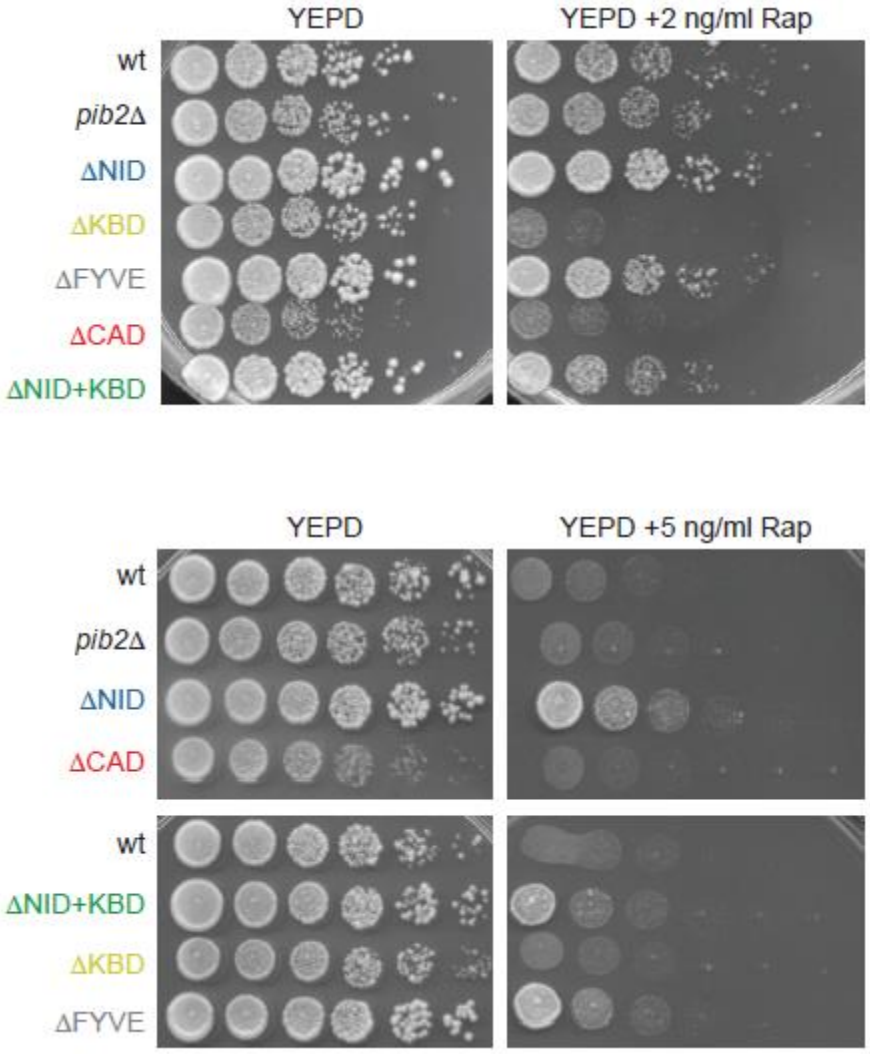

Fig. S4. Rapamycin sensitivity of Pib2 truncation mutants. The strains examined in Fig. 5 were spotted onto YEPD plates containing 0, 2 or 5 ng/ml rapamycin, with a five-fold dilution at each step.

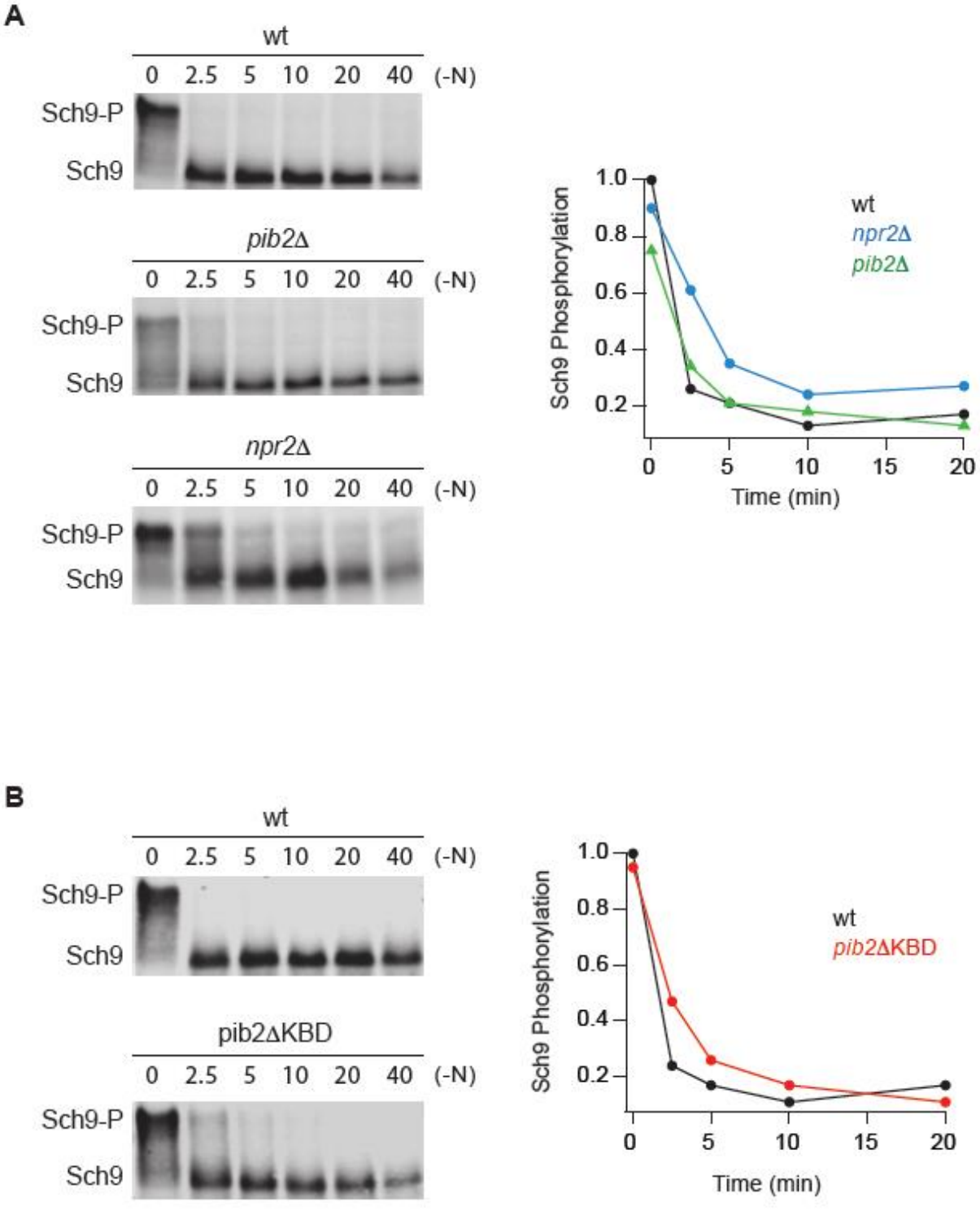
A
wt
0 2.5 5 10 20 40 (-N)
Sch9-P
Sch9
pib2Δ
0 2.5 5 10 20 40 (-N)
Sch9-P
Sch9
npr2Δ
0 2.5 5 10 20 40 (-N)
Sch9-P
Sch9
Sch9 Phosphorylation
1.0
0.8
0.6
0.4
0.2
0 5 10 15 20
Time (min)
wt
npr2Δ
pib2Δ
B
wt
0 2.5 5 10 20 40 (-N)
Sch9-P
Sch9
pib2ΔKBD
0 2.5 5 10 20 40 (-N)
Sch9-P
Sch9
Sch9 Phosphorylation
1.0
0.8
0.6
0.4
0.2
0 5 10 15 20
Time (min)
wt
pib2ΔKBD

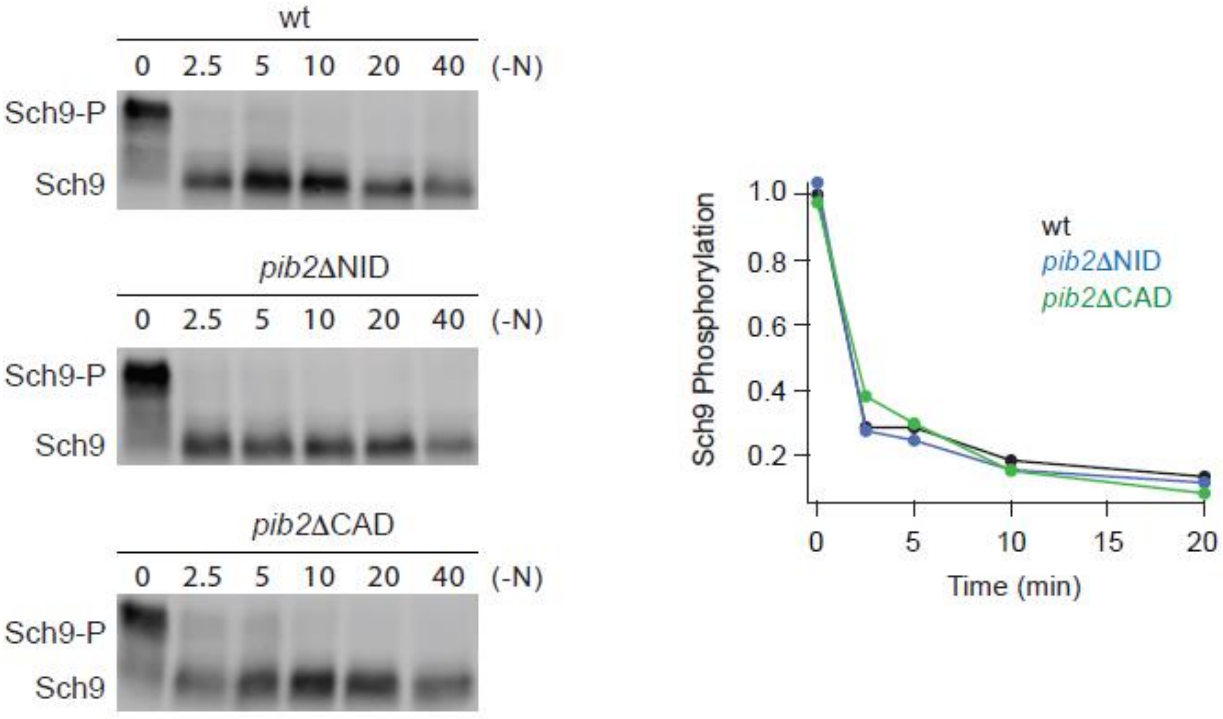

Fig. S5+S6. Sch9 phosphorylation kinetics of Pib2 truncation mutants during nitrogen starvation. Western blots following Sch9 phosphorylation during nitrogen starvation in the wild-type strain, npr2Δ□ and select Pib2 truncation mutants (Fig. 5). Experiments were performed and analyzed as described in Figs. 3d and e.

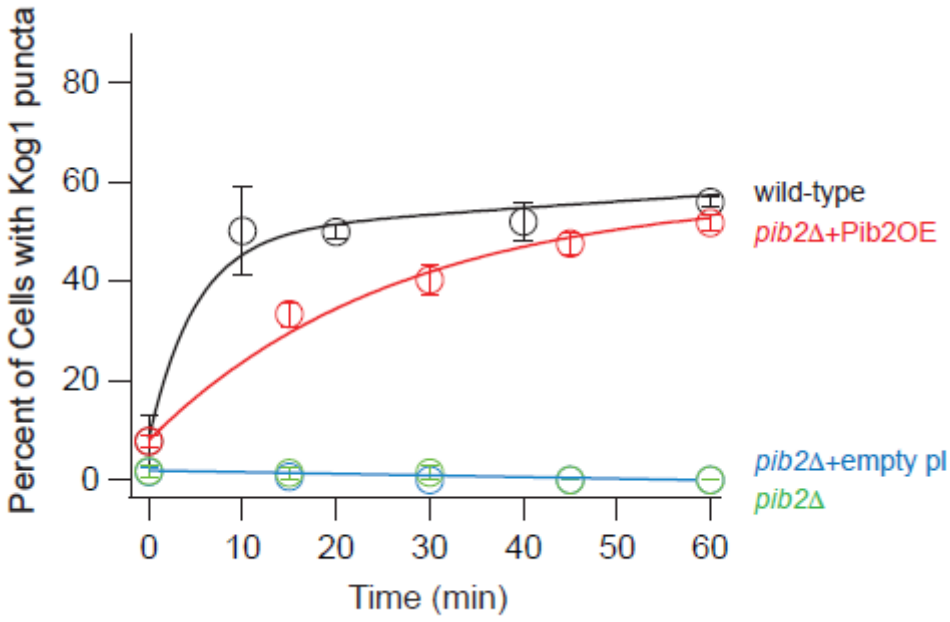

Fig. S7. Overexpression of Pib2 slows TORC1-body formation. Time-course data showing the fraction of cells containing Kog1-YFP puncta in the wild-type strain and strains missing Pib2, missing Pib2 and carrying an empty p415 plasmid (pib2Δ + empty vector), or missing Pib2 and carrying a p415 plasmid with Pib2 under control of a CYC1 promoter (pib2Δ + Pib2OE). Each time-point shows the average and standard deviation from three experiments, with 100-300 cells per time-point, per replicate.

CHAPTER 4: DISCUSSION AND FUTURE DIRECTIONS

Both studies presented here highlight the complex nature of growth control in a living cell. I believe our work has shed some light on the nature of TORC1 signaling while also opening new and exciting questions. Research directed at discovering the molecular basis of each input and output of TORC1 in single cellular systems and mTORC1 in humans has gone on for decades and likely will for many years to come, both as a pursuit in basic science and to further our knowledge of the roles TORC1 plays in aging, development, and disease.

4.1 Uncovering regulators in stress conditions

Though our high-throughput assay proved robust on a technical level it is known that some strains in the yeast knock-out library have acquired suppressor mutations, which may be even be more abundant in genes that affect growth control, and thus could lead to false negatives or false positives in our work (Ben-Shitrit et al., 2012; Giaever & Nislow, 2014; S. Huang & O'Shea, 2005; Hughes et al., 2000). One method to unearth some of these errors is to perform the assay on both the mating type A and alpha libraries and cancel out genes that do not have matching data output. I believe that since the strength of our assay is based in the ability to grow and isolate DNA/RNA from yeast strains in a high-throughput manner that we are also in a position to obtain more data than just the expression of one ribosomal biogenesis gene and one control gene. For instance, we could use a multiplexed optical DNA coding nanobeads (MOCNBs) (L. Li et al., 2015) system to interrogate multiple targets/controls at the same time; this would both give more data about the

cells' transcriptional programming but may also offer ways to combat false readings with more controls. Similarly, if it ever becomes less expensive for thousands of samples, we could instead do whole transcriptome sequencing on our purified RNA. Running more screens in this fashion but with other stress or nutrient starvation conditions may also highlight which gene/pathways are core to the larger TORC1 signaling network and which are specific to one type of stress. Systems wide studies like these do not overtly tell us the direct regulators of TORC1 that we seek, but rather they give us hints of where to focus future deeper work. The addition of Pib2 to the TORC1 body screen in Chapter 3 is an example of this.

4.2 Expanding the TORC1 network

More questions remain concerning TORC1-bodies. Foremost, it is unclear if TORC1, EGOC and Pib2 are the only components in the body. One study has noted that a number of yeast kinases move into a focus in stationary phase (Shah et al., 2014). Whether or not this a common feature for kinase regulation in yeast and if any of these foci interact with each other is an interesting question. We show that TORC1 is inactive by observing levels of Sch9 phosphorylation under conditions of starvation – even when unable to form a body – but others have postulated that in yeast the Tor1 kinase maybe be constitutively active which raises the question of whether TORC1's active site is occluded when in an aggregate or if it has new and unknown substrates that can associate with the body (Prouteau et al., 2017; Yang et al., 2013).

The EGOC foci and its role in growth and starvation are also interesting for future work. The Rag GTPases, Gtr1/2, do have suggested TORC1-independent roles in endocytosis (MacDonald & Piper, 2017). It would be interesting if the EGOC foci was also the location of Gtr1/2 loading onto Ego1/2/3 post-endocytosis or if it is some other configuration of the complex. Further, it has been shown that the I-BAR protein Ivy1 co-localizes to the EGOC foci (Itoh, Kida, Hanawa-Suetsugu, & Suetsugu, 2016; Numrich et al., 2015; Wang, Miao, & Chang, 2014) and in late starvation re-localizes with EGOC proteins to segmented domains of the vacuole that are sterol rich and sites of lipophagy, suggesting yet another role for EGOC proteins (Wang et al., 2014). Interestingly, in cells I have viewed that have these domains present, the TORC1-body appears to stay at the edge between two or more of these domains (data not shown); whether it can sense lipophagy or is simply sequestered is an open question.

In stress conditions Ivy1 also activates the PI3P-5 kinase Fab1, converting PI3P to PI3P-5 (Malia et al., 2018). Fab1 was a moderate defect in our screen in Chapter 3, and it is possible that the homeostasis of different phospholipids changes the ability of TORC1 to aggregate or find interactions (Elbaz-Alon et al., 2014; Hönscher et al., 2014; Jin, Lang, & Weisman, 2016a, 2016b; Jin et al., 2014; Murley et al., 2015; Numrich et al., 2015). The ability of Ivy1 to move out of a focus seems dependent on being bound to the GTPase Ytp7, which also binds the GEF for Gtr1, Vam6, and has interactions with the vacuole-mitochondria complex vCLAMP (Murley & Nunnari, 2016; Numrich et al., 2015). The complex interplay between TORC1, the vacuole, and these components, when changing from growth to starvation conditions, is an exciting new area of study.

As with EGOC most of the work being done by other groups looking at the PI3P binding protein Pib2 in recent years has been focused in its role in amino acid signaling to TORC1 (Kim & Cunningham, 2015; Michel et al., 2017; Ukai et al., 2018; Varlakhanova, Mihalevic, Bernstein, & Ford, 2017), but as we show in Chapter 3 it is also an important regulator in starvation conditions. The importance of the NID domain and the CAD domain of Pib2 (Kim & Cunningham, 2015; Michel et al., 2017) in TORC1 signaling and body formation highlights a difficulty in the study of the protein. Tagging either the N-terminal or C-terminal ends of the protein with a fluorescent or epitope tag could have undesired effects in its ability to signal to TORC1 as a full-length protein. Likewise creating an internal tag could disrupt the Kog1 binding domain or the FYVE domain. As pointed out by the Cunningham group, there is a distant homolog in humans to Pib2, LAPF/phafin1(Kim & Cunningham, 2015), and although the N-terminal domain of Pib2 is missing in LAPF/phafin1 I would be curious if it assists in the regulation of mTORC1 signaling/localization in mammalian systems. Future work on the Pib2 protein and its role in TORC1 signaling will help our understanding with the nature of its regulation.

APPENDIX A – PERMISSIONS

CHAPTER 2 Permissions

From: http://www.g3journal.org/content/permissions

‘G3 articles are published as open-access articles distributed under the terms of the Creative Commons Attribution 4.0 International License (http://creativecommons.org/licenses/by/4.0/), which permits unrestricted use, distribution, and reproduction in any medium, provided the original work is properly cited.’

CHAPTER 3 Permissions

From: https://www.molbiolcell.org/permissions

Effective 1-28-2019

‘Under the License and Publishing Agreement, authors grant to the general public, effective two months after publication of (i.e., the appearance of the edited manuscript in an online issue of MBoC), the nonexclusive right to copy, distribute, or display the manuscript subject to the terms of the Creative Commons–Noncommercial–Share Alike 3.0 Unported license (http://creativecommons.org/licenses/by-nc-sa/3.0).

For further information, please see http://creativecommons.org/licenses/by-nc-sa/3.0’

REFERENCES

Adami, A., García-Álvarez, B., Arias-Palomo, E., Barford, D., & Llorca, O. (2007a). *Structure of TOR and Its Complex with KOG1*. *Molecular Cell* (Vol. 27). Retrieved from http://www.sciencedirect.com/science/article/pii/S1097276507003723

Adami, A., García-Álvarez, B., Arias-Palomo, E., Barford, D., & Llorca, O. (2007b). Structure of TOR and Its Complex with KOG1. *Molecular Cell*, *27*(3), 509–516. https://doi.org/10.1016/J.MOLCEL.2007.05.040

Alejandro-Osorio, A. L., Huebert, D. J., Porcaro, D. T., Sonntag, M. E., Nillasithanukroh, S., Will, J. L., & Gasch, A. P. (2009). The histone deacetylase Rpd3p is required for transient changes in genomic expression in response to stress. *Genome Biology*, *10*(5), R57. https://doi.org/10.1186/gb-2009-10-5-r57

Algret, R., Fernandez-Martinez, J., Shi, Y., Kim, S. J., Pellarin, R., Cimermancic, P., … Dokudovskaya, S. (2014). Molecular architecture and function of the SEA complex, a modulator of the TORC1 pathway. *Molecular & Cellular Proteomics : MCP*, *13*(11), 2855–2870. https://doi.org/10.1074/mcp.M114.039388

Ashrafi, K., Farazi, T. A., & Gordon, J. I. (1998). A role for Saccharomyces cerevisiae fatty acid activation protein 4 in regulating protein N-myristoylation during entry into stationary phase. *The Journal of Biological Chemistry*, *273*(40), 25864–25874. https://doi.org/10.1074/JBC.273.40.25864

Bar-Peled, L., & Sabatini, D. M. (2014). Regulation of mTORC1 by amino acids. *Trends in Cell Biology*. https://doi.org/10.1016/j.tcb.2014.03.003

Bar-Peled, L., Schweitzer, L. D., Zoncu, R., & Sabatini, D. M. (2012). Ragulator is a GEF for the rag GTPases that signal amino acid levels to mTORC1. *Cell*, *150*(6), 1196–1208. https://doi.org/10.1016/j.cell.2012.07.032

Barbet, N. C., Schneider, U., Helliwell, S. B., Stansfield, I., Tuite, M. F., & Hall, M. N. (1996). TOR controls translation initiation and early G1 progression in yeast. *Molecular Biology of the Cell*, *7*(1), 25–42. https://doi.org/10.1091/mbc.7.1.25

Beck, T., & Hall, M. N. (1999). The TOR signalling pathway controls nuclear localization of nutrient-regulated transcription factors. *Nature*, *402*(6762), 689–692. https://doi.org/10.1038/45287

Ben-Shitrit, T., Yosef, N., Shemesh, K., Sharan, R., Ruppin, E., & Kupiec, M. (2012). Systematic identification of gene annotation errors in the widely used yeast mutation collections. *Nature Methods*, *9*(4), 373–378. https://doi.org/10.1038/nmeth.1890

Betz, C., & Hall, M. N. (2013). Where is mTOR and what is it doing there? *The Journal of Cell Biology*, *203*(4), 563–574. https://doi.org/10.1083/jcb.201306041

Binda, M., Péli-Gulli, M.-P., Bonfils, G., Panchaud, N., Urban, J., Sturgill, T. W., … De Virgilio, C. (2009). The Vam6 GEF controls TORC1 by activating the EGO complex. *Molecular Cell*, *35*(5), 563–573. https://doi.org/10.1016/j.molcel.2009.06.033

Bonfils, G., Jaquenoud, M., Bontron, S., Ostrowicz, C., Ungermann, C., & De Virgilio, C. (2012). Leucyl-tRNA synthetase controls TORC1 via the EGO complex. *Molecular Cell*, *46*(1), 105–110. https://doi.org/10.1016/j.molcel.2012.02.009

Bosotti, R., Isacchi, A., & Sonnhammer, E. L. (2000). FAT: a novel domain in PIK-related

kinases. *Trends in Biochemical Sciences*, *25*(5), 225–227. https://doi.org/10.1016/S0968-0004(00)01563-2

Braun, K. A., Vaga, S., Dombek, K. M., Fang, F., Palmisano, S., Aebersold, R., & Young, E. T. (2014). Phosphoproteomic analysis identifies proteins involved in transcription-coupled mRNA decay as targets of Snf1 signaling. *Science Signaling*, *7*(333), ra64. https://doi.org/10.1126/scisignal.2005000

Breitkreutz, A., Choi, H., Sharom, J. R., Boucher, L., Neduva, V., Larsen, B., … Tyers, M. (2010). A global protein kinase and phosphatase interaction network in yeast. *Science (New York, N.Y.)*, *328*(5981), 1043–1046. https://doi.org/10.1126/science.1176495

Cafferkey, R., Young, P. R., McLaughlin, M. M., Bergsma, D. J., Koltin, Y., Sathe, G. M., … Livi, G. P. (1993). Dominant missense mutations in a novel yeast protein related to mammalian phosphatidylinositol 3-kinase and VPS34 abrogate rapamycin cytotoxicity. *Molecular and Cellular Biology*, *13*(10), 6012–6023. Retrieved from http://www.ncbi.nlm.nih.gov/pubmed/8413204

Carroll, B., Maetzel, D., Maddocks, O. D. K., Otten, G., Ratcliff, M., Smith, G. R., … Korolchuk, V. I. (2016). Control of TSC2-Rheb signaling axis by arginine regulates mTORC1 activity. *ELife*. https://doi.org/10.7554/eLife.11058.001

Causton, H. C., Ren, B., Koh, S. S., Harbison, C. T., Kanin, E., Jennings, E. G., … Young, R. A. (2001). Remodeling of Yeast Genome Expression in Response to Environmental Changes. *Mol. Biol. Cell*, *12*, 323–337. Retrieved from http://www.molbiolcell.org/cgi/content/abstract/12/2/323

Chantranupong, L., Wolfson, R. L., & Sabatini, D. M. (2015). Nutrient-sensing mechanisms across evolution. *Cell*, *161*(1). https://doi.org/10.1016/j.cell.2015.02.041

Choi, J., Chen, J., & Schreiber, S. L. (1996). Structure of the FKBP1 2-Rapamycin Complex Interacting. *Science*, 239–242.

Dames, S. A., Mulet, J. M., Rathgeb-Szabo, K., Hall, M. N., & Grzesiek, S. (2005). The solution structure of the FATC domain of the protein kinase target of rapamycin suggests a role for redox-dependent structural and cellular stability. *The Journal of Biological Chemistry*, *280*(21), 20558–20564. https://doi.org/10.1074/jbc.M501116200

De Virgilio, C. (2012). The essence of yeast quiescence. *FEMS Microbiology Reviews*, *36*(2), 306–339. https://doi.org/10.1111/j.1574-6976.2011.00287.x

De Virgilio, C., & Loewith, R. (2006). The TOR signalling network from yeast to man. *The International Journal of Biochemistry & Cell Biology*, *38*(9), 1476–1481. https://doi.org/10.1016/j.biocel.2006.02.013

Dechant, R., Binda, M., Lee, S. S., Pelet, S., Winderickx, J., & Peter, M. (2010). Cytosolic pH is a second messenger for glucose and regulates the PKA pathway through V-ATPase. *The EMBO Journal*, *29*. https://doi.org/10.1038/emboj.2010.138

Demetriades, C., Doumpas, N., & Teleman, A. A. (2014). Regulation of TORC1 in response to amino acid starvation via lysosomal recruitment of TSC2. *Cell*, *156*(4), 786–799. https://doi.org/10.1016/j.cell.2014.01.024

Dubouloz, F., Deloche, O., Wanke, V., Cameroni, E., & De Virgilio, C. (2005). The TOR and EGO protein complexes orchestrate microautophagy in yeast. *Molecular Cell*, *19*(1), 15–26. https://doi.org/10.1016/j.molcel.2005.05.020

Durán, R. V, & Hall, M. N. (2012). Regulation of TOR by small GTPases. *EMBO Reports*,

13(2), 121–128. https://doi.org/10.1038/embor.2011.257
Düvel, K., Yecies, J. L., Menon, S., Raman, P., Lipovsky, A. I., Souza, A. L., … Manning, B. D. (2010). Activation of a metabolic gene regulatory network downstream of mTOR complex 1. *Molecular Cell*, *39*(2), 171–183. https://doi.org/10.1016/j.molcel.2010.06.022
Efeyan, A., Comb, W. C., & Sabatini, D. M. (2015). Nutrient-sensing mechanisms and pathways. *Nature*, *517*(7534), 302–310. https://doi.org/10.1038/nature14190
Elbaz-Alon, Y., Rosenfeld-Gur, E., Shinder, V., Futerman, A. H., Geiger, T., & Schuldiner, M. (2014). A Dynamic Interface between Vacuoles and Mitochondria in Yeast. *Developmental Cell*, *30*(1), 95–102. https://doi.org/10.1016/j.devcel.2014.06.007
Gasch, a P., Spellman, P. T., Kao, C. M., Carmel-Harel, O., Eisen, M. B., Storz, G., … Brown, P. O. (2000). Genomic expression programs in the response of yeast cells to environmental changes. *Molecular Biology of the Cell*, *11*(12), 4241–4257. Retrieved from http://www.pubmedcentral.nih.gov/articlerender.fcgi?artid=15070&tool=pmcentrez&rendertype=abstract
Gaubitz, C., Prouteau, M., Kusmider, B., & Loewith, R. (2016). TORC2 Structure and Function. *Trends in Biochemical Sciences*. https://doi.org/10.1016/j.tibs.2016.04.001
Giaever, G., & Nislow, C. (2014). The yeast deletion collection: a decade of functional genomics. *Genetics*, *197*(2), 451–465. https://doi.org/10.1534/genetics.114.161620
González, A., & Hall, M. N. (2017). Nutrient sensing and TOR signaling in yeast and mammals. *The EMBO Journal*, *36*(4), 397–408. https://doi.org/10.15252/embj.201696010
Hallett, J. E. H., Luo, X., Capaldi, A. P., Hughes Hallett, J. E., Luo, X., & Capaldi, A. P. (2014). State Transitions in the TORC1 Signaling Pathway and Information Processing in Saccharomyces cerevisiae. *Genetics*. https://doi.org/10.1534/genetics.114.168369
Hedbacker, K., & Carlson, M. (2008). SNF1/AMPK pathways in yeast. *Frontiers in Bioscience : A Journal and Virtual Library*, *13*, 2408–2420. Retrieved from http://www.ncbi.nlm.nih.gov/pubmed/17981722
Helliwell, S. B., Wagner, P., Kunz, J., Deuter-Reinhard, M., Henriquez, R., & Hall, M. N. (1994). TOR1 and TOR2 are structurally and functionally similar but not identical phosphatidylinositol kinase homologues in yeast. *Molecular Biology of the Cell*, *5*(1), 105–118. Retrieved from http://www.ncbi.nlm.nih.gov/pubmed/8186460
Hönscher, C., Mari, M., Auffarth, K., Bohnert, M., Griffith, J., Geerts, W., … Ungermann, C. (2014). Cellular Metabolism Regulates Contact Sites between Vacuoles and Mitochondria. *Developmental Cell*, *30*(1), 86–94. https://doi.org/10.1016/j.devcel.2014.06.006
Hsu, P. P., Kang, S. A., Rameseder, J., Zhang, Y., Ottina, K. A., Lim, D., … Sabatini, D. M. (2011). The mTOR-regulated phosphoproteome reveals a mechanism of mTORC1-mediated inhibition of growth factor signaling. *Science (New York, N.Y.)*, *332*(6035), 1317–1322. https://doi.org/10.1126/science.1199498
Huang, J., & Manning, B. D. (2008). The TSC1-TSC2 complex: a molecular switchboard controlling cell growth. *The Biochemical Journal*, *412*(2), 179–190. https://doi.org/10.1042/BJ20080281
Huang, S., & O'Shea, E. K. (2005). A systematic high-throughput screen of a yeast deletion collection for mutants defective in PHO5 regulation. *Genetics*, *169*(4), 1859–1871. https://doi.org/10.1534/genetics.104.038695
Huber, A., Bodenmiller, B., Uotila, A., Stahl, M., Wanka, S., Gerrits, B., … Loewith, R. (2009).

Characterization of the rapamycin-sensitive phosphoproteome reveals that Sch9 is a central coordinator of protein synthesis. *Genes & Development*, *23*(16), 1929–1943. https://doi.org/10.1101/gad.532109

Huber, A., French, S., Tekotte, H., & Yerlikaya, S. (2011). Sch9 regulates ribosome biogenesis via Stb3, Dot6 and Tod6 and the histone deacetylase complex RPD3L. *The EMBO …*, *30*(15), 3052–3064. https://doi.org/10.1038/emboj.2011.221

Hughes Hallett, J. E., Luo, X., Capaldi, A. P., Adami, A., García-Alvarez, B., Arias-Palomo, E., … Sabatini, D. (2015). Snf1/AMPK promotes the formation of Kog1/Raptor-bodies to increase the activation threshold of TORC1 in budding yeast. *ELife*, *4*, 509–516. https://doi.org/10.7554/eLife.09181

Hughes, T. R., Roberts, C. J., Dai, H., Jones, A. R., Meyer, M. R., Slade, D., … Marton, M. J. (2000). Widespread aneuploidy revealed by DNA microarray expression profiling. *Nature Genetics*, *25*(3), 333–337. https://doi.org/10.1038/77116

Inoki, K., Zhu, T., & Guan, K.-L. (2003). TSC2 mediates cellular energy response to control cell growth and survival. *Cell*, *115*(5), 577–590. https://doi.org/10.1016/S0092-8674(03)00929-2

Itoh, Y., Kida, K., Hanawa-Suetsugu, K., & Suetsugu, S. (2016). Yeast Ivy1p Is a Putative I-BAR-domain Protein with pH-sensitive Filament Forming Ability in vitro. *Cell Structure and Function*, *41*(1), 1–11. https://doi.org/10.1247/csf.15014

Jiang, Y., & Broach, J. R. (1999). Tor proteins and protein phosphatase 2A reciprocally regulate Tap42 in controlling cell growth in yeast. *The EMBO Journal*, *18*(10), 2782–2792. https://doi.org/10.1093/emboj/18.10.2782

Jin, N., Lang, M. J., & Weisman, L. S. (2016a). Phosphatidylinositol 3,5-bisphosphate: regulation of cellular events in space and time. *Biochemical Society Transactions*, *44*(1), 177–184. https://doi.org/10.1042/BST20150174

Jin, N., Lang, M. J., & Weisman, L. S. (2016b). Phosphatidylinositol 3,5-bisphosphate: regulation of cellular events in space and time. *Biochemical Society Transactions*, *44*(1), 177–184. https://doi.org/10.1042/BST20150174

Jin, N., Mao, K., Jin, Y., Tevzadze, G., Kauffman, E. J., Park, S., … Weisman, L. S. (2014). Roles for PI(3,5)P2 in nutrient sensing through TORC1. *Molecular Biology of the Cell*, *25*(7), 1171–1185. https://doi.org/10.1091/mbc.E14-01-0021

Jorgensen, P., Rupes, I., Sharom, J. R., Schneper, L., Broach, J. R., & Tyers, M. (2004). A dynamic transcriptional network communicates growth potential to ribosome synthesis and critical cell size. *Genes & Development*, *18*(20), 2491–2505. https://doi.org/10.1101/gad.1228804

Kamada, Y., Funakoshi, T., Shintani, T., Nagano, K., Ohsumi, M., & Ohsumi, Y. (2000). Tor-mediated induction of autophagy via an Apg1 protein kinase complex. *The Journal of Cell Biology*, *150*(6), 1507–1513. Retrieved from http://www.ncbi.nlm.nih.gov/pubmed/10995454

Kim, A., & Cunningham, K. W. (2015). A LAPF/phafin1-like protein regulates TORC1 and lysosomal membrane permeabilization in response to endoplasmic reticulum membrane stress. *Molecular Biology of the Cell*, *26*(25), 4631–4645. https://doi.org/10.1091/mbc.E15-08-0581

Kira, S., Kumano, Y., Ukai, H., Takeda, E., Matsuura, A., & Noda, T. (2016). Dynamic

relocation of the TORC1-Gtr1/2-Ego1/2/3 complex is regulated by Gtr1 and Gtr2. *Molecular Biology of the Cell*, *27*(2), 382–396. https://doi.org/10.1091/mbc.E15-07-0470

Kliegman, J. I., Fiedler, D., Ryan, C. J., Xu, Y.-F., Su, X.-Y., Thomas, D., … Shokat, K. M. (2013). Chemical genetics of rapamycin-insensitive TORC2 in S. cerevisiae. *Cell Reports*, *5*(6), 1725–1736. https://doi.org/10.1016/j.celrep.2013.11.040

Laxman, S., Sutter, B. M., Shi, L., & Tu, B. P. (2014). Npr2 inhibits TORC1 to prevent inappropriate utilization of glutamine for biosynthesis of nitrogen-containing metabolites. *Science Signaling*, *7*(356), ra120. https://doi.org/10.1126/scisignal.2005948

Lempiäinen, H., Uotila, A., Urban, J., Dohnal, I., Ammerer, G., Loewith, R., & Shore, D. (2009). Sfp1 interaction with TORC1 and Mrs6 reveals feedback regulation on TOR signaling. *Molecular Cell*, *33*(6), 704–716. https://doi.org/10.1016/j.molcel.2009.01.034

Li, H., Tsang, C. K., Watkins, M., Bertram, P. G., & Zheng, X. F. S. (2006). Nutrient regulates Tor1 nuclear localization and association with rDNA promoter. *Nature*, *442*(7106), 1058–1061. https://doi.org/10.1038/nature05020

Li, L., Shen, L., Zhang, X., Shui, L., Sui, B., Zhang, X., … Jin, W. (2015). Multiplexed optical coding nanobeads and their application in single-molecule counting analysis for multiple gene expression analysis. *Analytica Chimica Acta*, *886*, 123–132. https://doi.org/10.1016/J.ACA.2015.05.042

Liko, D., Slattery, M. G., & Heideman, W. (2007). Stb3 binds to ribosomal RNA processing element motifs that control transcriptional responses to growth in Saccharomyces cerevisiae. *The Journal of Biological Chemistry*, *282*(36), 26623–26628. https://doi.org/10.1074/jbc.M704762200

Lippman, S. I., & Broach, J. R. (2009). Protein kinase A and TORC1 activate genes for ribosomal biogenesis by inactivating repressors encoded by Dot6 and its homolog Tod6. *Proceedings of the National Academy of Sciences of the United States of America*, *106*(47), 19928–19933. https://doi.org/10.1073/pnas.0907027106

Loewith, R., & Hall, M. N. (2011). Target of rapamycin (TOR) in nutrient signaling and growth control. *Genetics*, *189*(4), 1177–1201. https://doi.org/10.1534/genetics.111.133363

Loewith, R., Jacinto, E., Wullschleger, S., Lorberg, A., Crespo, J. L., Bonenfant, D., … Hall, M. N. (2002). Two TOR complexes, only one of which is rapamycin sensitive, have distinct roles in cell growth control. *Molecular Cell*, *10*(3), 457–468. https://doi.org/10.1016/S1097-2765(02)00636-6

MacDonald, C., & Piper, R. C. (2017). Genetic dissection of early endosomal recycling highlights a TORC1-independent role for Rag GTPases. *The Journal of Cell Biology*, *216*(10), 3275–3290. https://doi.org/10.1083/jcb.201702177

Malia, P. C., Numrich, J., Nishimura, T., González Montoro, A., Stefan, C. J., & Ungermann, C. (2018). Control of vacuole membrane homeostasis by a resident PI-3,5-kinase inhibitor. *Proceedings of the National Academy of Sciences of the United States of America*, *115*(18), 4684–4689. https://doi.org/10.1073/pnas.1722517115

Marion, R. M., Regev, A., Segal, E., Barash, Y., Koller, D., Friedman, N., & O'Shea, E. K. (2004). Sfp1 is a stress- and nutrient-sensitive regulator of ribosomal protein gene expression. *Proceedings of the National Academy of Sciences of the United States of America*, *101*(40), 14315–14322. https://doi.org/10.1073/pnas.0405353101

Martin, D. E., Powers, T., & Hall, M. N. (2006). Regulation of ribosome biogenesis: where is

TOR? *Cell Metabolism*, *4*(4), 259–260. https://doi.org/10.1016/j.cmet.2006.09.002
Menon, S., Dibble, C. C., Talbott, G., Hoxhaj, G., Valvezan, A. J., Takahashi, H., … Manning, B. D. (2014). Spatial control of the TSC complex integrates insulin and nutrient regulation of mTORC1 at the lysosome. *Cell*, *156*(4), 771–785. https://doi.org/10.1016/j.cell.2013.11.049
Michel, A. H., Hatakeyama, R., Kimmig, P., Arter, M., Peter, M., Matos, J., … Kornmann, B. (2017). Functional mapping of yeast genomes by saturated transposition. *ELife*, *6*, e23570. https://doi.org/10.7554/eLife.23570
Murley, A., & Nunnari, J. (2016). The Emerging Network of Mitochondria-Organelle Contacts. https://doi.org/10.1016/j.molcel.2016.01.031
Murley, A., Sarsam, R. D., Toulmay, A., Yamada, J., Prinz, W. A., & Nunnari, J. (2015). Ltc1 is an ER-localized sterol transporter and a component of ER–mitochondria and ER–vacuole contacts. *J Cell Biol*, *209*(4), 539–548. https://doi.org/10.1083/JCB.201502033
Noda, T., & Ohsumi, Y. (1998). Tor, a phosphatidylinositol kinase homologue, controls autophagy in yeast. *The Journal of Biological Chemistry*, *273*(7), 3963–3966. https://doi.org/10.1074/JBC.273.7.3963
Numrich, J., Péli-Gulli, M.-P., Arlt, H., Sardu, A., Griffith, J., Levine, T., … Ungermann, C. (2015). The I-BAR protein Ivy1 is an effector of the Rab7 GTPase Ypt7 involved in vacuole membrane homeostasis. *Journal of Cell Science*, *128*(13).
Obrig, T. G., Culp, W. J., McKeehan, W. L., & Hardesty, B. (1971). The mechanism by which cycloheximide and related glutarimide antibiotics inhibit peptide synthesis on reticulocyte ribosomes. *The Journal of Biological Chemistry*, *246*(1), 174–181. Retrieved from http://www.ncbi.nlm.nih.gov/pubmed/5541758
Pé Rez-Sampietro, M., Casas, C., & Herrero, E. (2013). The AMPK Family Member Snf1 Protects Saccharomyces cerevisiae Cells upon Glutathione Oxidation. *PLoS ONE*, *8*(3). https://doi.org/10.1371/journal.pone.0058283
Péli-Gulli, M. P., Sardu, A., Panchaud, N., Raucci, S., & De Virgilio, C. (2015). Amino Acids Stimulate TORC1 through Lst4-Lst7, a GTPase-Activating Protein Complex for the Rag Family GTPase Gtr2. *Cell Reports*, *13*(1). https://doi.org/10.1016/j.celrep.2015.08.059
Powis, K., Zhang, T., Panchaud, N., Wang, R., De Virgilio, C., & Ding, J. (2015). Crystal structure of the Ego1-Ego2-Ego3 complex and its role in promoting Rag GTPase-dependent TORC1 signaling. *Cell Research*, *25*(9). https://doi.org/10.1038/cr.2015.86
Prouteau, M., Desfosses, A., Sieben, C., Bourgoint, C., Lydia Mozaffari, N., Demurtas, D., … Loewith, R. (2017). TORC1 organized in inhibited domains (TOROIDs) regulate TORC1 activity. *Nature*. https://doi.org/10.1038/nature24021
Reinke, A., Anderson, S., Mccaffery, J. M., Yates Iii, J., Aronova, S., Chu, S., … Powers, T. (2004). TOR Complex 1 Includes a Novel Component, Tco89p (YPL180w), and Cooperates with Ssd1p to Maintain Cellular Integrity in Saccharomyces cerevisiae*. https://doi.org/10.1074/jbc.M313062200
Reinke, A., Anderson, S., McCaffery, J. M., Yates, J., Aronova, S., Chu, S., … Powers, T. (2004). TOR complex 1 includes a novel component, Tco89p (YPL180w), and cooperates with Ssd1p to maintain cellular integrity in Saccharomyces cerevisiae. *The Journal of Biological Chemistry*, *279*(15), 14752–14762. https://doi.org/10.1074/jbc.M313062200
Riggi, M., Niewola-Staszkowska, K., Chiaruttini, N., Colom, A., Kusmider, B., Mercier, V., …

Loewith, R. (2018). Decrease in plasma membrane tension triggers PtdIns(4,5)P2 phase separation to inactivate TORC2. *Nature Cell Biology*, *20*(9), 1043–1051. https://doi.org/10.1038/s41556-018-0150-z

Roosen, J., Engelen, K., Marchal, K., Mathys, J., Griffioen, G., Cameroni, E., … Winderickx, J. (2005). PKA and Sch9 control a molecular switch important for the proper adaptation to nutrient availability. *Molecular Microbiology*, *55*(3), 862–880. https://doi.org/10.1111/j.1365-2958.2004.04429.x

Rosner, M., & Hengstschlager, M. (2008). Cytoplasmic and nuclear distribution of the protein complexes mTORC1 and mTORC2: rapamycin triggers dephosphorylation and delocalization of the mTORC2 components rictor and sin1. *Human Molecular Genetics*, *17*(19), 2934–2948. https://doi.org/10.1093/hmg/ddn192

Saito, H., & Posas, F. (2012). Response to hyperosmotic stress. *Genetics*, *192*(2), 289–318. https://doi.org/10.1534/genetics.112.140863

Sancak, Y., Bar-Peled, L., Zoncu, R., Markhard, A. L., Nada, S., & Sabatini, D. M. (2010). Ragulator-Rag complex targets mTORC1 to the lysosomal surface and is necessary for its activation by amino acids. *Cell*, *141*(2), 290–303. https://doi.org/10.1016/j.cell.2010.02.024

Saxton, R. A., & Sabatini, D. M. (2017). mTOR Signaling in Growth, Metabolism, and Disease. *Cell*, *168*(6), 960–976. https://doi.org/10.1016/j.cell.2017.02.004

Schawalder, S. B., Kabani, M., Howald, I., Choudhury, U., Werner, M., & Shore, D. (2004). Growth-regulated recruitment of the essential yeast ribosomal protein gene activator Ifh1. *Nature*, *432*(7020), 1058–1061. https://doi.org/10.1038/nature03200

Sengupta, S., Peterson, T. R., & Sabatini, D. M. (2010). Regulation of the mTOR complex 1 pathway by nutrients, growth factors, and stress. *Molecular Cell*, *40*(2), 310–322. https://doi.org/10.1016/j.molcel.2010.09.026

Shah, K. H., Nostramo, R., Zhang, B., Varia, S. N., Klett, B. M., & Herman, P. K. (2014). Protein kinases are associated with multiple, distinct cytoplasmic granules in quiescent yeast cells. *Genetics*, *198*(4), 1495–1512. https://doi.org/10.1534/genetics.114.172031

Soulard, A., Cremonesi, A., Moes, S., Schütz, F., Jenö, P., & Hall, M. N. (2010). The rapamycin-sensitive phosphoproteome reveals that TOR controls protein kinase A toward some but not all substrates. *Molecular Biology of the Cell*, *21*(19), 3475–3486. https://doi.org/10.1091/mbc.E10-03-0182

Stephan, J. S., Yeh, Y. Y., Ramachandran, V., Deminoff, S. J., & Herman, P. K. (2009). The Tor and PKA signaling pathways independently target the Atg1/Atg13 protein kinase complex to control autophagy. *Proc Natl Acad Sci U S A*, *106*, 17049–17054. Retrieved from http://www.ncbi.nlm.nih.gov/entrez/query.fcgi?cmd=Retrieve&db=PubMed&dopt=Citation&list_uids=19805182

Sturgill, T. W., Cohen, A., Diefenbacher, M., Trautwein, M., Martin, D. E., & Hall, M. N. (2008). TOR1 and TOR2 have distinct locations in live cells. *Eukaryotic Cell*, *7*(10), 1819–1830. https://doi.org/10.1128/EC.00088-08

Suzuki, K., & Ohsumi, Y. (2010). Current knowledge of the pre-autophagosomal structure (PAS). *FEBS Letters*. https://doi.org/10.1016/j.febslet.2010.02.001

Takahara, T., & Maeda, T. (2012). Transient sequestration of TORC1 into stress granules during heat stress. *Molecular Cell*, *47*(2), 242–252. https://doi.org/10.1016/j.molcel.2012.05.019

Thedieck, K., Holzwarth, B., Prentzell, M. T., Boehlke, C., Kläsener, K., Ruf, S., … Baumeister,

R. (2013). Inhibition of mTORC1 by astrin and stress granules prevents apoptosis in cancer cells. *Cell*, *154*(4), 859–874. https://doi.org/10.1016/j.cell.2013.07.031

Ukai, H., Araki, Y., Kira, S., Oikawa, Y., May, A. I., & Noda, T. (2018). Gtr/Ego-independent TORC1 activation is achieved through a glutamine-sensitive interaction with Pib2 on the vacuolar membrane. *PLoS Genetics*, *14*(4), e1007334. https://doi.org/10.1371/journal.pgen.1007334

Urban, J., Soulard, A., Huber, A., Lippman, S., Mukhopadhyay, D., Deloche, O., … Loewith, R. (2007a). Sch9 is a major target of TORC1 in Saccharomyces cerevisiae. *Molecular Cell*, *26*(5), 663–674. https://doi.org/10.1016/j.molcel.2007.04.020

Urban, J., Soulard, A., Huber, A., Lippman, S., Mukhopadhyay, D., Deloche, O., … Loewith, R. (2007b). Sch9 is a major target of TORC1 in Saccharomyces cerevisiae. *Molecular Cell*, *26*(5), 663–674. https://doi.org/10.1016/j.molcel.2007.04.020

Varlakhanova, N. V, Mihalevic, M. J., Bernstein, K. A., & Ford, M. G. J. (2017). Pib2 and the EGO complex are both required for activation of TORC1. *Journal of Cell Science*, *130*, 3878–3890. https://doi.org/10.1242/jcs.207910

Wang, C.-W., Miao, Y.-H., & Chang, Y.-S. (2014). A sterol-enriched vacuolar microdomain mediates stationary phase lipophagy in budding yeast. *The Journal of Cell Biology*, *206*(3).

Warner, J. R. (1999). The economics of ribosome biosynthesis in yeast. *Trends in Biochemical Sciences*, *24*(11), 437–440. Retrieved from http://www.sciencedirect.com/science/article/pii/S0968000499014607

Wedaman, K. P., Reinke, A., Anderson, S., Yates, J., McCaffery, J. M., Powers, T., & Powers, T. (2003). Tor kinases are in distinct membrane-associated protein complexes in Saccharomyces cerevisiae. *Molecular Biology of the Cell*, *14*(3), 1204–1220. https://doi.org/10.1091/mbc.e02-09-0609

Wei, Y., & Zheng, X. (2009). Sch9 partially mediates TORC1 signaling to control ribosomal RNA synthesis. *Cell Cycle (Georgetown, Tex.)*, *8*(24), 4085–4090. Retrieved from http://www.ncbi.nlm.nih.gov/pmc/articles/PMC3023923/

Worley, J., Luo, X., & Capaldi, A. P. (2013). Inositol pyrophosphates regulate cell growth and the environmental stress response by activating the HDAC Rpd3L. *Cell Reports*, *3*(5), 1476–1482. https://doi.org/10.1016/j.celrep.2013.03.043

Wullschleger, S., Loewith, R., & Hall, M. N. (2006). TOR signaling in growth and metabolism. *Cell*, *124*(3), 471–484. https://doi.org/10.1016/j.cell.2006.01.016

Wullschleger, S., Loewith, R., Oppliger, W., & Hall, M. N. (2005). Molecular organization of target of rapamycin complex 2. *The Journal of Biological Chemistry*, *280*(35), 30697–30704. https://doi.org/10.1074/jbc.M505553200

Wyant, G. A., Abu-Remaileh, M., Frenkel, E. M., Laqtom, N. N., Dharamdasani, V., Lewis, C. A., … Sabatini, D. M. (2018). NUFIP1 is a ribosome receptor for starvation-induced ribophagy. *Science (New York, N.Y.)*, *360*(6390), 751–758. https://doi.org/10.1126/science.aar2663

Yadav, R. B., Burgos, P., Parker, A. W., Iadevaia, V., Proud, C. G., Allen, R. A., … Botchway, S. W. (2013). mTOR direct interactions with Rheb-GTPase and raptor: sub-cellular localization using fluorescence lifetime imaging. *BMC Cell Biology*, *14*(1), 3. https://doi.org/10.1186/1471-2121-14-3

Yan, G., Lai, Y., & Jiang, Y. (2012). TOR under stress: targeting TORC1 by Rho1 GTPase. *Cell*

Cycle (Georgetown, Tex.), *11*(18), 3384–3388. https://doi.org/10.4161/cc.21461
Yan, G., Shen, X., & Jiang, Y. (2006). Rapamycin activates Tap42-associated phosphatases by abrogating their association with Tor complex 1. *The EMBO Journal*, *25*(15), 3546–3555. https://doi.org/10.1038/sj.emboj.7601239
Yang, H., Jiang, X., Li, B., Yang, H. J., Miller, M., Yang, A., … Pavletich, N. P. (2017). Mechanisms of mTORC1 activation by RHEB and inhibition by PRAS40. *Nature*, *552*(7685), 368–373. https://doi.org/10.1038/nature25023
Yang, H., Rudge, D. G., Koos, J. D., Vaidialingam, B., Yang, H. J., & Pavletich, N. P. (2013). mTOR kinase structure, mechanism and regulation. *Nature*, *497*(7448), 217–223. https://doi.org/10.1038/nature12122
Yip, C. K., Murata, K., Walz, T., Sabatini, D. M., & Kang, S. A. (2010). Structure of the human mTOR complex I and its implications for rapamycin inhibition. *Molecular Cell*, *38*(5), 768–774. https://doi.org/10.1016/j.molcel.2010.05.017
Zheng, Y., & Jiang, Y. (2005). The yeast phosphotyrosyl phosphatase activator is part of the Tap42-phosphatase complexes. *Molecular Biology of the Cell*, *16*(4), 2119–2127. https://doi.org/10.1091/mbc.e04-09-0797
Zhou, X., Clister, T. L., Wong, G. W., Correspondence, J. Z., Lowry, P. R., Seldin, M. M., & Zhang, J. (2015). Dynamic Visualization of mTORC1 Activity in Living Cells Resource Dynamic Visualization of mTORC1 Activity in Living Cells. *CellReports*, *10*, 1767–1777. https://doi.org/10.1016/j.celrep.2015.02.031